

國立交通大學

電子工程學系

電子研究所碩士班

碩士論文

矽奈米線生物感測器之分析與模擬



Analysis and Simulation for Silicon Nanowire
Biosensors

研究生：呂昆諺

指導教授：蘇 彬 教授

中華民國九十八年九月

矽奈米線生物感測器之分析與模擬
Analysis and Simulation for Silicon Nanowire
Biosensors

研究生：呂昆諺

Student: Kun-Yen Lu

指導教授：蘇 彬

Advisor: Pin Su

國立交通大學

電子工程學系 電子研究所



Submitted to Department of Electronics Engineering & Institute of Electronics

College of Electrical and Computer Engineering

National Chiao Tung University

in Partial Fulfillment of the requirements

for the Degree of Master

in

Electronic Engineering

September 2009

Hsinchu, Taiwan

中華民國九十八年九月

矽奈米線生物感測器之分析與模擬

研究生: 呂昆諺

指導教授: 蘇 彬

國立交通大學電子工程學系 電子研究所碩士班

摘要

在本論文中提供一個廣泛適用於矽奈米線生物感測器模擬的架構。使用這種模擬的架構，我們系統化地探討元件設計對生物感測器靈敏度的所造成影響。同時，我們也探討因為本質參數變異對矽奈米線生物感測器所造成的影響，其中包含了隨機參雜濃度變動 (Random Dopant Fluctuation)、線邊緣的粗糙程度 (Line-edge Roughness)。經由模擬的結果，我們得知一個擁有較低參雜濃度、較小通道半徑與較短通道長度的矽奈米線生物感測器有更好的靈敏度與抵抗靈敏度擾動的能力。而當通道半徑小於十奈米，量子效應會進一步的驅動生物感測器靈敏度的成長。另一方面，我們研究在電解液中使用擴散型電子流抑制遮蔽效應對生物感測器所造成的影響。研究發現，使用擴散型電子流十分有效的抑制遮蔽效應，在一個輕參雜、小通道半徑的生物感測器上靈敏度會明顯的增加，特別是在參雜原子與待測分子的之間所帶電性相反的情況下。除此之外，天線型矽奈米線生物感測器的分析與模擬，在本論文中也將做進一步的討論。

Analysis and Simulation for Silicon Nanowire Biosensors

Student: Kun-Yen Lu

Advisor: Pin Su

Department of Electronics Engineering

Institute of Electronics

National Chiao Tung University

Abstract

This thesis provides a comprehensive simulation framework for silicon nanowire (Si-NW) biosensors. Using this simulation framework, we have systematically investigated the impact of device design on the sensitivity of Si-NW biosensors. In addition, we have examined the impacts of intrinsic parameter fluctuations such as random dopant fluctuations (RDF) and line-edge roughness (LER). Our study indicates that Si-NW biosensors with smaller diameter, shorter channel length, and lower channel doping have better sensitivity and less sensitivity variation. When diameter is smaller than $\sim 10\text{nm}$, the quantum effect further enhances the sensitivity. Regarding the suppression of screening effects, our simulations indicate that the electro-diffusion flow can significantly suppress the screening effects in the electrolyte solution, and Si-NW biosensors with lower channel doping and smaller diameter have more enhancements in the sensitivity, especially for the accumulation mode. Besides, the structure of Si-NW biosensor with antenna has been simulated and analyzed.

誌 謝

從剛進實驗室時的懵懵懂懂，到今日畢業在即一切卻又顯得如此的離情依依，兩年的歲月在不知不覺中流過。剎那間，驪歌響起、微風輕拂，又要向下一個人生階段邁進。兩年的光陰，不論是與教授的討論，或是在實驗室與大家一起為研究努力、打拼的情景，一切的酸、甜、苦、辣，都是我最深的懷念。

得之於人者太多，出之於己者太少。在此時此刻，這兩句話不禁浮然躍於心頭之上。在碩士班兩年的時間，特別感謝指導老師-蘇彬教授，老師對學術上的熱忱以及對學術嚴謹的要求都是我學習的榜樣。同時，也很感謝吳育昇學長、胡璧合學姐、郭俊延學長、范銘隆學長、王生圳學長、陳伯年學長、謝欣原學弟以及余昌鴻學弟在日常生活中，不論是課業上或是研究上的幫助。能和大家在同一個實驗室，是我在這段求學期間中最幸福也是最幸運的事。此外林鴻志教授門下的徐行徽學長及生科所楊裕雄教授門下的蕭程允學長，對我論文的完成給予我相當大的幫助在此一並感謝。

最後，感謝我的家人，不論我處在任何的困境都有你們的陪伴。謝謝我的爸爸呂元春先生和媽媽葉月嬌女士，你們辛苦的工作撫育我，為我所做一切的事都是支持我能不斷向前邁進的動力。

就像是陳之藩所說的：『要感謝的人太多了，所以就謝天吧!』。謹以此論文獻給所有給幫助過我的人。

2009/9/1 呂昆諺于風城

Contents

Abstract (Chinese)	
Abstract (English)	
Acknowledgement	
Contents	
Figure Captions	
Chapter 1 Introduction	
1-1 Background.....	1
1-2 Organization of the Thesis.....	3
1-3 References	3
Chapter 2 Device Design of Silicon Nanowire Biosensors Considering Intrinsic Parameter Fluctuations	
2-1 Introduction	5
2-2 Simulation Approach and Calibration	6
2-2.1 Simulation Approach	8
2-2.2 Calibration.....	10
2-3 Impact of Process Variations on Si-NW Biosensors	11
2-3.1 Impact of Diameter Variation on the Sensitivity of Si-NW Biosensors	11
2-3.2 Impact of Channel Length Variation on the Sensitivity of Si-NW Biosensors	13
2-3.3 Impact of Random Dopant Fluctuations on the Sensitivity of Si-NW Biosensors	14
2-4 Quantum Mechanical Effects on the Sensitivity of Silicon Nanowire Biosensors.....	17
2-5 Summary.....	19
2-6 References	20
Chapter 3 Investigation of Si-NW Biosensors with Electro-Diffusion Flow	

3-1	Introduction	39
3-2	Simulation Approach and Calibration	40
3-2.1	Equivalent Circuit Model.....	40
3-2.2	Simulation Approach	41
3-2.3	Calibration	44
3-3	Sensitivity of Si-NW Biosensors Operating in the Accumulation Mode and Depletion Mode	45
3-3.1	Accumulation Mode	45
3-3.2	Depletion Mode	48
3-4	Quantum Mechanical Effects on Small-Diameter Si-NW Biosensors.....	49
3-5	Summary.....	50
3-6	References	51

**Chapter 4 Simulation and Analysis for Silicon Nanowire Biosensors with
Antenna**

4-1	Introduction	69
4-2	Simulation Approach and Calibration	69
4-2.1	Simulation Approach	70
4-2.2	Simulation Results.....	72
4-3	Analytical Sensitivity Model for Long channel Si-NW biosensors with Antenna in Subthreshold Region.....	74
4-4	Summary.....	77
4-5	References	78

Chapter 5 Conclusions

5-1	Conclusions.....	89
5-2	References.....	91

Figure Captions

Fig. 2-1.	Schematic sketch of a Si-NW biosensor.....	23
Fig. 2-2.	(a) The biomolecules detecting system, which can be separated to (b) the electrolyte solution region, and (c) the semiconductor region.	24
Fig. 2-3.	Simulation procedure for a Si-NW biosensor.....	25
Fig. 2-4.	Simulation of the PSA molecule. (a) The net charge of a PSA molecule depends on the pH value of solution. (b) Comparison of simulation results with the Harvard experimental data [2.16]......	26
Fig. 2-5.	Sensitivity of Si-NW biosensors as a function of (a) channel length, and (b) diameter for various channel doping concentrations.	27
Fig. 2-6.	In the Si-NW biosensors, the resistance change is insensitive to the channel length scaling.	28
Fig. 2-7.	Schematic sketch of a Si-NW biosensor with $\pm 3\sigma$ diameter variation.....	29
Fig. 2-8.	Impact of diameter variation on the sensitivity for various channel doping concentrations.....	30
Fig. 2-9.	The percentage change of sensitivity variation in diameter for various doping concentrations.....	31
Fig. 2-10.	(a) Schematic sketch of a Si-NW biosensors with channel length variation, ΔL . (b) Gaussian distribution of the channel length variation. The figure includes 500 ensembles.	32
Fig. 2-11.	Sensitivity variation in channel length for (a) heavily doped cases, and (b) lightly doped cases.	33
Fig. 2-12.	Schematic sketch of a Si-NW device with (a) continuous doping, and (b) individually dopants distributed in the channel.....	34
Fig. 2-13.	Statistical fluctuations in sensitivity due to random dopant fluctuations..	35
Fig. 2-14.	Impact of the random dopant fluctuations for (a) heavily-doped, and (b) lightly-doped Si-NW biosensors for various channel length.	36
Fig. 2-15.	When the density gradient parameter $\gamma=15$, the exact solution of coupled Poisson-Schrodinger equations can be captured well by our ISE simulation.	37
Fig. 2-16.	Impact of quantum effects on (a) heavily-doped, and (b) lightly-doped Si-NW biosensors.....	38
Fig. 3-1.	The proposed biomolecules detecting system [4], which can be separated to (b) the electrolyte solution region, and (c) the semiconductor region...	53
Fig. 3-2.	The equivalent circuit models of two screening effect behaviors:	

- (a) Without solution bias, the biomolecule is shielded by the accumulated ions. (b) With solution bias, the electro-current suppresses the screening effect of biomolecule, and increases the Q_{SI} in silicon.....54
- Fig. 3-3.** The simulation procedure for a Si-NW biosensor with solution bias.55
- Fig. 3-4.** Our simulation results agree well with the Stanford simulation results. The ratio of the induced charge Q' to Q_{dop} increases with the solution bias because the solution bias induces more charges in the biosensor.....56
- Fig. 3-5.** The potential change is defined as $\log_{10}(\Delta\psi)$. (a) At solution bias=0V, the potential change is limited in the vicinity of biomolecule because of the serious screening effect. (b) At solution bias=1V, the screening effect is suppressed and the potential change spreads over a border space.57
- Fig. 3-6.** Two operation modes of Si-NW biosensors: (a) the accumulation mode which means the biological charge is opposite to the charge of carriers in the silicon, and (b) the depletion mode that is contrary to the accumulation mode.58
- Fig. 3-7.** (a) Schematic structure of a Si-NW with an approximated rod for ds DNA & ss DNA. (b) The device design parameters for our Si-NW biosensor simulations.....59
- Fig. 3-8.** With increasing the solution bias, the Si-NW biosensor has more induced charge Q' in the channel. Comparing (a) and (b), we can find that the $R_{Q'/Q_{dop}}$ for 20mM solution is larger than the $R_{Q'/Q_{dop}}$ for 100mM solution.60
- Fig. 3-9.** In the accumulation mode, the sensitivity has the largest value through an optimized solution bias. (a) For 20mM, the largest sensitivity of dsDNA and ssDNA are ~ 6.1 and ~ 4.3 , respectively. (b) For 100mM, the corresponding values are ~ 3.5 and ~ 2.1 . The biosensor operating in the light electrolyte concentration has larger sensitivity compared to in the heavy electrolyte concentration.61
- Fig. 3-10.** In the accumulation mode, the sensitivity increases with decreasing channel diameter of the nanowire biosensor.62
- Fig. 3-11.** In the accumulation mode, the sensitivity increases with decreasing doping concentration of the nanowire biosensor.63
- Fig. 3-12.** In depletion mode, the induced charge Q' increases rapidly with the solution bias and has an enhancement of $\sim 3.5X/\sim 3X$ compared to the Q_{dop} in 20mM/100mM (at solution bias=3V), respectively. It means the biosensor operating in light ion concentrations has better performance. ..64
- Fig. 3-13.** The corresponding largest sensitivity for dsDNA/ssDNA are (a) 0.95/0.92 for the 20mM electrolyte concentration, and (b) 0.86/0.77 for the 100mM

electrolyte concentration.	65
Fig. 3-14. In the depletion mode, the sensitivity of a Si-NW biosensor increases with decreasing diameter because of the increased surface to volume ratio.	66
Fig. 3-15. The sensitivity does not increase with decreasing channel doping concentration because the sensitivity is saturated in the depletion mode.	67
Fig. 3-16. Impact of quantum effects on the sensitivity of small-diameter Si-NW biosensors.	68
Fig. 4-1. The proposed biomolecules detecting system [4.3] which can be separated to (b) the sensing region, and (c) the semiconductor region.	80
Fig. 4-2. The simulation procedure for a Si-NW biosensor with antenna.	81
Fig. 4-3. Simulation of the surface potential change in the electrolyte solution with pH 6 and pH 7. Our simulation results agree well with the experimental results [4.11].	82
Fig. 4-4. The sensitivity of Si-NW biosensors with antenna operating in the subthreshold and superthreshold region for various (a) channel diameters, and (b) channel lengths.....	83
Fig. 4-5. The subthreshold swing of Si-NW biosensors with antenna depends on various device design parameters such as (a) diameter, (b) channel length, and (c) channel doping.	84
Fig. 4-6. Schematic sketch of a Si-NW structure [4.4]. The origin ($r=0$ and $y=0$) is defined at the center of the channel/source junction.	85
Fig. 4-7. The simulation results are captured well by our analytical model in the (a) I_d versus V_g curves, and (b) I_d versus V_d curves.	86
Fig. 4-8. Comparison of the analytical sensitivity model with simulation results for various doping concentrations.	87
Fig. 4-9. Comparison of the analytical sensitivity model with simulation results for various diameters.	87
Fig. 4-10. The corresponding sensitivity of Si-NW biosensors for various subthreshold slopes, from 60mV/dec ~180mV/dec.	88

Chapter 1

Introduction

1.1 Background

Biosensor is one of the most widely researched topics in bio-technology over past decades. For better sensitivity and faster analysis, the size of biosensors has been progressively miniaturized. In 2001, the research group at Harvard [1.1] has demonstrated silicon nanowire (Si-NW) served as a highly sensitive sensor for charged biological molecules and chemical species. Moreover, Si-NW biosensors have been used to demonstrate detection of DNA and proteins [1.2]-[1.4] at very low concentrations. With scaling the size of biosensors, device design and analysis become crucial and critical issues.

Moreover, for devices in the nanometer regime, several process variations such as random dopant fluctuation, channel length variation, and diameter variation may become pronounced because of the smaller device critical dimensions. It is difficult to capture device variability by investigating single device or using conventional simulation approach. Instead, using full Monte Carlo simulations to collect a large amount of identical devices and analyze the impacts of process variations on Si-NW biosensors is needed.

Besides, the electrostatic screening due to the ions in the electrolyte solution is also an important issue [1.5]. In 2008 IEDM, the research group at Stanford [1.6] has proposed a novel method to suppress the screening-induced performance limits of

Si-NW biosensors. In [1.6], the proposed method has significantly improved the performance of Si-NW biosensors, but it only considers the Si-NW biosensors operating in different electrolyte concentrations. The impacts of other device design parameters are short of discussion. Moreover, with scaling the size of biosensors, the quantum effect may play an important role. We provide a systematic investigation of Si-NW biosensors design and consider the electro-diffusion flow in the electrolyte solution.

Finally, we compare the ISFET of traditional bulk structure with a novel structure with antenna proposed by the research group at NCTU [1.7]. The new structure shows a superior subthreshold swing and higher on/off current ratio than the traditional bulk device. Although these advantages can further improve the performance of biosensors, the characteristics of the new structure with antenna have not been well understood. In addition to establishing a simulation methodology for the new structure, we demonstrate an analytical sensitivity model [1.8] for Si-NW biosensors with antenna operating in subthreshold regime. This model may provide more physical insights for Si-NW biosensors.

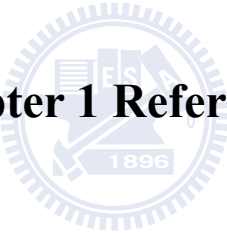
In this work, we have developed three distinct simulation frameworks to individually address the design considerations of Si-NW biosensors. The first simulation framework is for the direct-detection Si-NW biosensors. It considers that the biomolecules are directly accepted on the surface of Si-NW biosensors and change the conductance of Si-NWs. The second simulation framework is for Si-NW biosensors with solution bias. It considers the screening effect in the electrolyte solution. The third simulation framework is for the Si-NW biosensor with antenna. It considers that the charged biomolecules is uniformly distributed on the antenna

surface and the surface potential changes as detecting the biomolecules.

1.2 Organization of this Thesis

This thesis is organized as follows. In chapter 2, we investigate the impacts of intrinsic device parameter fluctuations on Si-NW biosensors and discuss the impacts of quantum effects on small-diameter Si-NW biosensors. In chapter 3, the effects of electro-diffusion current flow on Si-NW biosensors are assessed using our combined simulation procedure. In chapter 4, we investigate the Si-NW biosensors with antenna and demonstrate an analytical sensitivity model for Si-NW biosensors with antenna operating in subthreshold regime. Chapter 5 concludes this work.

Chapter 1 References

- 
- [1.1] Y. Cui, Q. Wei, H. Park, and C. M. Lieber, “Nanowire nanosensors for highly sensitive and selective detection of biological and chemical species,” *Science*, vol. 293, no. 5533, pp. 1289-1292, Aug. 2001.
 - [1.2] G. Zheng, F. Patlowsky, Y. Cui, W. U. Wang, and C. M. Lieber, “Multiplexed electrical detection of cancer markers with nanowire sensor arrays,” *Nat. Biotechnol.*, vol. 23, no. 10, pp. 1294-1031, Oct. 2005.
 - [1.3] J. Hahn and C. M. Lieber, “Direct ultrasensitive electrical detection of DNA and DNA sequence variations using nanowire nanosensors,” *Nano. Lett.*, vol. 4, no. 1, pp. 51-55, 2004.
 - [1.4] E. Stern, J. F. Klemic, D. A. Routenberg, P. N. Wyrembak, D. B. Turner-Evans, A. D. Hamilton, D. A. LaVan, T. M. Fahmy, and M. A. Reed, “Label-free immunodetection with CMOS compatible semiconducting nanowires,” *Nature*, vol. 445, no. 7127, pp. 519-523, Feb. 2007.
 - [1.5] P. E. Sheehan, and L. J. Whitman, “Detection limits for nanoscale biosensors,” *Nano Letters*, vol. 5, no. 4, pp. 803-807, 2005.
 - [1.6] Y. Liu, K. Lilja, C. Heitzinger, R. W. Dutton, “Overcoming the

screening-induced performance limits of nanowire biosensors: a simulation study on the effect of electro-diffusion flow,” in *IEDM Tech. Dig.*, pp. 491–494, 2008.

- [1.7] H. H. Hsu, T. W. Liu, L. Chan, C. D. Lin, T. Y. Huang, and H. C. Lin, “Fabrication and characterization of multiple-gated poly-si nanowire thin-film transistors and impacts of multiple-gate structures on device fluctuations,” *IEEE TED*, vol. 55, no. 11, NOV. 2008.
- [1.8] Y. S. Wu, and P. Su, “Sensitivity of gate-all-around nanowire MOSFETs to process variations-a comparison with multi-gate MOSFETs,” *IEEE TED*, vol. 55, no. 11, NOV. 2008.



Chapter2

Device Design of Silicon Nanowire Biosensors Considering Intrinsic Parameter Fluctuations

2-1 Introduction

In the past decades, the detection of biological and chemical device has progressively developed and served at many areas such as diagnosis of diseases [2.1], new drug discovery, homeland security [2.2]-[2.3], health monitor, and so on. Since the early 1970s, the ion-sensitive field effect transistors (ISFET) have been as a low-cost alternative to a traditional pH sensor [2.4]. It resembles a conventional MOSFET, but the channel is exposed to the solution to enable ions to serve as a gate [2.5]. However, the ISFET is not sensitive enough for fast detection of biomolecules at ultra-low concentration, and its detection limits is about nanomolar level [2.6]. In recent years, chemical sensors with fluorescent labeling and parallel optical detection techniques have been demonstrated for the fast detection of biomolecules at ultra-low concentration [2.7], but the pre-work and post-work for manipulating the detection system are too expensive and time-consumption. Hence, developing a new device that can enable direct detection, ultra-sensitive and rapid analysis of the biological molecules becomes an emerging topic.

Due to the superior surface to volume ratio [2.8], silicon nanowire (Si-NW) is a good candidate for a direct label-free and ultra-sensitive sensor. The Si-NW biosensors have been demonstrated [2.9]. Compared with the ISFETs, the detection

limit of Si-NW biosensors is three to four orders of magnitude higher [2.6]. Hence, the size of Si-NW biosensors has been progressively reduced to nanometer scale for larger surface to volume ratio and better performance. When Si-NW biosensors are scaled to nanometer dimension, intrinsic device parameter fluctuation may play an important role [2.10]. In [2.11], the research group at Purdue has indicated that there exists a lower limit of channel doping concentration N_D for Si-NW biosensors. When channel doping density is below N_D , the sensitivity will have unpredictable variations. However, the impacts of other device parameter variations, such as channel length and diameter, on Si-NW biosensors are still short of discussion. Moreover, with diameter scaling, biosensors may need to consider the quantum effect. How the quantum effect affect the performance of Si-NW biosensor merits investigation.

Therefore, in this chapter, we investigate the device design of Si-NW biosensors considering the impacts of several process variations and the quantum effects. In Section 2-2, we develop a simulation flow considering Poisson-Boltzmann equation and investigate the impacts of various design parameters on Si-NW biosensors. In Section 2-3, we consider several process variations on Si-NW biosensors and calculate the corresponding sensitivity variation for different device design parameters. Section 2-4 gives the details of quantum effects for small-diameter Si-NW biosensors and discusses the influence of quantum effects for heavily- and lightly-doped cases. Section 2-5 summarizes the essential results of this chapter.

2-2 Simulation Approach and Calibration

Fig. 1 shows the detecting system of Si-NW biosensors. The detecting system

consists of two electrodes (source and drain) and a functionalized surface around channel. The functionalized surface with specified receptors only conjugates with the target biomolecules. When the surface of biosensors receives target biomolecules, the potential distribution in the vicinity of biomolecules will be modulated. We assume Si-NW biosensors are operating in the accumulation mode because our simulation results indicate that the sensitivity of Si-NW biosensors is not determined by the doping type (n- or p-type). It is consistent with the Purdue's simulation results [2.11]. The carriers in the channel are attracted by the biomolecules so they accumulate in the vicinity of conjugated receptors. Due to the charge redistribution in the channel, the conductivity of Si-NW biosensors will be changed. Hence, we can define the sensitivity, S , of a Si-NW biosensor as below:

$$\text{Sensitivity (S)} = \frac{G-G_0}{G_0} = \frac{\Delta G}{G_0}, \quad (2-1)$$

where G/G_0 is the conductance of Si-NW biosensors with/without detecting biomolecules, and ΔG is the difference between G and G_0 . Although the sensitivity is a good criterion to evaluate Si-NW biosensors, it is not intuitive enough to realize the relationship between the device design parameters and the sensitivity. We can approximate the biomolecule on the surface by a constant surface density σ and redefine the expression of sensitivity as the relative change in charge as below:

$$\text{Sensitivity(S)} = \frac{\Delta Q}{Q_0} = \frac{\pi\sigma d}{qN_{\text{eff}}\pi(\frac{d}{2})^2} = \frac{\sigma}{qN_{\text{eff}}} \left(\frac{4}{d}\right), \quad (2-2)$$

where q is the elementary charge, N_{eff} is the effective doping concentration in the channel, and d is the channel diameter. Equation 2-2 suggests that Si-NW biosensors with smaller diameters and lower doping densities are expected to have higher

sensitivity. It also explains why the surface to volume ratio ($\frac{4}{d}$) increases with decreasing diameter.

2-2.1 Simulation Approach

The system of a Si-NW biosensor can be divided into two sub-regions, as shown in Fig. 2-2. Fig. 2-2(b) is the first sub-region, A, which contains the electrolyte solution, target biomolecules, and the various ions. Although these ions can provide the necessary buffer for the stability of biomolecule-receptor binding, they can also shield the biomolecules. The electrostatic potential in this region can be described by the nonlinear Poisson-Boltzmann (PB) equation [2.12]-[2.13]:

$$-\nabla(\epsilon_{\omega}\nabla\Phi(\mathbf{r})) + \kappa^2 \sinh(\beta\Phi) = q \sum_i Z_i \delta(\mathbf{r} - \mathbf{r}_i), \quad (2-3)$$

where ϵ_{ω} is the dielectric constant of water, q is the elementary charge, Φ is the electrostatic potential, $\beta=k_B/T$ (k_B is the Boltzmann constant, T is the temperature), κ is the modified Debye-Huckel parameter [2.13], and Z_i is the fixed charge of biomolecules.

Fig. 2-2(c) is the second sub-region, B, which contains the silicon channel and oxide. In this region, we assume the silicon and oxide are perfect without any defects or traps, and the impurities in the channel are completely ionized. The carrier transport and the potential distribution in this region can be described by the drift-diffusion equation and Poisson's equation, respectively.

$$J_{e,h} = q\mu_{e,h}\nabla\Phi \pm qD_{e,h}\nabla n_{e,h} \quad (2-4)$$

$$-\nabla(\epsilon_{Si}\nabla\Phi) = q(p - n + N_{dop}) \quad (2-5)$$

where J is the current density, q is the elementary charge, μ is the mobility, n/p are the electron/hole density, Φ is the electrostatic potential, D is the diffusion coefficient, and N_{dop} is the net impurity concentration. The subscripts “e,h” correspond to electron / hole, respectively.

Equation (2-3)-(2-5) are the physical models used in the calculation of the Si-NW biosensor. We separate the numerical method into five main steps to solve the above equations.

In the first step: We use a numerical solver, COMSOL physical simulation tool [2.14] to solve the Poisson-Boltzmann equation and compute the electrical field distribution in the region A. Through the Gauss’s theorem, we can estimate the charge density in the water/oxide interface by integrating the electrical field. The differential form of Gauss’s law is expressed as:

$$\nabla \cdot \mathbf{E} = \frac{\rho}{\epsilon_0}, \quad (2-6)$$

where E is the electric field, ρ is the charge density, and ϵ_0 is the electric constant of water.

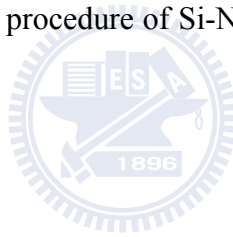
In the second step: In the region B, the coupled drift-diffusion equation and Poisson-Boltzmann equation are solved by the semiconductor simulation tool, ISE [2.15]. We take the first step result, the interface charge density, as the boundary condition of ISE simulation.

In the third step: Give specified operating bias to calculate the sensitivity of Si-NW biosensors.

In the fourth step: Vary the device design parameters in the first, second, and third steps, sequentially. In addition, we collect and categorize the simulation results to build the sensitivity table for various design parameters.

In the fifth step: We investigate and analyze the sensitivity for various design parameters, and systematically optimize the design parameters of Si-NW biosensors.

In summary, the simulation procedure of Si-NW biosensors is shown in the Fig. 2-3.

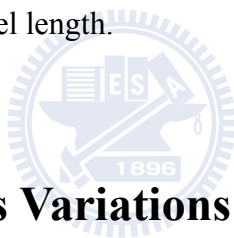


2.2.2 Calibration

In this section, we provide our simulation results for the detection of prostate-specific antigen (PSA) calibrated with the Harvard experimental data [2.16]. The research group at Harvard has successfully demonstrated highly-sensitive and label-free electrical detection of PSA by using Si-NW devices. The prostate-specific antigen is a marker for prostate cancer and its net charge on the surface depends on the pH of solution [2.17]. The simulation of PSA can be separated into three steps. In the first step, we find the sequence of PSA in the protein data bank [2.18]. In the second step, we use the protein calculator [2.19] to estimate the net charge on the various pH of solution. In the final step, we use our established simulation flow to investigate the relative conductance change of Si-NW biosensors. Fig. 2-4(a) shows

that the net charge depends on the pH of solution. Fig. 2-4(b) shows that our simulation results are very close to the Harvard experimental data [2.16].

In addition, we demonstrate the sensitivity of Si-NW biosensors for various design parameters. Fig. 2-5(a) and Fig 2-5 (b) show that the sensitivity increases with shorter channel length, smaller diameter, and lower channel doping concentration. These results are well expected from equation (2-2) except the dependence of channel length. For further investigating the dependence of sensitivity on length, the sensitivity can be rewritten as $S=\Delta R/R_0$, where ΔR is the change in resistance due to Si-NW biosensors detecting the target molecules, and R_0 is the initial resistance. Fig. 2-6 shows that the change in resistance, ΔR , remains the same. It makes the sensitivity increase reversely with the channel length.



2-3 Impact of Process Variations on Si-NW Biosensors

2-3.1 Impact of Diameter Variation on The Sensitivity of Si-NW Biosensors

To access the impact of diameter variation on Si-NW biosensors, we assume that the device design parameter D has a $\pm 3\sigma$ variation (in Fig. 2-7). This 3σ value is estimated from the combination of process variations such as lithography variation, etch variation, and resist trim variation [2.20]. According to the 2008 ITRS [2.20], the value of 3σ is very close to 3nm. Therefore, the corresponding sensitivity variation in diameter can be calculated as:

$$\Delta S_D = | S_{D_{+3\sigma}} - S_{D_{-3\sigma}} | \quad (2-7)$$

where $S_{D_{+3\sigma}} / S_{D_{-3\sigma}}$ represents the sensitivity of Si-NW biosensors with $D+3\sigma/D-3\sigma$, and the sensitivity variation ΔS_D is the difference between $S_{D_{+3\sigma}}$ and $S_{D_{-3\sigma}}$.

Fig. 2-8 shows our simulation results of the sensitivity variation in diameter for different channel doping concentrations. The figure clearly shows that the sensitivity variation increases reversely with the channel diameter. This is because the diameter is the critical dimension and its fraction of 3σ variation over diameter ($3\sigma/D$) increases with smaller diameter. Moreover, it can be seen that Si-NW biosensors have smaller sensitivity variation in diameter as the heavily-doped channel is employed. In summaries, Si-NW biosensors with higher channel doping density and larger diameter seem to have more advantages on the device design. To further our examination, we define the percentage change of sensitivity variation in diameter as below:

The percentage change of sensitivity variation in diameter (P_{Diameter}),

$$P_{\text{Diameter}} = \frac{\Delta S_D}{S} \times 100\% \quad (2-8)$$

In other words, we normalize the sensitivity variation with its self-sensitivity. This definition can help us more accuracy to determine the impact of the diameter variation.

Fig. 2-9 shows the P_{Diameter} for different channel doping concentrations. The figure indicates that the P_{Diameter} decreases with reduced channel doping. This is because the sensitivity, S , increases faster than the ΔS_D . In other word, Si-NW biosensors should be designed at lower doping concentrations for smaller percentage of sensitivity variation in diameter.

2-3.2 Impact of Channel Length Variation on The Sensitivity of Si-NW Biosensors

To access the impact of channel length variation, we use the Gaussian autocorrelation function [2.21] in this study. The Gaussian autocorrelation function is based on the 1-D Fourier synthesis technique [2.21]:

$$S_E(\mathbf{k}) = \sqrt{\pi}\Delta^2\Lambda e^{-(k^2\Lambda^2/4)}, \quad (2-9)$$

where Δ is the rms amplitude of the channel length variation, Λ is the correlation length, and k is the index of sampling points defined as $k=i (2\pi/Ndx)$ with dx , the space of sampling points.

A schematic sketch for Si-NW biosensor with channel length variation, ΔL , is shown in Fig. 2-10(a). In our simulation, ΔL is estimated by the Gaussian autocorrelation function. With appropriate choices of rms amplitude $\Delta=1.5$ nm and correlation length $\Lambda=20$ nm [2-22], we generate a database with 500 samples for ΔL (Fig. 2-10(b)). Each simulated biosensor is randomly assigned a value of ΔL from the database.

We have performed Monte Carlo simulation with 100 samples to capture the stochastic behavior of channel length variation in Si-NW biosensors. In addition, we have defined the percentage change of sensitivity variation in channel length as:

The percentage change of sensitivity variation in channel length(P_{Lenght})

$$P_{Lenght} = \frac{\sigma_{S_L}}{\langle S_L \rangle} \times 100\%, \quad (2-10)$$

where $\langle S_L \rangle$ is the average of the sensitivity variation in channel length, and σS_L is the standard deviation of the sensitivity variation in channel length.

Fig. 2-11(a) shows the impact of channel length variation on the heavily-doped cases. It can be seen that $\langle S_L \rangle$ and σS_L increase with decreasing channel length. This is because the sensitivity scales reversely with the channel length. Fig. 2-11(b) shows the impact of channel length variation on the lightly doped cases. It can be seen that $\langle S_L \rangle$ slowly increases with decreasing channel length. However, the σS_L decreases with the channel length because the sensitivity in short-channel-length devices is saturated. In other words, the sensitivity in short channel length only has a small fluctuation of considering the channel length variation. Furthermore, our simulation indicates that P_{Length} is negligible, no matter for lightly- or heavily-doped cases. Hence, lightly-doped channel and short channel length should be employed for higher sensitivity.

2-3.3 Impact of Random Dopant Fluctuation on The Sensitivity of Si-NW Biosensors

In this section, we investigate the impact of random dopant fluctuations (RDF) by performing 3-D atomistic simulation [2.23]. Fig. 2-12(a) shows a Si-NW biosensor with the traditional simulation approach. It can be seen that the dopants are continuously distributed in the Si-NW. However, a Si-NW biosensor is performed with 3-D atomistic simulation shown in Fig. 2-12(b). Each dopant is treated as individually distributed in the channel.

The simulation methodology of atomistic simulation approaches can be divided into three steps: In the first step: The dopant number fluctuations are governed by Poisson distribution function [2.24] expressed as:

$$P = (x, N_{mean}) = \frac{N_{mean}^x \cdot e^{-N_{mean}}}{x!}, \quad (2-11)$$

where N_{mean} is the expected dopant number in Si-NW, x is the number of occurrences of the dopant number, and P is the probability of x occurrences. The dopant numbers in the channel can be randomly generated by equation (2-11). In the second step: We build a large matrix equivalent to the lattice structure in the Si-NW region and randomly place dopants in it. In the third step: Each dopant in the Si-NW region is assigned to the nearest grid of lattice structure with a corresponding doping concentration, $\frac{N_{grid}}{V_{Si_NW}}$. Where N_{grid} is the total number of grids, and V_{Si_NW} is the volume of Si-NW.

We have performed Monte Carlo simulation with 100 samples to capture the stochastic behavior of random dopant fluctuations in Si-NW biosensors. Fig.2-13 shows the statistical fluctuations for 100 different Si-NW biosensors. It can be seen that the sensitivity of Si-NW biosensors shows large fluctuations from the mean value. The variations due to the ransom dopant fluctuations would be a severely problem for the detection of one biomolecule. As mentioned before [2.11], there exists a lower limit of channel doping concentration N_D for Si-NW biosensors. When channel doping density is below N_D , the sensitivity will have unpredictable variations. For further examination, we have defined the percentage change of sensitivity variation in RDF as:

The percentage change of sensitivity variation in RDF (P_{RDF})

$$P_{\text{RDF}} = \frac{\sigma_{\text{S}_{\text{RDF}}}}{\langle \text{S}_{\text{RDF}} \rangle} \times 100\%, \quad (2-12)$$

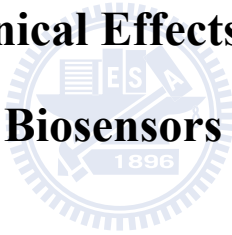
where $\langle \text{S}_{\text{RDF}} \rangle$ is the average of the sensitivity variation in RDF, and $\sigma_{\text{S}_{\text{RDF}}}$ is the standard deviation of the sensitivity variation in RDF.

Fig. 2-14(a) shows the impact of random dopant fluctuations on the heavily-doped cases. It can be seen that $\langle \text{S}_{\text{RDF}} \rangle$ and $\sigma_{\text{S}_{\text{RDF}}}$ increase inversely with the channel length. However, the P_{RDF} decreases with the channel length because $\langle \text{S}_{\text{RDF}} \rangle$ increases faster than $\sigma_{\text{S}_{\text{RDF}}}$ with decreasing channel length. When the channel length is $1.75\mu\text{m}/0.1\mu\text{m}$, the corresponding P_{RDF} is $78.5\%/28.6\%$, and the corresponding $\langle \text{S}_{\text{RDF}} \rangle$ is $0.004/0.424$, respectively. For the heavily-doped cases, our simulation results indicate that the short-channel Si-NW biosensor has smaller percentage change of sensitivity variation in RDF and larger sensitivity than the long-channel case.

Fig. 2-14(b) shows the impact of random dopant fluctuations on the lightly-doped cases. It can be seen that $\langle \text{S}_{\text{RDF}} \rangle$ is insensitive with the channel length because the sensitivity in light doping is saturated. However, $\sigma_{\text{S}_{\text{RDF}}}$ decreases with the channel length because the sensitivity in short channel length is saturated. In other words, the sensitivity in short channel length only has a small change with random dopant fluctuations. Moreover, the figure shows that P_{RDF} decreases with the channel length. When the channel length is $1.75\mu\text{m}/0.1\mu\text{m}$, the corresponding P_{RDF} is $19.85\%/1.35\%$, and the corresponding $\langle \text{S}_{\text{RDF}} \rangle$ is $1.71/1.85$. For the lightly-doped cases, our simulation results indicate that the short-channel Si-NW biosensors have smaller percentage change of sensitivity variation in RDF and larger sensitivity than the long-channel cases.

For comparison of the lightly- and heavily-doped cases, the Si-NW biosensors with light doping have larger $\langle S_{\text{RDF}} \rangle$ and P_{RDF} than that with heavy doping. The conclusion is that Si-NW biosensors with shorter channel length and lower channel doping can suppress the RDF effects and improve the sensitivity. In other words, we believe that the lower limit N_{D} does not exist. Our simulation results seem to conflict with the Purdue' simulation results [2.11]. This is because they only consider the standard deviation of the sensitivity variation σS_{RDF} . However, sometimes, σS_{RDF} increases with the sensitivity. Hence, for the further examination of the impact of RDF on sensitivity, our criterion P_{RDF} is more reasonable and fair.

2-4 Quantum Mechanical Effects on The Sensitivity of Silicon Nanowire Biosensors



The quantum effects have been demonstrated to have an undeniable influence on the nanoscale devices [2.25]. However, the impact of quantum effects on the nanoscale biosensors has rarely been investigated. Therefore, we quantitatively investigate the quantum effects on small-diameter nanowire biosensors for lightly- and heavily-doped cases in this section.

In this work, we use the density gradient model [2.26]-[2.27] to approximate the quantum mechanical effect. The density gradient function is a partial different function with a parameter γ which is sensitive to the electron distribution. Therefore, how to accurately estimate the parameter γ is a crucial problem in this quantum-mechanical simulation. The full Schrödinger equation solver, Silvaco [2.28],

is used to be a criterion for determination of the parameter γ . In first step, we use Silvaco simulation tool to solve the Schrodinger equation and find the exact electron distribution in the biosensor. In second step, we use the density gradient model in ISE [2.15] and adjust the parameter γ to find the electron distribution in the biosensor. Finally, we compare the solutions from the first step and the second step, and set the discrepancy between the two solutions within 2%. The Fig. 2-15 shows that the density gradient model calibrates with the exact Poisson-Schrodinger solution well when the parameter $\gamma=15$. The discrepancy of the two solutions is about 1.94%.

Fig. 2-16(a) shows the sensitivity with and without considering the quantum effect for Si-NW biosensors with heavy doping. The figure shows that with diameter scaling from 10nm to 3nm, the sensitivity without considering the quantum effect has a $\sim 1.37X$ enhancement because of the increased surface to volume ratio. When considering the quantum effect, the enhancement of sensitivity can reach $\sim 1.42X$. According to equation (2-2), the driving force of the sensitivity enhancements can be divided into the surface to volume ratio ($d/4$) part and the effective doping concentration ($1/N_{\text{eff}}$) part. Compared with excluding the quantum effect, the sensitivity of Si-NW biosensors with considering the quantum effect has more improvements because of the effective doping concentration limited by the quantum effects [2.29].

Fig. 2-16(b) shows the sensitivity with and without considering the quantum effects for Si-NW biosensors with light doping. The figure shows that with diameter scaling from 10nm to 3nm, the sensitivity without/with considering the quantum effect has a $\sim 1.13X/\sim 1.19X$ enhancement.

For the further examination, we define the percentage enhancements of considering the quantum effect as:

$$S_{\text{increase}} = \frac{S_{\text{with}} - S_{\text{without}}}{S_{\text{without}}} \cdot 100\%, \quad (2-13)$$

where S_{with} is the sensitivity of Si-NW biosensors with considering the quantum effect, S_{without} is the sensitivity of Si-NW biosensors without considering the quantum effect. The comparison of the S_{increase} for lightly- and heavily-doped Si-NW biosensors indicates that sensitivity in the heavily-doped case has more enhancements. Even though the sensitivity is enhanced more by the quantum effects in the heavily-doped case, the sensitivity for heavy doping concentration is far less than that for lightly doping concentration. Hence, even considering the quantum effect, the lightly-doped channel is still a better choice. Moreover, it can be seen that when the diameter near $\sim 10\text{nm}$, the S_{increase} are 3.95% and 0.4% for heavily- and lightly-doped cases, respectively. The quantum effects on the sensitivity do not seem to have significant enhancements, especially in lightly-doped cases. In other word, we can only consider the classical model when diameter beyond $\sim 10\text{nm}$.

2.5 Conclusion

Our conclusions for this chapter are summarized as follows:

- (1) Our simulation flow for Si-NW biosensors has been demonstrated.
- (2) The sensitivity of Si-NW biosensors increases with smaller diameter, shorter channel length, and lower channel doping concentration.
- (3) The sensitivity variation in diameter increases with decreasing diameter. Hence, for suppression of the sensitivity variation in diameter, the Si-NW biosensors with should be design at lower doping.

- (4) Because the normalized sensitivity variation in the channel length is negligible, shorter channel length and lower doping concentration should be employed for the Si-NW biosensor design.
- (5) Considering the impact of RDF on the sensitivity variation, the short-channel Si-NW biosensors have larger $\langle S_{RDF} \rangle$ and smaller P_{RDF} than the long-channel cases. Hence, shorter channel length and lower channel doping should be employed for smaller RDF effects and higher sensitivity of Si-NW biosensors.
- (6) Though the sensitivity is enhanced more by the quantum effect in the heavily-doped case, the sensitivity in the heavily-doped case is far less than in the lightly-doped case. Hence, even considering the quantum effect, the lightly-doped channel is still a better choice.



References

- [2.1] D. C. H. Burgess, J. Wasserman, and C. A. Dahl, "Global health diagnostics," *Nature*, vol. 444, pp. 1-2, 2006.
- [2.2] D. V. Lim, M. M. Simpson, E. A. Kearns, "Current and developing technologies for monitoring agents of bioterrorism and biowarfare," *Clin. Microbiol. Rev.*, vol. 18, no.4, pp. 583-607, Oct. 2005.
- [2.3] F. S. Ligier and J. S. Erickson, "Bioengineering: diagnosis on disc," *Nature*, vol. 440, no. 7081, pp. 159-160m Nar, 2006.
- [2.4] W. M. Siu and R. S. C. Cobbold, "Basic properties of the electrolyte-sio2-si system: physical and theoretical aspects," *IEEE Trans. Electron devices*, vol. 26, no. 11, NOV. 1979.
- [2.5] S. M. Sze, *Physics of Semiconductor Devices*, third edition 2007.
- [2.6] P. R. Nair, and M. A. Alam, "Performance limits of nanobiosensors," *Applied Physics Letters*, vol. 88, 2006.
- [2.7] R. J. Lipschutz, S. P. A. Fodor et al, "High density synthetic oligonucleotide arrays," *Nat. Genet.*, vol. 21, pp.20-24, 1999.
- [2.8] M. Curreli et. al, "Real-time, label-free detection of biological entities using nanowire-based FETs," *IEEE Trans. Nanotech.*, vol. 7, no.6, NOV. 2008.

- [2.9] F. Patolsky, and C. M. Lieber, "Nanowire nanosensors," *Materials Today*, April, 2005.
- [2.10] A. Asenov, S. Kaya, and A. R. Brown, "Intrinsic parameter fluctuations in decananomwter MOSFETs intruded by Gage line edge roughness," *IEEE Trans. On Electron Devices*, vol. 50, no.5, May 2003.
- [2.11] P. R. Nair and A. M. Alam," Design considerations of silicon nanowire biosensors," *IEEE TED*, vol. 54, no. 12, December 2007.
- [2.12] D. McQuarrie, *Statistical Mechanics*. New York: Harper & Row,1976.
- [2.13] M. Holst, "The Poisson-Boltzmann equation: analysis and multilevel numerical solution," in "Applied Mathematics and CRPC," California inst. Technol., Pasadena, CA, 1994. Tech. Rep.
- [2.14] <http://www.comsol.com/>
- [2.15] <http://www.synopsys.com/home.aspx>
- [2.16] G. Zheng et. al, "Multiplexed electrical detection of cancer markers with nanowire sensor arrays," *Nat. Biotechnol.*, vol. 23, no. 10, pp. 1294-1301, Oct. 2005.
- [2.17] A. L. Carvalho, L. Sanz, D. Baretino, A. Romero, J. J. Calvete, and M. J. Romao, "Crystal structure of prostate kallikrein isolated from stallion seminal plasma: A homologue of human PSA," *J. Mol. Biol.*, vol. 322-337, Sep. 2002.
- [2.18] <http://www.ncbi.nlm.nih.gov/protein/24158620?report=GenPept>
- [2.19] <http://www.scripps.edu/~cdputnam/protcalc.html>
- [2.20] <http://www.itrs.net/>
- [2.21] A. Dixit, K. G. Anil, E. Baravelli, P. Roussel, A. Mercha, C. Gustin, M. Bamal, E. Grossar, R. Rooyachers, E. Augendre, M. Jurczak, S. Biesemans, and K. D. Meyer, "Impact of stochastic mismatch on measure SRAM performance of FinFETs with resist/ spacer-defined fins: role of line-edge-roughness," in *Proc. IEDM Tech. Dig.*, 2006.
- [2.22] E. Baravelli, M. Jurczak, N. Speciale, K. D. Meyer, and A. Dixit, "Impact of ler and random dopant fluctuations on FinFET matching performance," *IEEE Transactions on nanotechnology*, vol. 7, no. 3, MAY 2008.
- [2.23] D. J. Frank, Y. Taur, M. Jeong, and H-S P. Wong, "Monte carlo modeling of threshold variation due to dopant fluctuations," *Symp. On VLSI Tech. Dig.*, pp.171-172, 1999.
- [2.24] H. S. Wong and Y. Taur, "Three-Dimensional "atomistic" simulation of discrete random dopant distribution effects in sub-0.1 μ m MOSFETs," *IEDM Tech. Dig.*, pp. 705-708, 1993.
- [2.25] A. Asenov, A. R. Brown, and J. R. Watling, "Quantum corrections in the simulation of decanano MOSFETs," *Solid-State Electronics*, vol. 47, no. 7,

July 2003.

- [2.26] M. G. Ancona and H. F. Tiersten, “Macroscopic physics of the silicon inversion layer,” *Phys. Rev. B*, vol. 35, no. 15, pp. 7959–7965, May, 1987.
- [2.27] M. G. Ancona and G. J. Iafrate, “Quantum correction to the equation of state of an electron gas in a semiconductor,” *Phys. Rev. B*, vol. 39, no. 13, pp. 9536–9540, May, 1989.
- [2.28] <http://www.silvaco.com/>
- [2.29] S. Datta, *Quantum Transport: Atom to Transistor*, chapter 7.3, pp 170-176 (Cambridge University Press, New York, 2005).



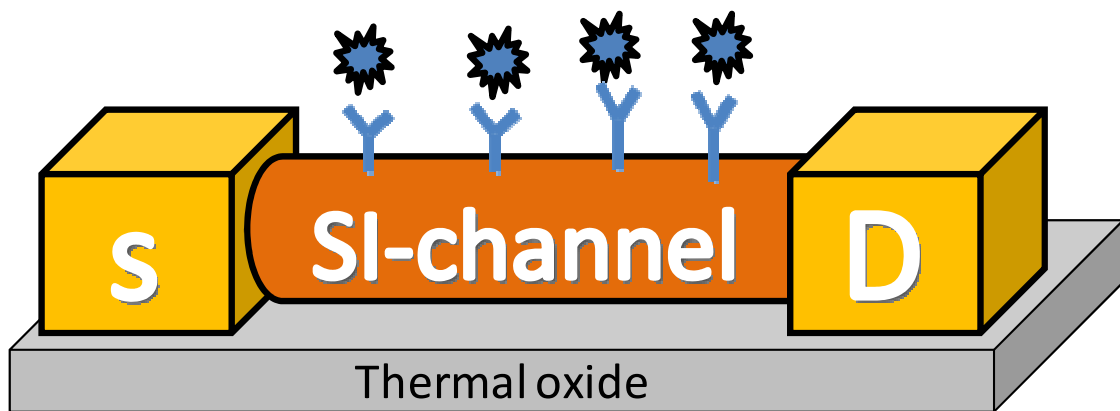
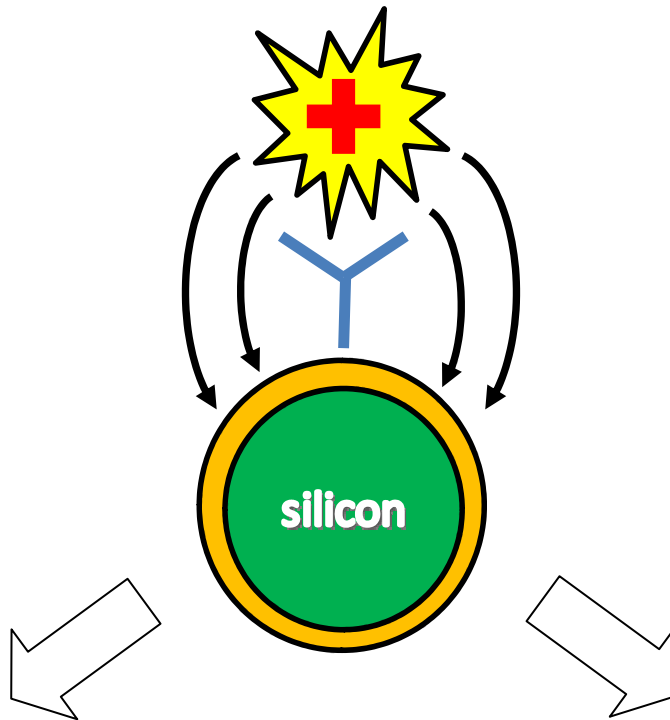
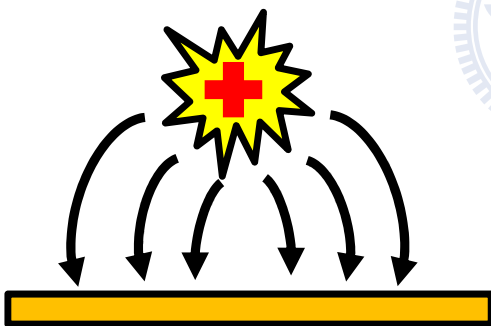


Fig. 2-1. Schematic sketch of a Si-NW biosensor.

(a) The cross-section of Si-NW biosensors



(b) The electrolyte solution region



(c) The semiconductor region

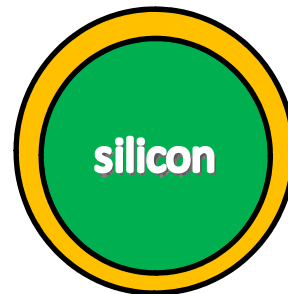


Fig. 2-2. (a) The biomolecules detecting system which can be separated to (b) the electrolyte region, and (c) the semiconductor region.

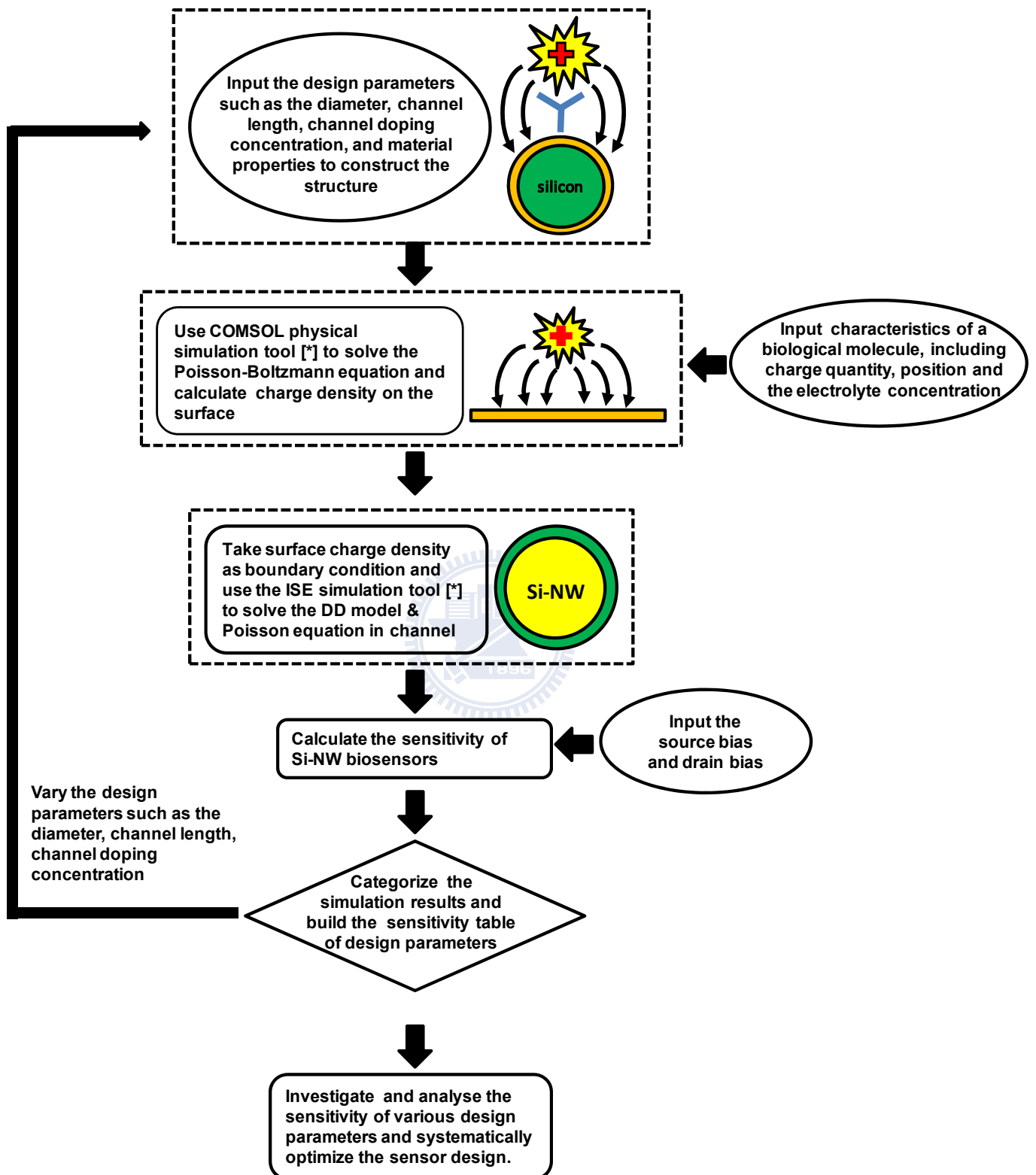


Fig. 2-3. Simulation procedure for a Si-NW biosensor.

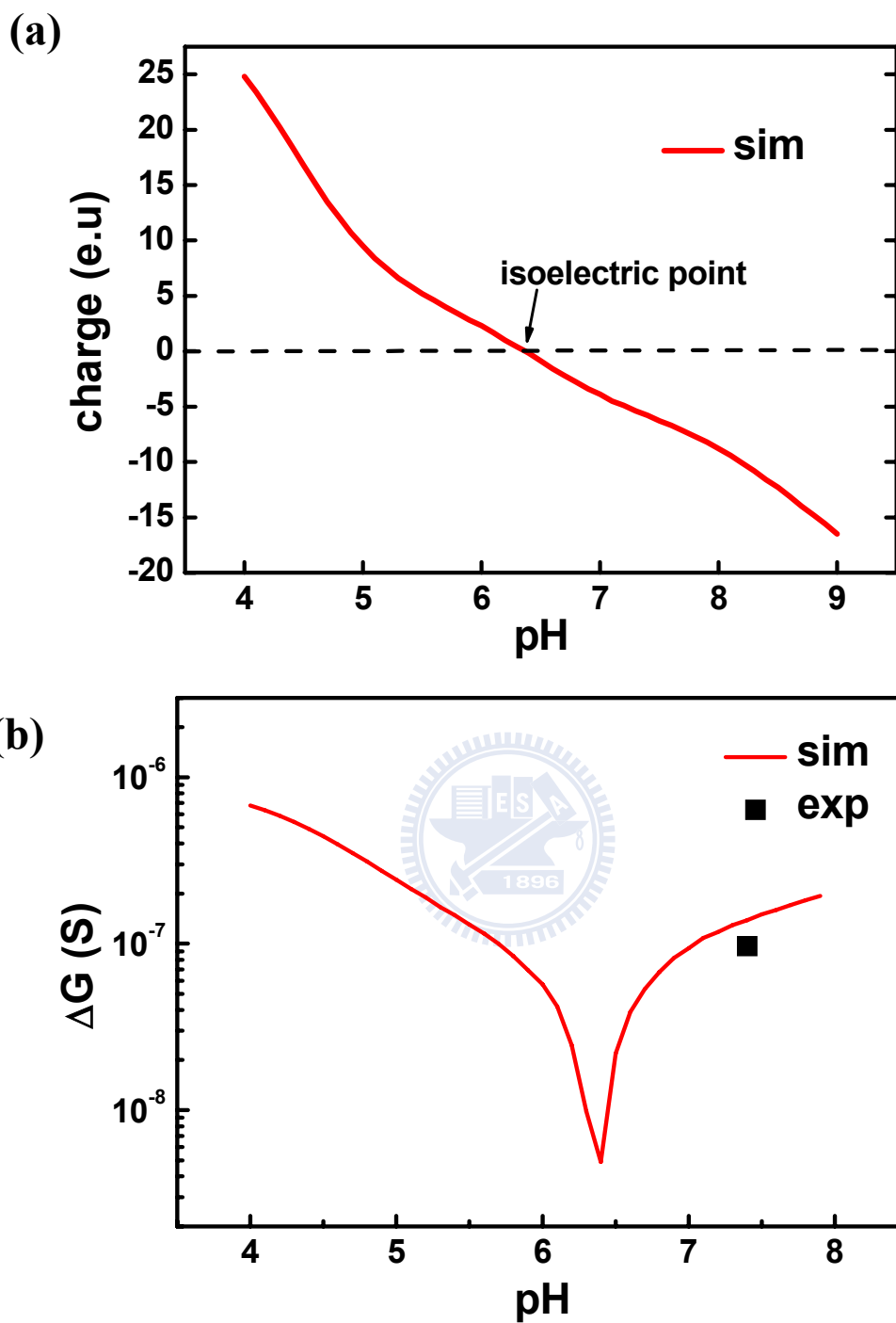


Fig. 2-4. Simulation of the PSA molecule. (a) The net charge of a PSA molecule depends on the pH value of solution. (b) Comparison of simulation results with the Harvard experimental data [2.16].

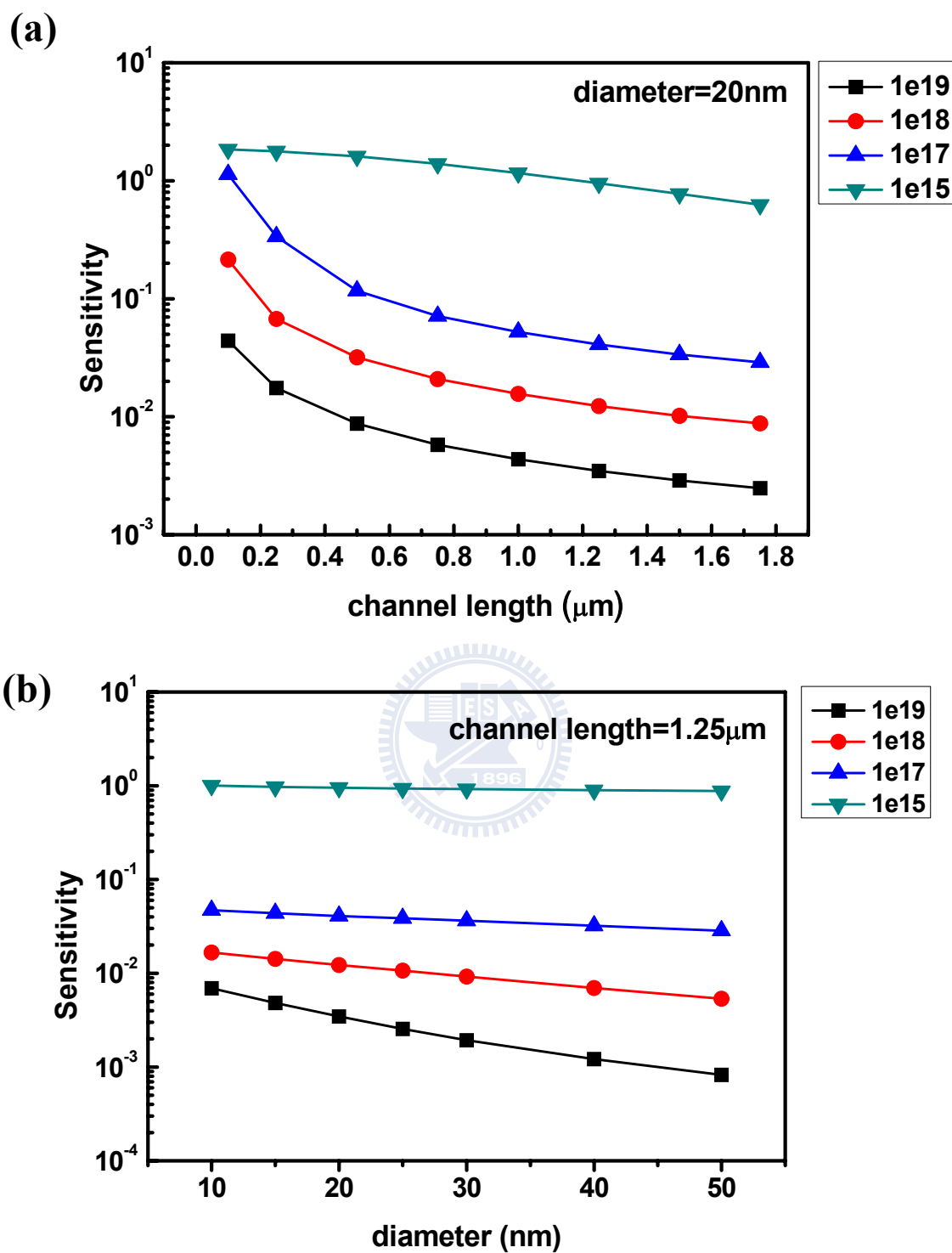


Fig. 2-5. Sensitivity of Si-NW biosensors as a function of (a) channel length, and (b) diameter for various channel doping concentrations.

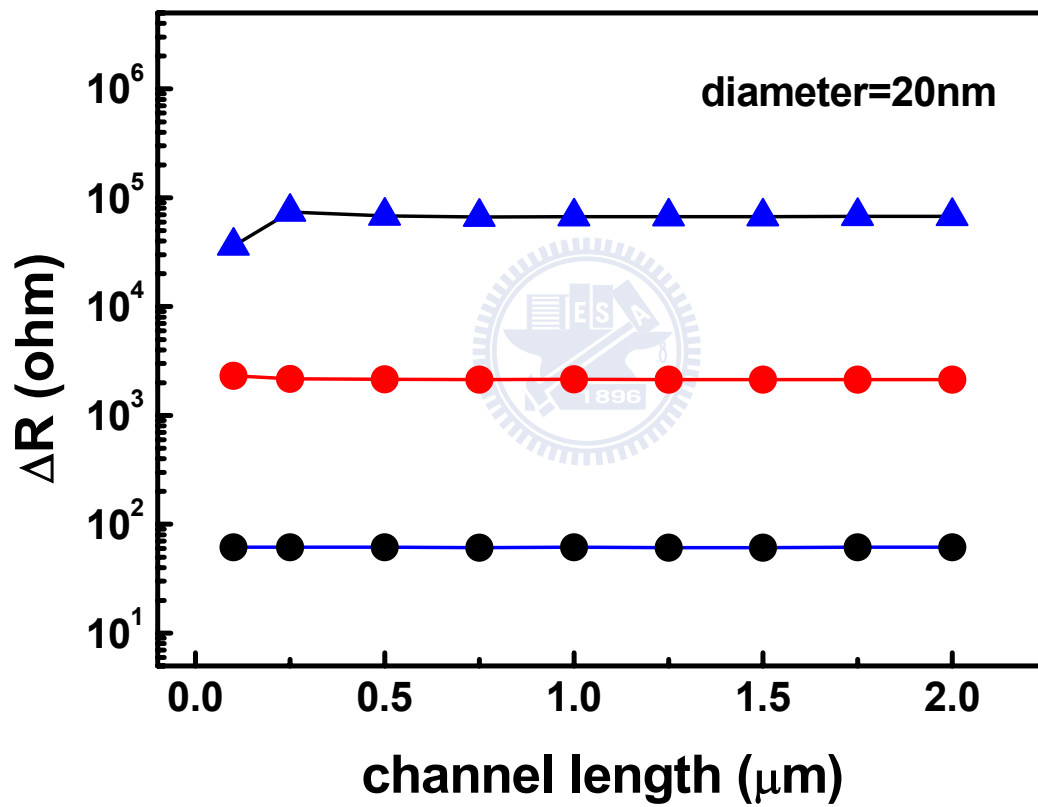


Fig. 2-6. In the Si-NW biosensors, the resistance change is insensitive to the channel length scaling.

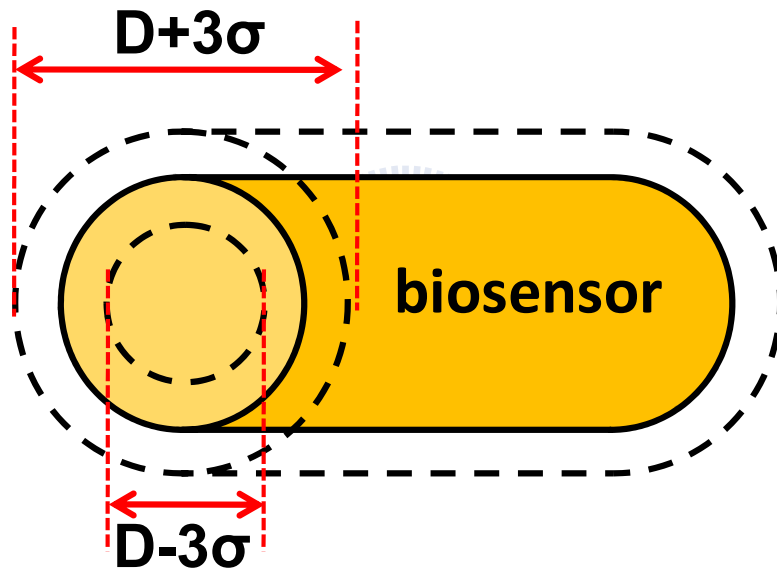


Fig. 2-7. Schematic sketch of a Si-NW biosensors with $\pm 3\sigma$ diameter variation.

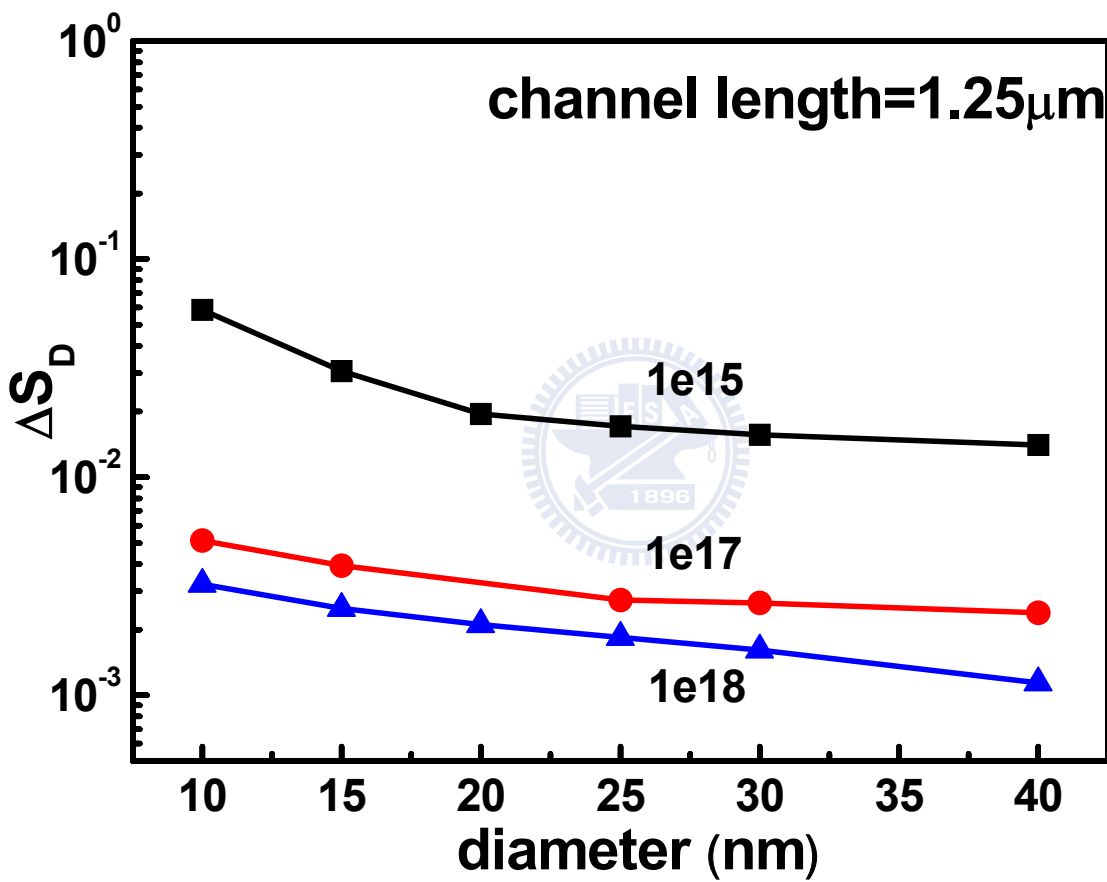


Fig. 2-8. Impact of diameter variation on the sensitivity of Si-NW biosensors for different channel doping concentrations.

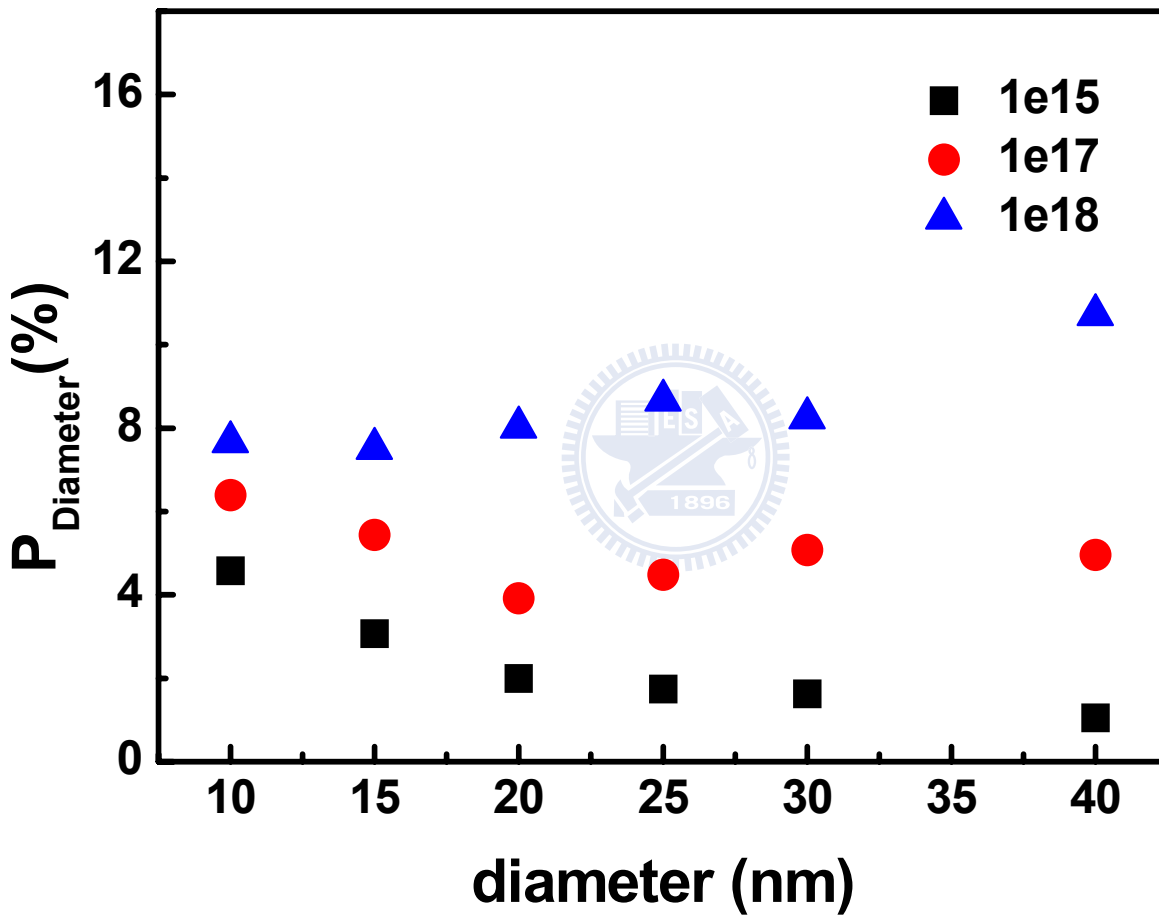
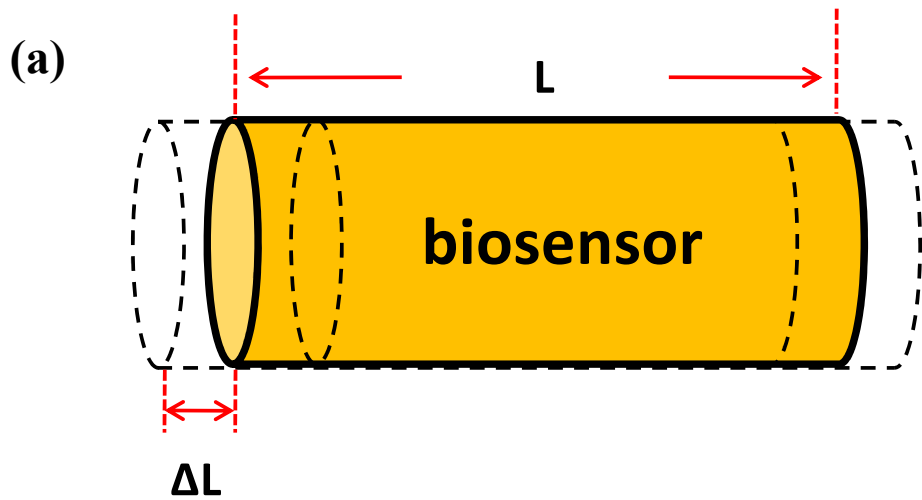


Fig. 2-9. The percentage change of the sensitivity variation for various diameters and channel doping.



channel length
variation

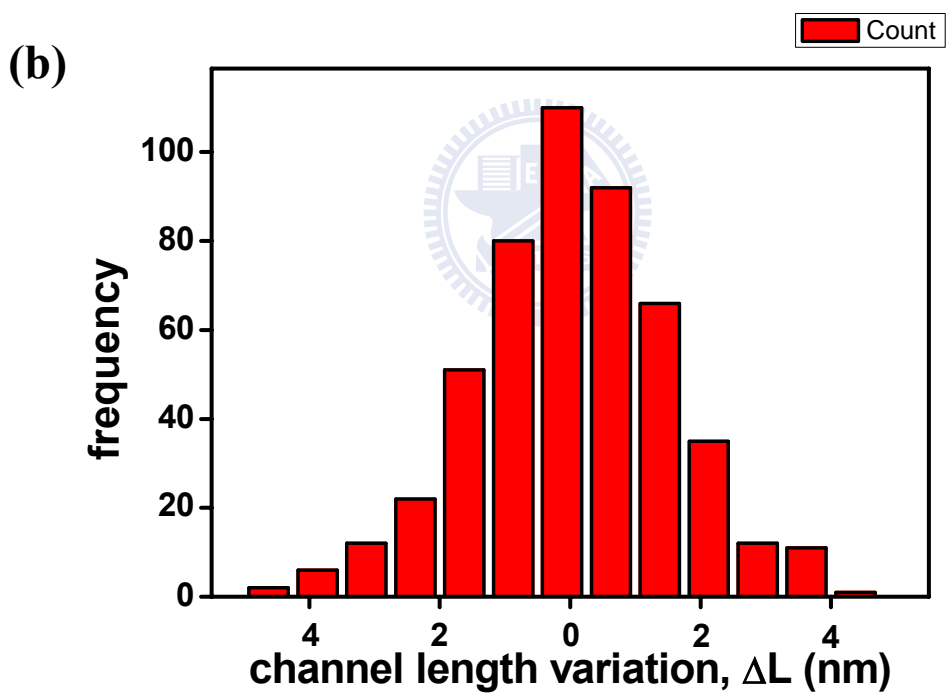


Fig. 2-10. (a) Schematic sketch of a Si-NW biosensors with channel length variation, ΔL . (b) Gaussian distribution of the channel length variation. The figure includes 500 ensembles.

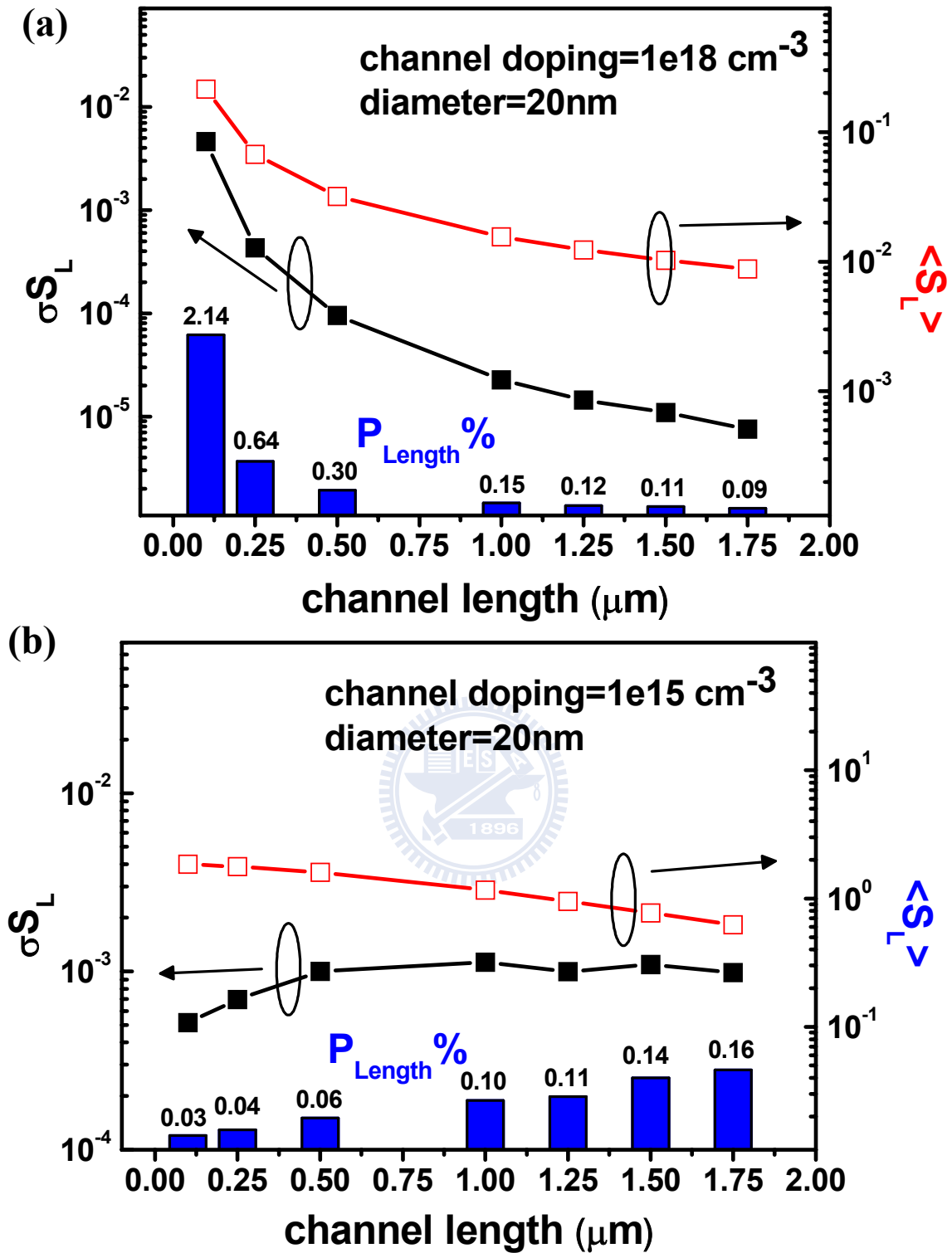


Fig. 2-11. Sensitivity variation in channel length for (a) heavily doped cases, and (b) lightly doped cases.

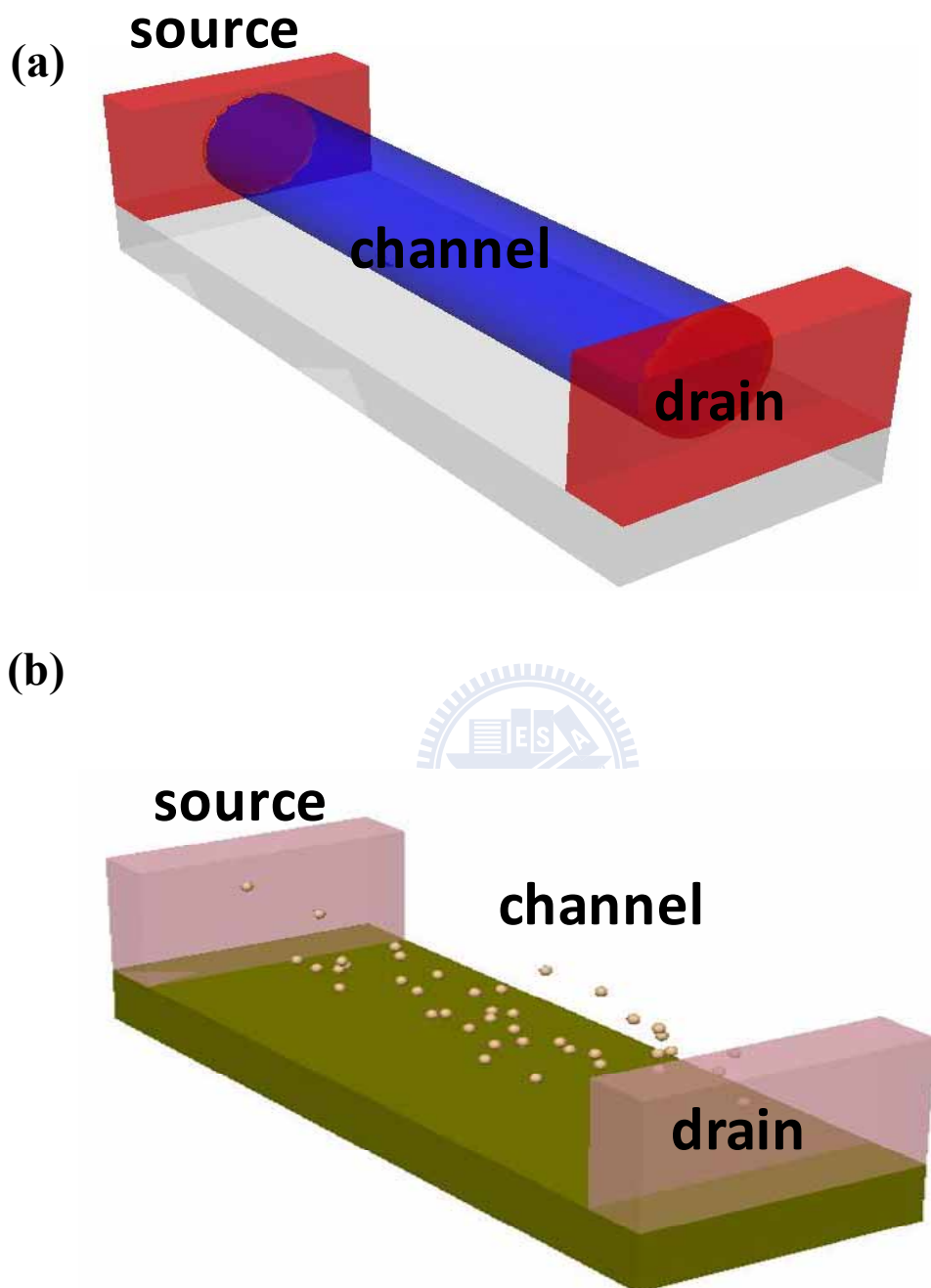


Fig. 2-12. Schematic sketch of a Si-NW device with (a) continuous doping, and (b) individually dopants distributed in the channel.

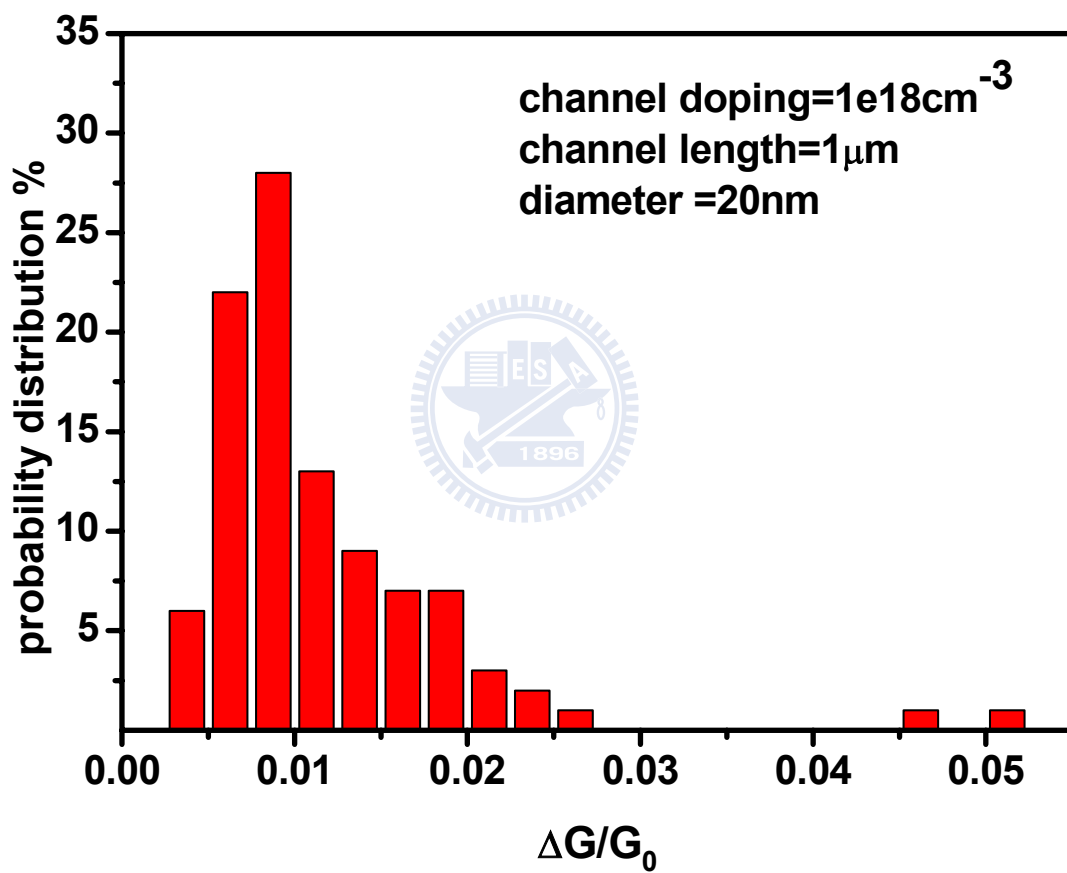


Fig. 2-13. Statistical fluctuations in sensitivity due to random dopant fluctuations.

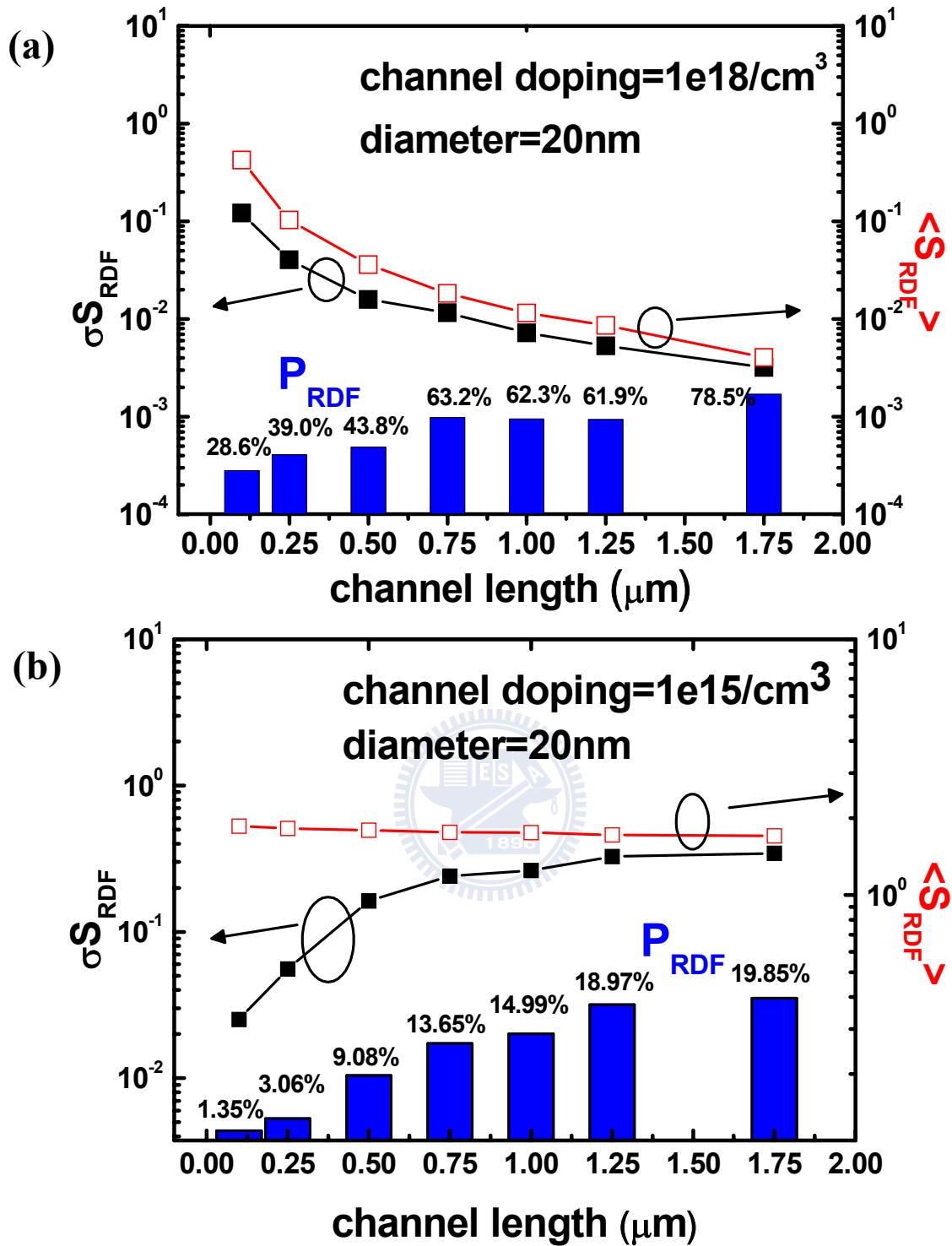


Fig. 2-14. Impact of the random dopant fluctuations for (a) heavily-doped, and (b) lightly-doped Si-NW biosensors for various channel length.

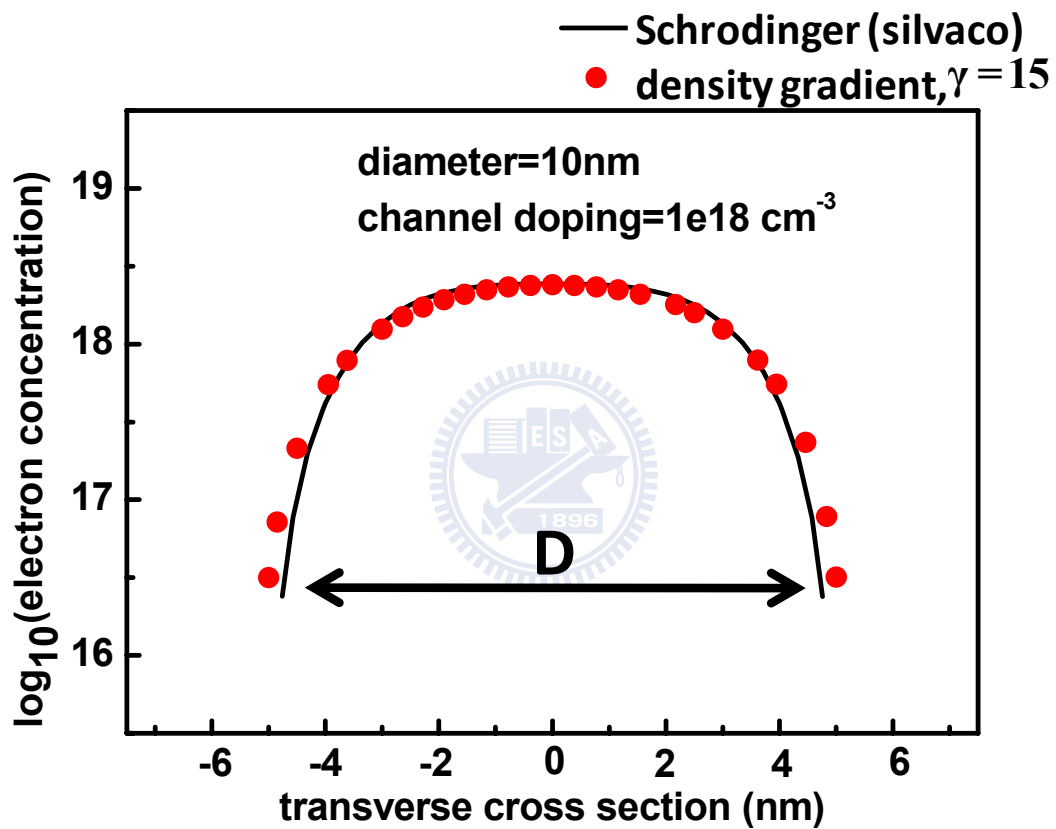


Fig. 2-15. When the density gradient parameter $\gamma=15$, the exact solution of coupled Poisson-Schrodinger equations can be captured well by our ISE simulation.

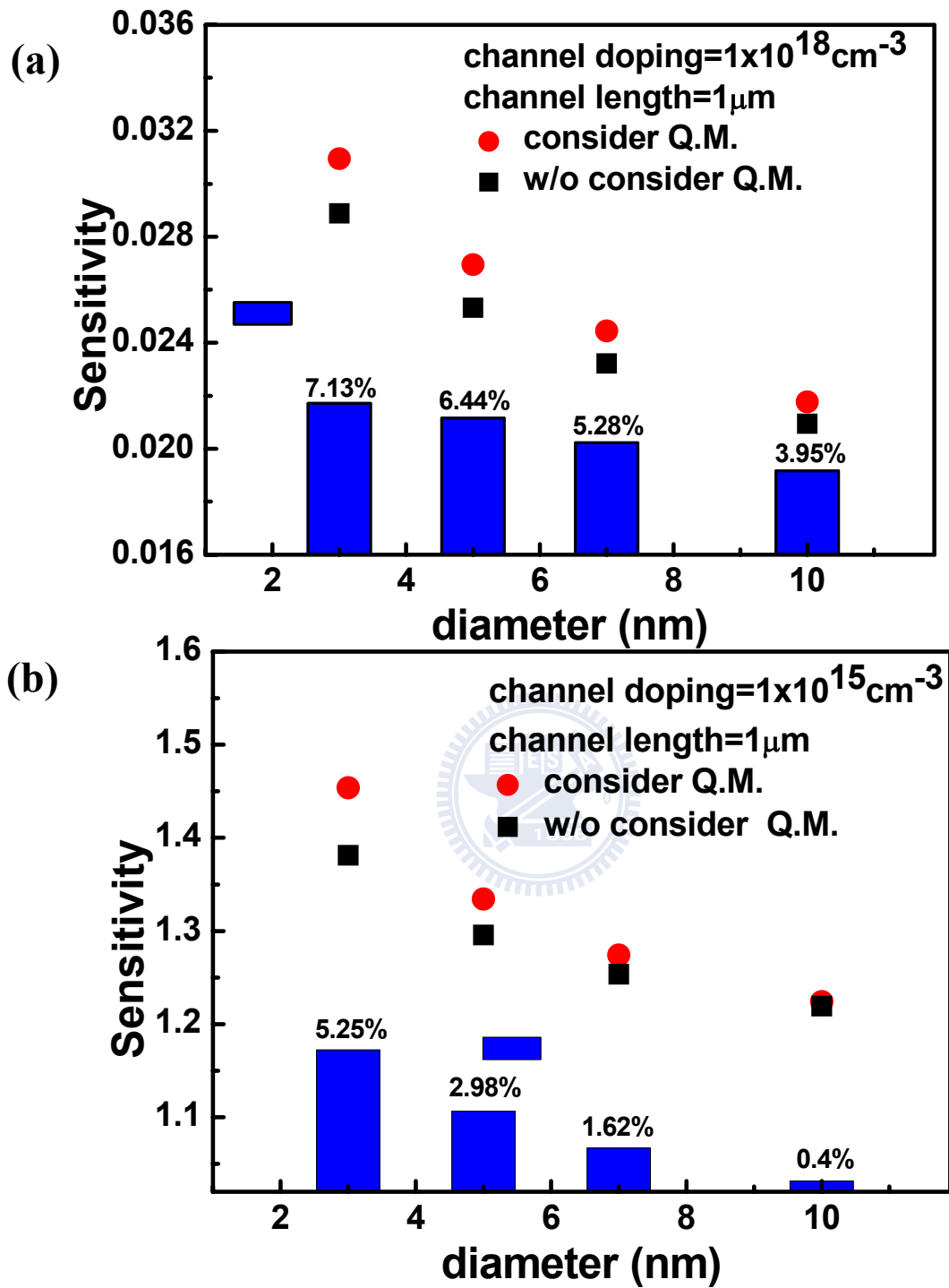


Fig. 2-16. Impact of quantum effects on (a) heavily-doped, and (b) lightly-doped Si-NW biosensors

Chapter3

Investigation of Si-NW Biosensors with Electro-Diffusion Flow

3-1 Introduction

In recent years, biosensor based on silicon nanowire (Si-NW) is one of the widely research topics in bio-technology, and it has been demonstrated to serve as a highly sensitive label-free sensor for charged biological molecules, such as DNAs and proteins [3.1]-[3.3]. The biomolecules in the electrolyte diffuse to the surface of Si-NW and get captured by the receptors in the oxide layer surface. And then, the conductivity of the Si-NW is modulated by the Coulomb interaction between the biomolecules in electrolyte solution and carriers in semiconductor. Therefore how to increase the Coulomb interaction and suppress the screening effect due to the ions around the charged biomolecules is a crucial issue. In 2008 IEDM, the research group at Stanford [3.4] has proposed a method using the electro-diffusion flow to overcome the screening-induced performance limits of Si-NW biosensors. This method has significantly improved the Si-NW signal strength and pointed out a new direction to design the Si-NW biosensor.

However, the Stanford's research only considers the performance of Si-NW biosensors operating in different electrolyte concentrations. The impacts of other design parameters, such as diameter and channel doping concentration, are short of discussion. Although it is generally accepted that the doping density determines the

sensitivity of Si-NW biosensors, not the doping type (n- or p-type) [3.5]-[3.6], whether it applies for Si-NW biosensors with electro-diffusion current flow remains unclear. Furthermore, in the past decade, the biosensors have been progressively miniaturized for the better performance [3.6]. With the device scaling, the quantum mechanical effects may play an important role in determining the performance of Si-NW biosensors. However, the impacts of quantum effects on the nanowire biosensors have rarely been investigated.

Therefore, in this chapter, we investigate the impacts of various design parameters and quantum effects on SI-NW biosensors. In Section 3-2, we develop a simulation flow considering the screening effect, and investigate the suppression of the screening effect by introducing electro-diffusion current flow in the electrolyte solution. In Section 3-3, we present our results for Si-NW biosensors operating in both accumulation mode and depletion mode with various channel diameters, channel doping concentrations, and ion concentrations in the electrolyte solution. Section 3-4 gives the details of quantum effects for small-diameter Si-NW biosensors with solution bias. In Section 3-5, we discuss and summarize the sensitivity of Si-NW biosensors associated with the design parameters.

3-2 Simulation Approach and Calibration

3-2.1 Equivalent Circuit Model

Fig. 3-1(a) is the proposed biomolecules detecting system [3.4] which consists of a Si-NW and two biased electrodes. The two biased electrode can generate the

electrical field and the mobile ions around the biomolecule is moved. The behavior of screening effect changed by the solution bias can be further illustrated as the Fig. 3-2. In the case (a): a biosensor without using solution bias (Fig. 3-2(a)). We assume there is a biomolecule with negative charge $-Q$ in serum which is effectively shielded by counter-ions and it is captured by a 2nm receptor. According to the Debye-Huckel theory, the Debye length is 0.7nm for 180mM ion concentration [3.7] that is very close the concentration of serum. It dictates that the negative charge $-Q$ cannot be detected when the detecting distance, from oxide surface to the biological charge (2nm), is beyond the Debye length (0.7nm).

We can use an equivalent circuit model to illustrate the behavior of screening effect with and without biased electrodes in Fig. 3-2(a) and Fig. 3-2(b), respectively. Where C_{SC} is a various capacitance of screening effect in the electrolyte solution and the C_{Si} is a capacitance in the silicon. The total image charge Q_{TOTAL} equals to the induced charge Q_{Si} in the silicon plus the induced charge Q_{SC} in the electrolyte solution and Q_{SC} are determined by the screening capacitance C_{SC} . In the case (b): a biosensor with solution bias (Fig. 3-1(b)). When the electro-diffusion flow diminishes the accumulated ions in the vicinity of biomolecules, the Debye length is no longer limited by the screening effect and the screening capacitance C_{SC} is dramatically reduced, which leads to the increase of Q_{Si} in silicon.

3-2.2 Simulation Approach

The system of a Si-NW biosensor with solution bias can be divided into two sub-regions, as shown in Fig. 3-1(b) and Fig. 3-1(c). The first region, A, is the electrolyte solution that contains target biomolecules and counter-ions around the

charged biomolecules. The second region, B, is Si-NW and oxide. In the following paragraph, we sequentially discuss the physical models for the two regions.

- 1) Region A: the ion transport in the electrolyte solution is modeled by the Poisson-Nearst-Plank (PNP) equations [3.8].

$$-\nabla \times (\boldsymbol{\varepsilon}_\omega \nabla \Phi) = q(C_+ - C_-), \quad (3-1)$$

$$\nabla \cdot (qD_+ \nabla C_+ + \mu_+ qC_+ \nabla \Phi) = 0, \quad (3-2)$$

$$\nabla \cdot (qD_- \nabla C_- - \mu_- qC_- \nabla \Phi) = 0, \quad (3-3)$$

where the subscripts +/- are corresponding to cation/anion, ε_ω is the dielectric constant in water, q is the elementary charge, C is the ion concentration, μ is the mobility, and Φ is the electrostatic potential. This continuum modeling approach has been firmly established in describing the transport of mobile ions in bulk condition [3.9]. It can be broadly applied to simulate ion transport in open ion channel when the pore radius is over two times of Debye length [3.10].

- 2) Region B: the carrier transport and the potential in Si-NW are modeled by the drift-diffusion equation and Poisson's equation.

$$J_{e,h} = q\mu_{e,h}n_{e,h}\nabla\Phi \pm qD_{e,h}\nabla n_{e,h}, \quad (3-4)$$

$$-\nabla \cdot (\boldsymbol{\varepsilon}_{Si} \nabla \Phi) = q(n_h - n_e + N_{dop}), \quad (3-5)$$

where J is the current density, q is the elementary charge, μ is the mobility, n is the carrier density, D is the diffusion coefficient, and N_{dop} is the net impurity concentration. Φ is the electrostatic potential which is determined by the potential applied at the electrodes. The subscripts "e,h" are corresponding to

electron / hole, respectively. We assume the dopants in silicon are completely ionized.

Equation (3-1)-(3-5) are the physical models for the Si-NW biosensor with solution bias. We separate the numerical method into following five main steps to solve the above equations.

In the first step: The PNP equation is solved self-consistently by a numerical solver, COMSOL physical simulation tool [3.11] in region A. We can categorize the numerical results, including the ion concentration and ionic flux, to build a parameter table “ P_{COMSOL} ”.

In the second step: We use the semiconductor simulation tool, ISE [3.12], to connect the “silicon region” and “electrolyte solution region”. Since the ISE simulation tool does not support the material of electrolyte solution, we have to create a new material $M_{\text{electrolyte solution}}$ to represent the electrolyte solution in the ISE simulation tool. The default parameter settings of $M_{\text{electrolyte solution}}$ is replaced by the parameter table “ P_{COMSOL} ”.

In the third step: We use the ISE simulation tool to solve those self-consistently coupled Equations (3-1)-(3-5), and the sensitivity of Si-NW biosensors can be calculated under specified operating bias.

In the fourth step: Vary the design parameters in the first, second, and third steps, sequentially. We collect and categorize the simulation results to build the sensitivity table for different design parameters.

In the fifth step: We investigate and analyze the sensitivity for various design parameters and systematically optimize the design parameters of Si-NW biosensors.

In summary, a scheme for the simulation procedure of Si-NW biosensors with the solution bias is shown in the Fig. 3-3.

3-2.3 Calibration

To confirm that our biosensors simulation results are robust and reliable, we demonstrate the behavior of “the induced charge Q' over the Q_{dop} ” ratio¹ in the Si-NW biosensor (in this case, the biosensor without binding any biomolecules) with varied solution bias from 0V to 3V. The induced charge Q' is defined as the integration of induced charge over the channel and the Q_{dop} is defined as the integration of channel doping concentration over the channel. Compared with the Stanford simulation results is shown in Fig. 3-4, we show our simulation results agree well with Stanford simulation results and the ratio of the induced charge Q' to Q_{dop} increases with the solution bias because electric field in the electrolyte solution increases with solution bias and induces more charge in the biosensor.

We demonstrate the potential change with and without applying solution bias in Fig. 3-5(a) and Fig. 3-5(b). At 0V, the screening effect severely limits the potential change within the Debye length. At 1V, the screening effect is suppressed by the electro-diffusion flow. Therefore, the potential change spreads over a much broader space and penetrates more into the Si-NW.

1. For convenient, “the induced charge Q' over the Q_{dop} ” ratio is abbreviated to $R_{Q'/Q_{\text{dop}}}$ in this chapter.

3-3 Sensitivity of Si-NW Biosensors Operating in the Accumulation Mode and Depletion Mode

In this section, we use our established simulation flow (Fig. 3-3) to investigate the sensitivity of Si-NW biosensors with solution bias in two operating modes: accumulation mode and depletion mode as shown in Fig. 3-6(a) and Fig. 3-6(b), respectively. The accumulation mode means that as the target biomolecule has opposite charge with the carriers in silicon and the carriers are attracted to accumulate in the oxide/silicon interface because of Coulomb force. The depletion mode is contrary to the accumulation mode.

The structure used for simulation is a 10 nm long Si-NW segment shown in Fig. 3-7(a). We assume that there is a DNA on the surface of Si-NW approximated by a small impermeable rod with the backbone charge uniformly distributed for simplicity and the electron concentration assigned for dsDNA / ssDNA are $2e/nm^3/4e/nm^3$ [3.13], respectively. The distance between two side electrodes is 100nm. The general scheme for the design parameters is shown in Fig. 3-7(b). In the following paragraph, we sequentially discuss the sensitivity in the accumulation mode and depletion mode for various design parameters.

3-3.1 Accumulation Mode

In Fig. 3-8 (a) and 3-8 (b), the induced charge Q' is plotted for different solution biases and ion concentrations. At low bias, the screening effect limits the potential change within the Debye length so the induced charge Q' in Si-NW is very small.

However, with increasing solution bias, the Si-NW biosensor without being screening-limited generate more induced charge Q' in the channel. In Fig 3-8(a), we can see that the induced charge Q' (dsDNA) has a significant enhancement more than 20X (the $R_{Q'/Q_{dop}}$ of dsDNA is from ~ 0.5 to ~ 10.3) when the solution bias is from 0V to 3V. Furthermore to examine the two different ion concentrations (Fig. 3-8(a) and Fig. 3-8(b)), the induced charge Q' (dsDNA) has an enhancement of $\sim 11X/\sim 9X$ (at the solution bias=3V) compared to the Q_{dop} in 20mM/100mM, respectively. It indicates that the Si-NW biosensor at lower ion concentrations has more improvement of performance.

In Fig. 3-8(a) and Fig. 3-8(b), the induced charge Q' is proportional to the solution bias, no matter for 20mM or 100mM electrolyte solution. Increasing the solution bias seems to enhance the performance of Si-NW biosensors. However, the question is “Does the performance of Si-NW biosensors always increase at higher solution bias?”. To answer the question, we introduce a criterion to evaluate the performance. The Sensitivity, S , of a Si-NW biosensor is defined as the relative change in charge quantity.

$$\text{Sensitivity (S)} = \frac{\Delta Q}{Q_{\text{initial}}} = \frac{Q_{\text{with_bio}} - Q_{\text{initial}}}{Q_{\text{initial}}} \quad (3-6)$$

where $Q_{\text{with_bio}}/Q_{\text{initial}}$ is the integration of total charge over the Si segment with/without the detection of bio-molecules. ΔQ is the difference between $Q_{\text{with_bio}}$ and Q_{initial} .

Fig. 3-9(a) and Fig. 3-9(b) show the sensitivity of a Si-NW biosensor for different ion concentrations. We can see the sensitivity at lower bias increases with the

solution bias, but at higher bias the sensitivity decreases with the solution bias. The different behaviors of sensitivity at lower/higher bias show two competing electrostatic fields, $E_{\text{biomolecula}}$ and $E_{\text{solution_bias}}$, in the biosensor. The $Q_{\text{with_bio}}$ can be separate into two partitions, as below:

$$Q_{\text{with_bio}} = Q_{E_bio} + Q_{E_sbias} \quad (3-7)$$

,where Q_{E_bio}/Q_{E_sbias} means the charge in biosensors is induced by the electrostatic field $E_{\text{biomolecula}}/E_{\text{solution_bias}}$. Based on the separated $Q_{\text{with_bio}}$, the Sensitivity, S , can be further simplified, as below:

$$S = \frac{Q_{\text{with_bio}} - Q_{\text{initial}}}{Q_{\text{initial}}} = \frac{Q_{E_bio} + Q_{E_sbias} - Q_{\text{initial}}}{Q_{\text{initial}}} \approx \frac{Q_{E_bio}}{Q_{E_sbias}} \quad (3-8)$$

At lower solution bias, the screening effect is diminished by electro-diffusion flow which makes the $E_{\text{biomolecula}}$ dramatically rise. Therefore, Q_{E_bio} increases faster than Q_{E_sbias} . The sensitivity increases with solution bias. However at higher solution bias, $E_{\text{solution_bias}}$ is the major component of electrostatic field which rapidly increases with solution bias and induces more Q_{E_sbias} in Si-NW. Hence, the sensitivity degrades at higher solution bias. The above analysis indicates that we can obtain a largest sensitivity, through an optimized solution bias. In our simulation case, the optimized solution bias is about 1V~1.5V.

Fig. 3-10 shows the sensitivity of a Si-NW biosensor for various diameters. With the smaller diameter, the sensitivity has a significant improvement because of the increased surface to volume ratio.

Fig. 3-11 shows that the sensitivity increases with decreasing channel doping

concentrations due to the decreased Q_{initial} in silicon channel.

3-3.2 Depletion Mode

Fig. 3-12(a) and Fig. 3-12(b) show the induced charge Q' increases rapidly with the solution bias and has an enhancement of $\sim 3.5X/\sim 3X$ compared to the Q_{dop} in 20mM/100mM (at solution bias=3V), respectively. Obviously, the Si-NW biosensor operating in the light electrolyte concentrations has more improvement of performance.

According to the equation (3-6), a general scheme for the sensitivity of a Si-NW biosensor can be derived from the Fig. 3-12(a) / Fig. 3-12(b) which is shown in Fig. 3-13(a) / Fig 3-13(b), respectively. For the same reasons, we must adjust the solution bias to obtain the largest sensitivity and the optimal range of solution bias is about 1V \sim 1.5V. The corresponding largest sensitivity for dsDNA/ssDNA are 0.95/0.92 in the 20mM electrolyte concentration and 0.86/0.77 in the 100mM electrolyte concentration.

Fig. 3-14 shows that the sensitivity of a Si-NW biosensor increases with decreasing diameter because of the increased “surface to volume ratio”. In our simulation case, it notes the sensitivity of Si-NW biosensors operating in depletion mode cannot beyond 1. This is because the quantity of depleted charge in the Si-NW is always smaller than originally existent charge.

Fig. 3-15 shows the sensitivity does not increase with reduced channel doping concentration because the sensitivity has saturated. Where the sensitivity saturation

means the quantity of depleted charge is very close with the originally existent charge, it cannot be improved anymore and its value is near 1.

3-4 Quantum Mechanical Effects on Small-Diameter Si-NW Biosensors

The sensitivity of a Si-NW biosensor increases with the diameter, no matter in the accumulation mode or depletion mode. However, when the diameter is within ~10 nm, the quantum mechanical effects need to be considered. In our simulation, we use the density gradient model [3.14]-[3.15] to approximate the quantum effect. The density gradient function is a partial differential function with a parameter γ . In earlier chapter 2-4, we have demonstrated that when the parameter γ is 15, the density gradient model agrees with the exact Poisson-Schrodinger solution well.

Fig. 3-16 shows that with the diameter scaling from 10nm to 7 nm, the sensitivity of Si-NW biosensors without considering the quantum effect has a ~2.5X (dsDNA) enhancement, because of the increased surface to volume ratio. When considering the quantum effect, the enhancement of sensitivity can reach ~3.7X (dsDNA). Compared with excluding the quantum effect, the sensitivity with considering the quantum effect has larger enhancement. We rewrite the definition of the sensitivity of Si-NW biosensors as:

$$\text{Sensitivity (S)} = \frac{\sigma}{qN_{\text{eff}}} \left(\frac{A}{d}\right), \quad (3-9)$$

where $\left(\frac{A}{d}\right)$ is the cylindrical surface of volume ratio, N_{eff} is the effective carrier

concentration, σ is a surface charge density for estimation of the charged biomolecules, q is the elementary charge. Without considering the quantum effect, the sensitivity increases reversely with the channel diameter. However, with considering the quantum effect, not only is the sensitivity determined by the surface to volume ratio, but the sensitivity is also determined by the effective carrier concentration. Therefore, considering the quantum effect has more enhancements in the sensitivity because of the limited effective doping concentration [3.16]-[3.17].

3-5 Summary

Our conclusions for this chapter are summarized as follows:

- (1) Our simulation flow of Si-NW biosensors with solution bias has been demonstrated.
- (2) The sensitivity of Si-NW biosensors with solution bias increases with the decreasing diameter and reducing ion concentrations.
- (3) The sensitivity in the depletion mode does not increase with decreasing channel doping because the sensitivity is saturated.
- (4) The Si-NW biosensor with solution bias operating in the accumulation mode can get more improvements of the sensitivity as compared with the depletion mode.
- (5) The sensitivity does not always increase with higher solution bias. We can obtain the largest sensitivity through an optimized solution bias.
- (6) The quantum effects on small-diameter can improve the sensitivity of Si-NW biosensors.

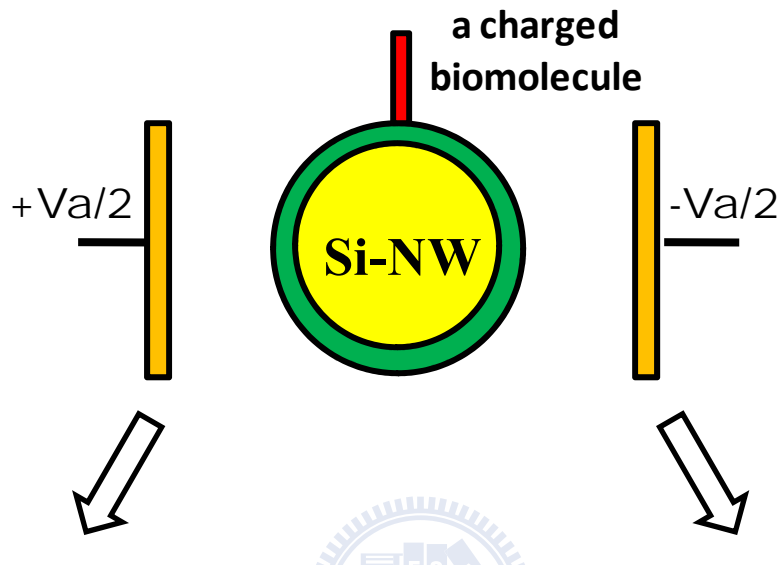
Chapter 3 References

- [3.1] G. Zheng, F. Patlowky, Y. Cui, W. U. Wang, and C. M. Lieber, "Multiplexed electrical detection of cancer markers with nanowire sensor arrays," *Nat. Biotechnol.*, vol. 23, no. 10, pp. 1294-1301, Oct. 2005.
- [3.2] J. Hahn and C. M. Lieber, "Direct ultrasensitive electrical detection of DNA and DNA sequence variations using nanowire nanosensors," *Nano. Lett.*, vol. 4, no. 1, pp. 51-55, 2004.
- [3.3] E. Stern, J. F. Klemic, D. A. Routenberg, P. N. Wyrembak, D. B. Turner-Evans, A. D. Hamilton, D. A. LaVan, T. M. Fahmy, and M. A. Reed, "Label-free immunodetection with CMOS compatible semiconducting nanowires," *Nature*, vol. 445, no. 7127, pp. 519-523, Feb. 2007.
- [3.4] Y. Liu, K. Lilja, C. Heitzinger, R. W. Dutton, "Overcoming the screening-induced performance limits of nanowire biosensors: a simulation study on the effect of electro-diffusion flow," in *IEDM Tech. Dig.*, pp. 491-494, 2008.
- [3.5] P. R. Nair, and M. A. Alam, "Design considerations of silicon nanowire biosensors," *IEEE Trans. Electron Devices*, vol. 54, no. 12, Dec. 2007.
- [3.6] M. Curreli, R. Zhang, F. N. Ishikawa, H.-K. Chang, R. J. Cote, C. Zhou, and M. E. Thompson, "Real-time, label-free detection of biological entities using nanowire-based FETs," *IEEE Trans. Nanotech.*, vol. 7, no. 6, Nov. 2008.
- [3.7] E. Stern, R. Wagner, F. J. Sigworth, R. Breaker, T. M. Fahmy, and M. A. Reed, "Importance of the Debye screening length on nanowire field effect transistor sensors," *Nano. Lett.*, vol. 7, pp. 3405-3409, 2007.
- [3.8] T. F. Weiss., *Cellular Biophysics* (MIT, Cambridge, MA, 1996), vol. 1.
- [3.9] B. Corry, S. Kuyucak, and S.-H. Chung, "Tests of Continuum Theories as Models of Ion Channels. II. Poisson-Nernst-Planck Theory versus Brownian Dynamics," *Biophys. J.*, vol. 78, Issue 5, May 2000.
- [3.10] B. Corry, S. Kuyucak, and S.-H. Chung, "Test of continuum theories as model of ion channels. . Poisson-Nernst-Planck theory versus Brownian Dynamics," *Biophys. J.* 78, 2364, 2000.
- [3.11] <http://www.femlab.com/products/multiphysics/>
- [3.12] <http://www.synopsys.com/TOOLS/TCAD/DEVICESIMULATION/Pages/SentaurusDevice.aspx>
- [3.13] Y. Liu, J. Sauer, and R. W. Dutton, "Effect of electrodiffusion current flow on electrostatic screening in aqueous pores," *J. Applied Physics.*, vol. 103, 2008.

- [3.14] M. G. Ancona and H. F. Tiersten, “Macroscopic physics of the silicon inversion layer,” *Phys. Rev. B*, vol. 35, no. 15, pp. 7959–7965, May, 1987.
- [3.15] M. G. Ancona and G. J. Iafrate, “Quantum correction to the equation of state of an electron gas in a semiconductor,” *Phys. Rev. B*, vol. 39, no. 13, pp. 9536–9540, May, 1989.
- [3.16] <http://www.silvaco.com/>
- [3.17] J. P. Colinge, J. C. Alderman, W. Xiong, and C. R. Cleavelin, “Quantum-mechanical effect in trigate SOI MOSFETs,” *IEEE Transactions on Electron Devices*, vol. 53, no. 5, MAY 2006.
- [3.18] S. Datta, *Quantum Transport: Atom to Transistor*, chapter 7.3, pp 170-176 (Cambridge University Press, New York, 2005).



(c) A Si-NW biosensor with two electrodes



(b) The electrolyte solution region

(a) The semiconductor region

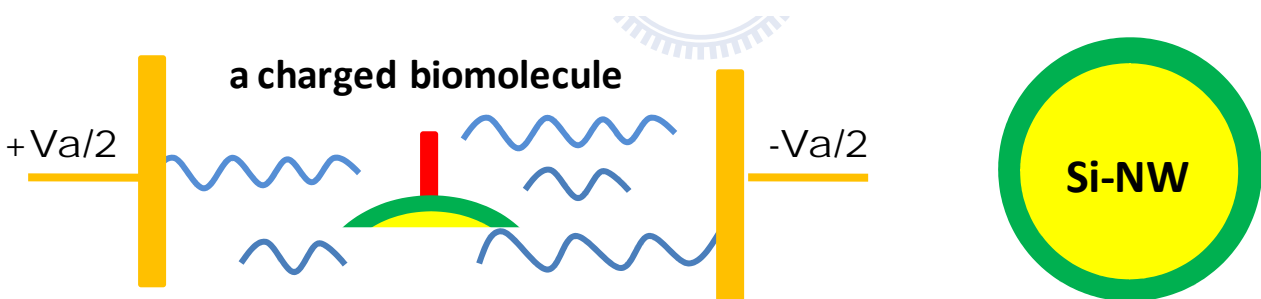
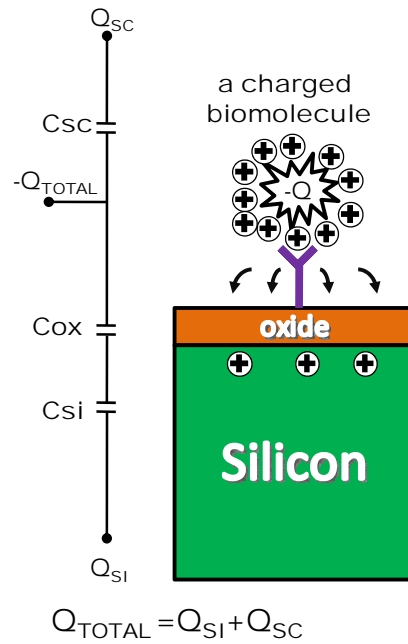


Fig. 3-1. (a) The proposed biomolecules detecting system [4], which can be separated to (b) the electrolyte solution region, and (c) the semiconductor region.

(a) Without solution bias



(b) With solution bias

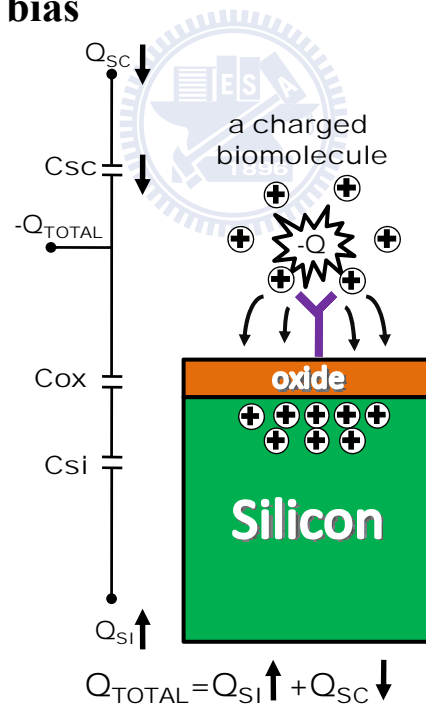


Fig. 3-2. The equivalent circuit models of two screening effect behaviors:
(a) Without solution bias, the biomolecule is shielded by the accumulated ions.
(b) With solution bias, the electro-current suppresses the screening effect of biomolecule, and increases the Q_{SI} in silicon.

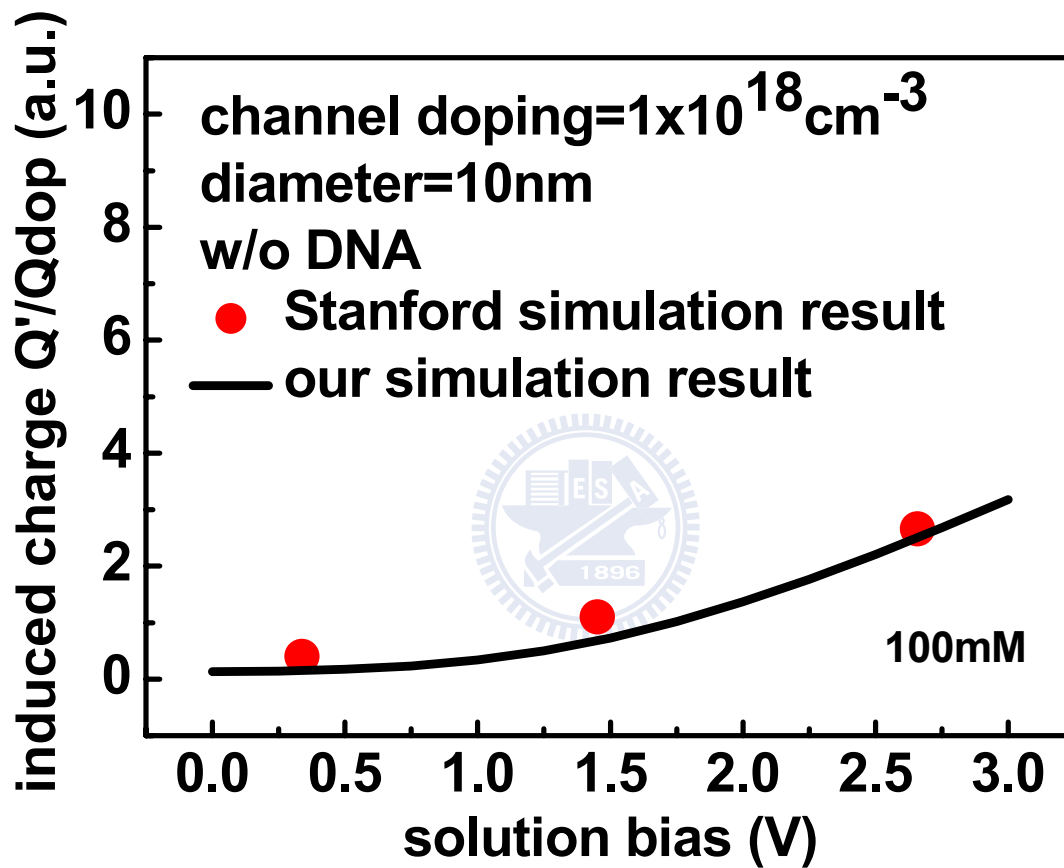


Fig. 3-4. Our simulation results agree well with the Stanford simulation results. The ratio of the induced charge Q' to Q_{dop} increases with the solution bias because the solution bias induces more charges in the biosensor.

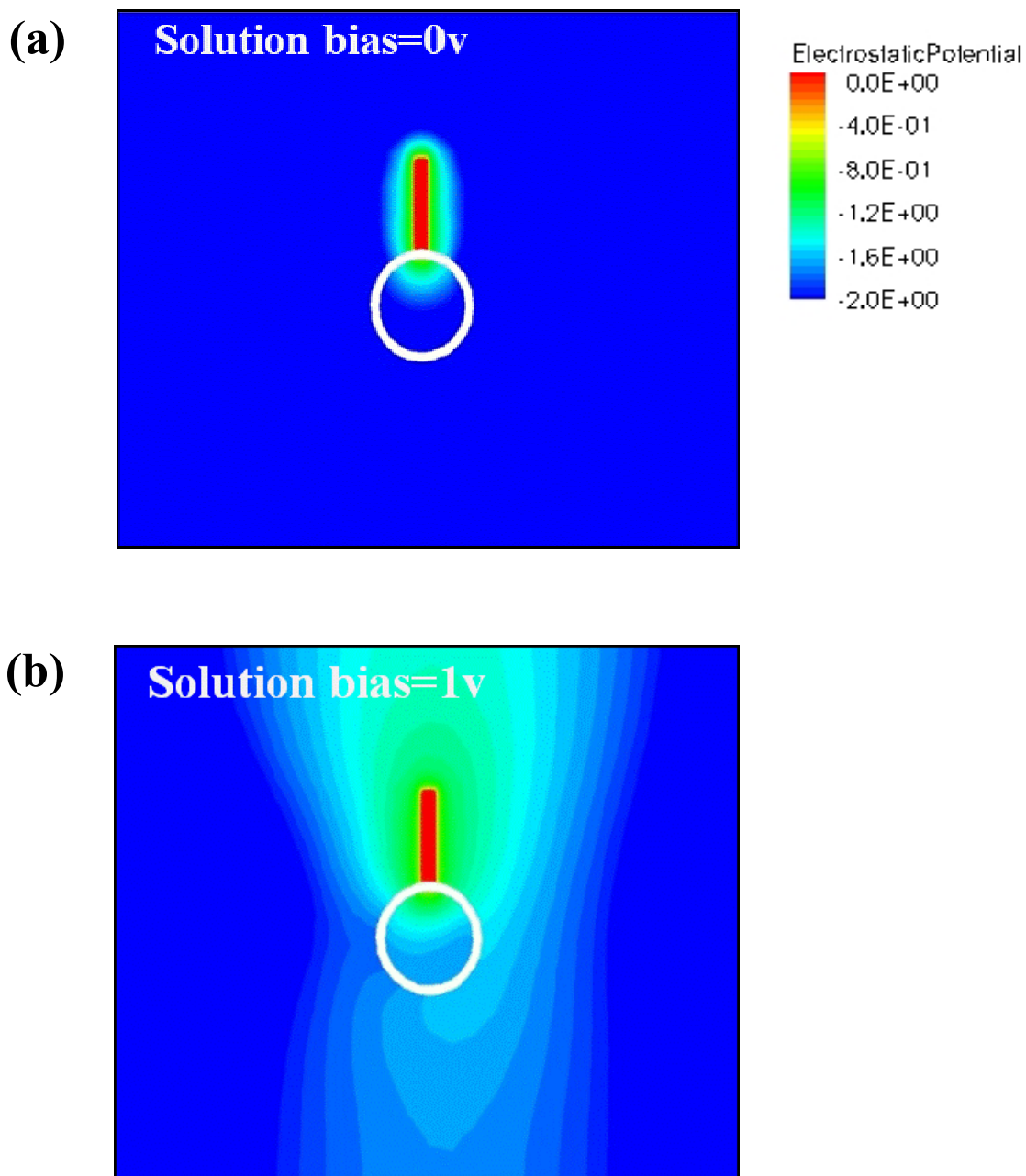
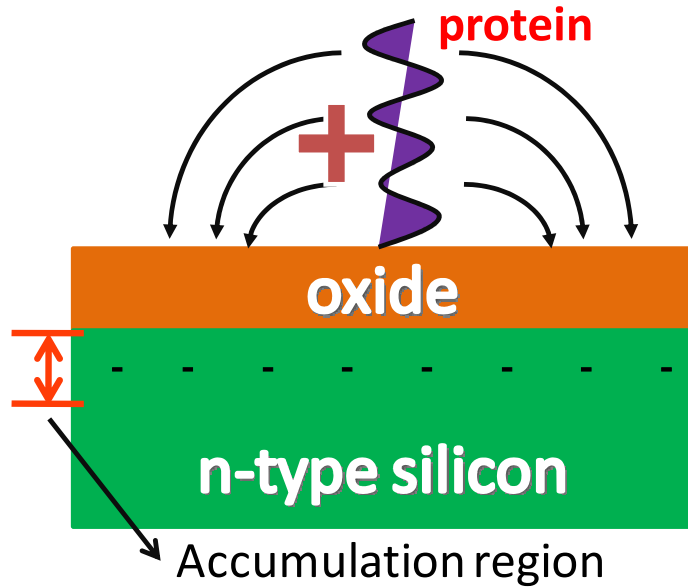


Fig. 3-5. The potential change is defined as $\log_{10}(\Delta\psi)$. (a) At solution bias=0V, the potential change is limited in the vicinity of biomolecule because of the serious screening effect. (b) At solution bias=1V, the screening effect is suppressed and the potential change spreads over a border space.

a) Accumulation Mode



b) Depletion Mode

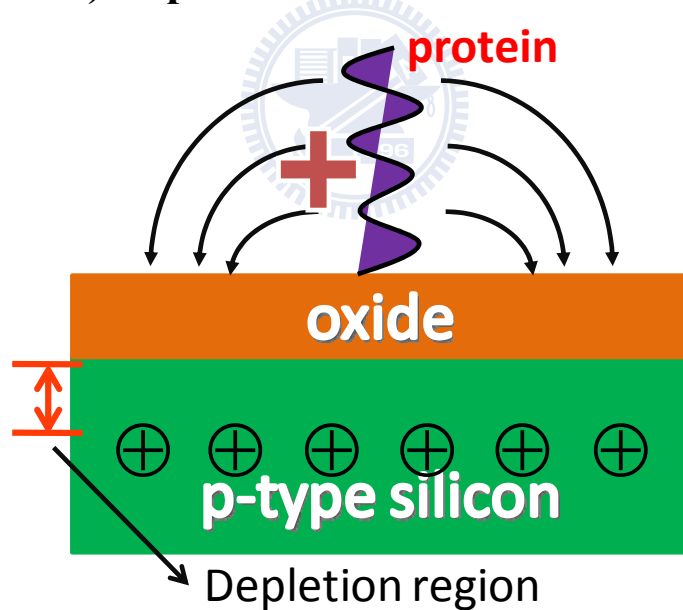
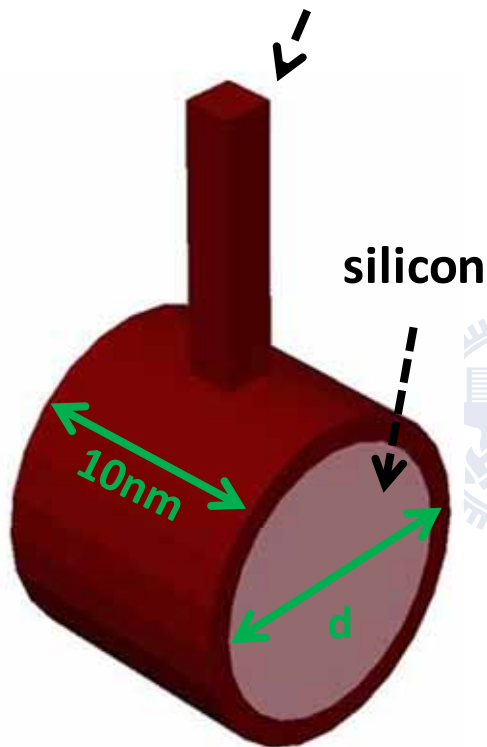


Fig. 3-6. Two operation modes of Si-NW biosensors: (a) the accumulation mode which means the biological charge is opposite to the charge of carriers in the silicon, and (b) the depletion mode that is contrary to the accumulation mode

(a)

ssDNA and dsDNA are approximated by a rod



(b)

Design parameters	unit
channel length	10 (nm)
diameter	d (nm)
channel doping concentration	N_{dop} (cm^{-3})
ion concentration	N_{ion} (mole/l)
the distance between two side electrodes	100 (nm)
solution bias	V_a (V)

Fig. 3-7. (a) Schematic structure of a Si-NW with an approximated rod for ds DNA & ss DNA. (b) The device design parameters for our Si-NW biosensor simulations.

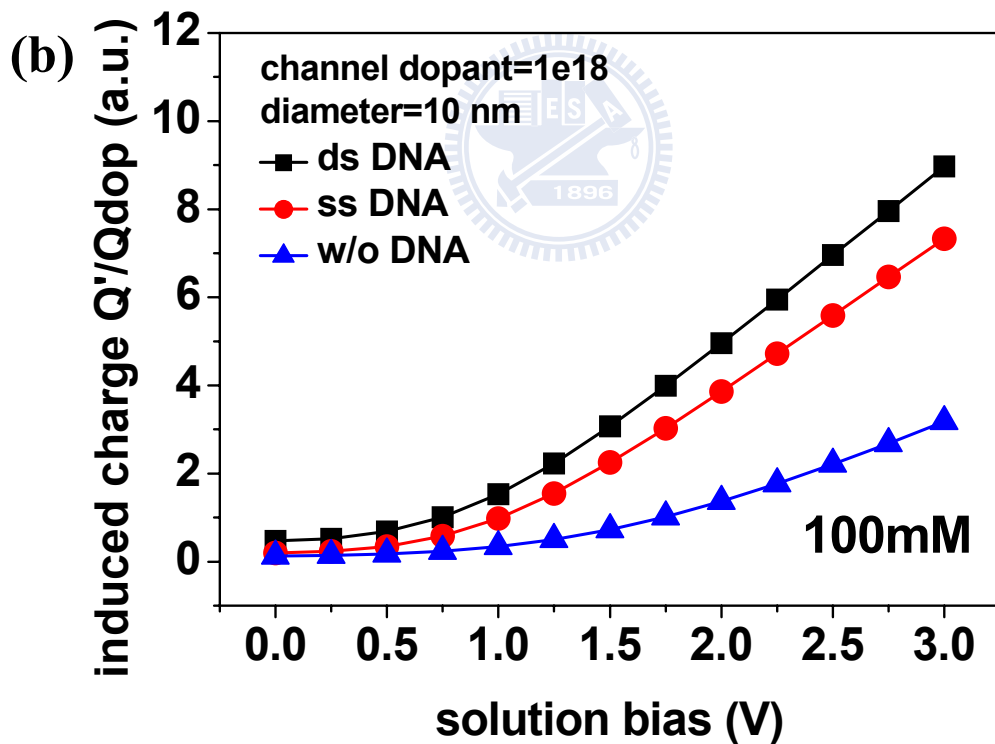
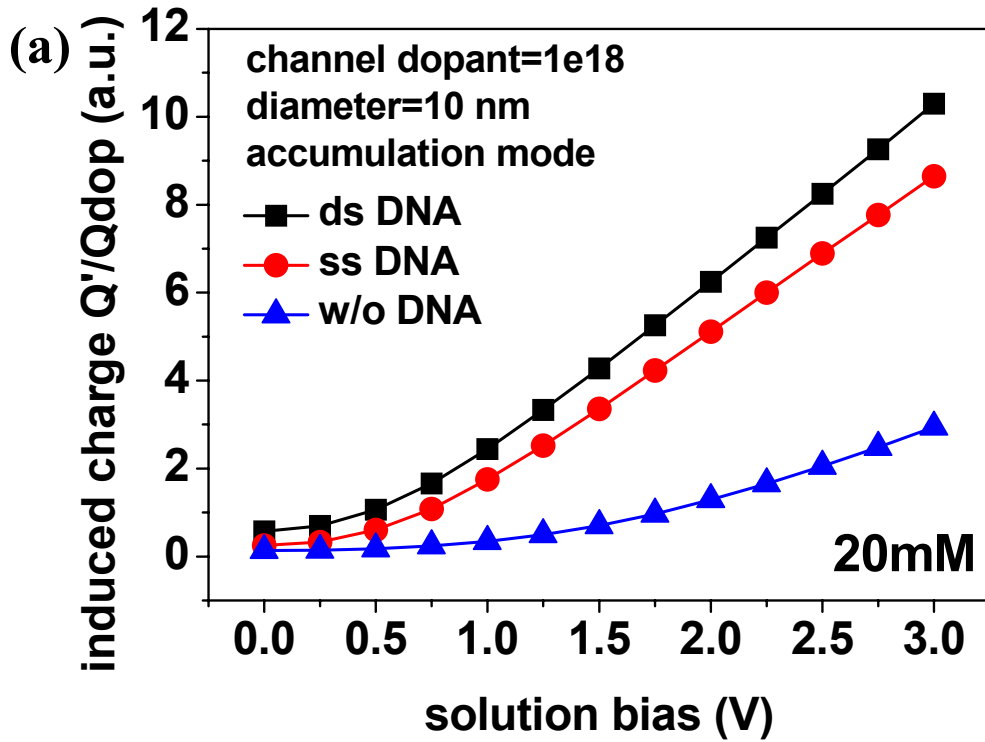


Fig. 3-8. With increasing the solution bias, the Si-NW biosensor has more induced charge Q' in the channel. Comparing (a) and (b), we can find that the $R_{Q'/Q_{dop}}$ for 20mM solution is larger than the $R_{Q'/Q_{dop}}$ for 100mM solution.

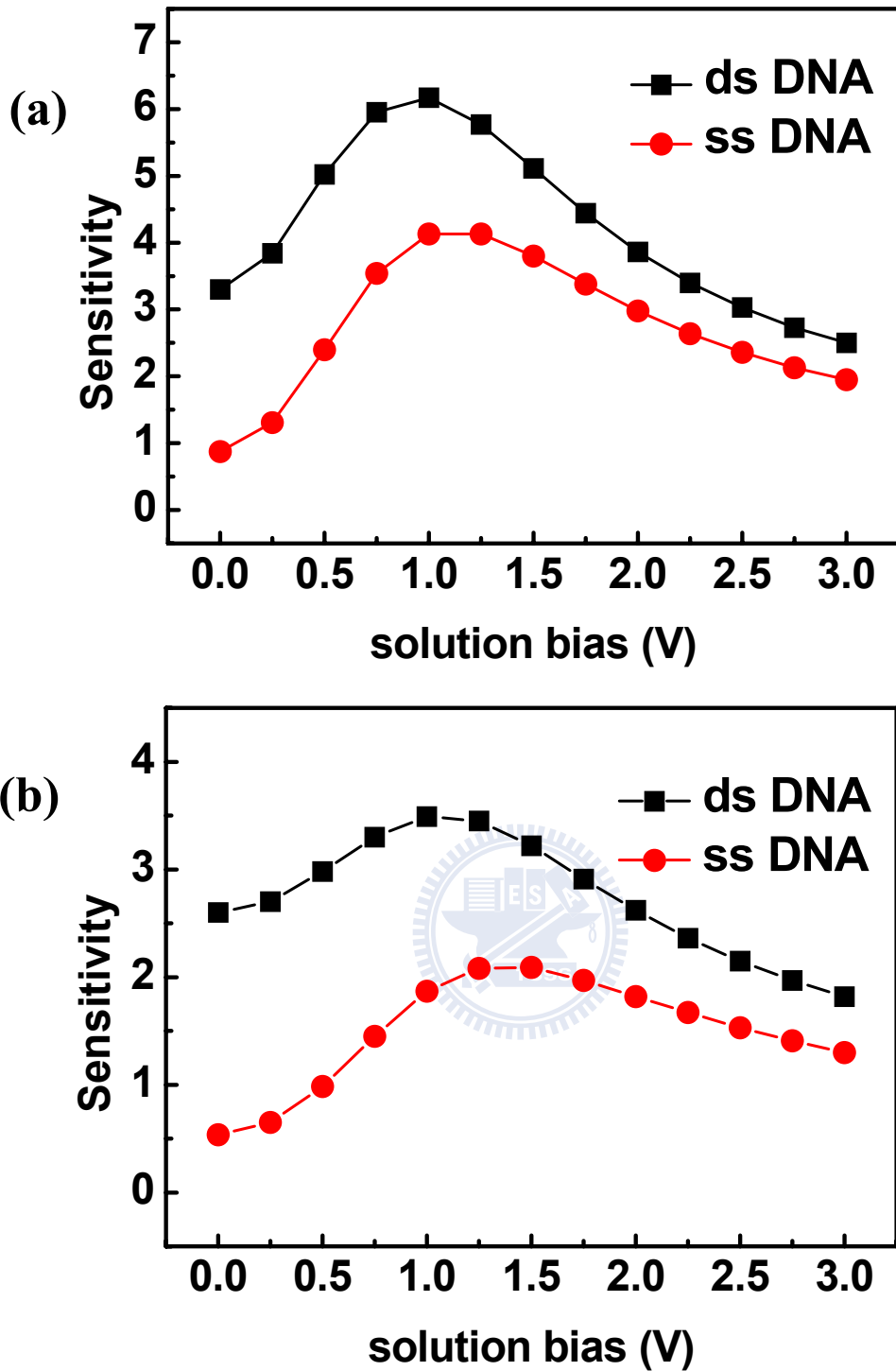


Fig. 3-9. In the accumulation mode, the sensitivity has the largest value through an optimized solution bias. (a) For 20mM, the largest sensitivity of dsDNA and ssDNA are ~6.1 and ~4.3, respectively. (b) For 100mM, the corresponding values are ~3.5 and ~2.1. The biosensor operating in the light electrolyte concentration has larger sensitivity compared to in the heavy electrolyte concentration.

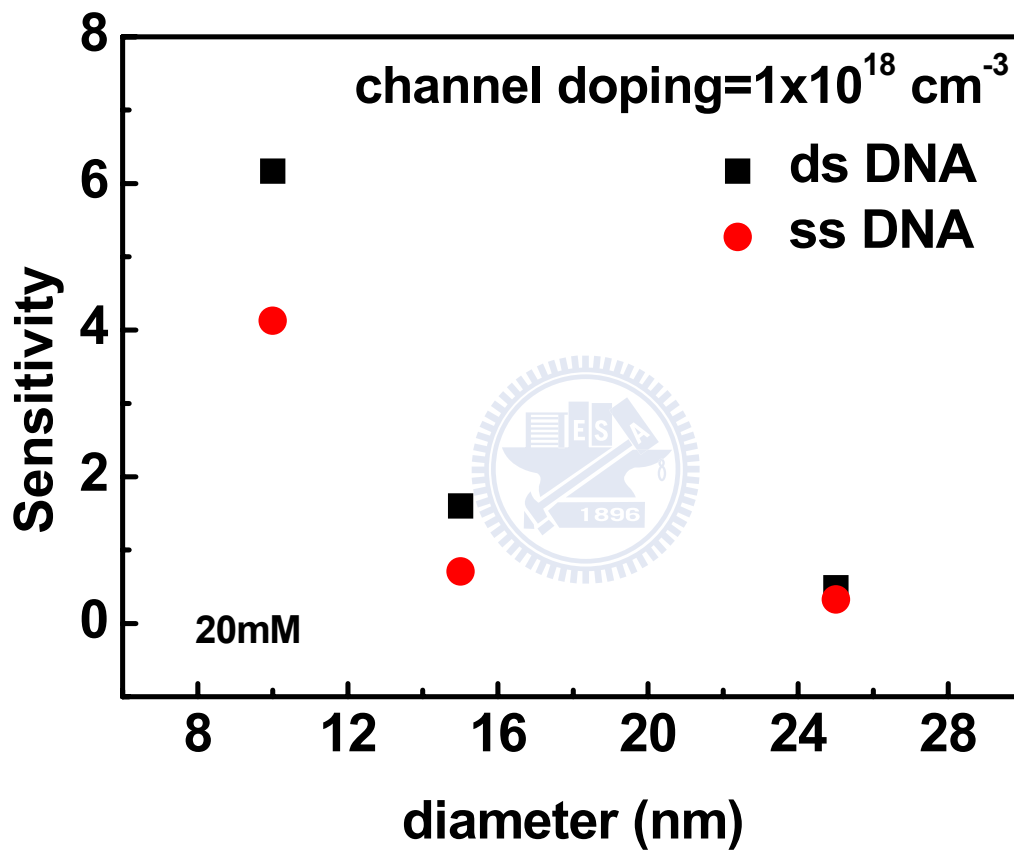


Fig. 3-10. In the accumulation mode, the sensitivity increases with decreasing channel diameter of the nanowire biosensor.

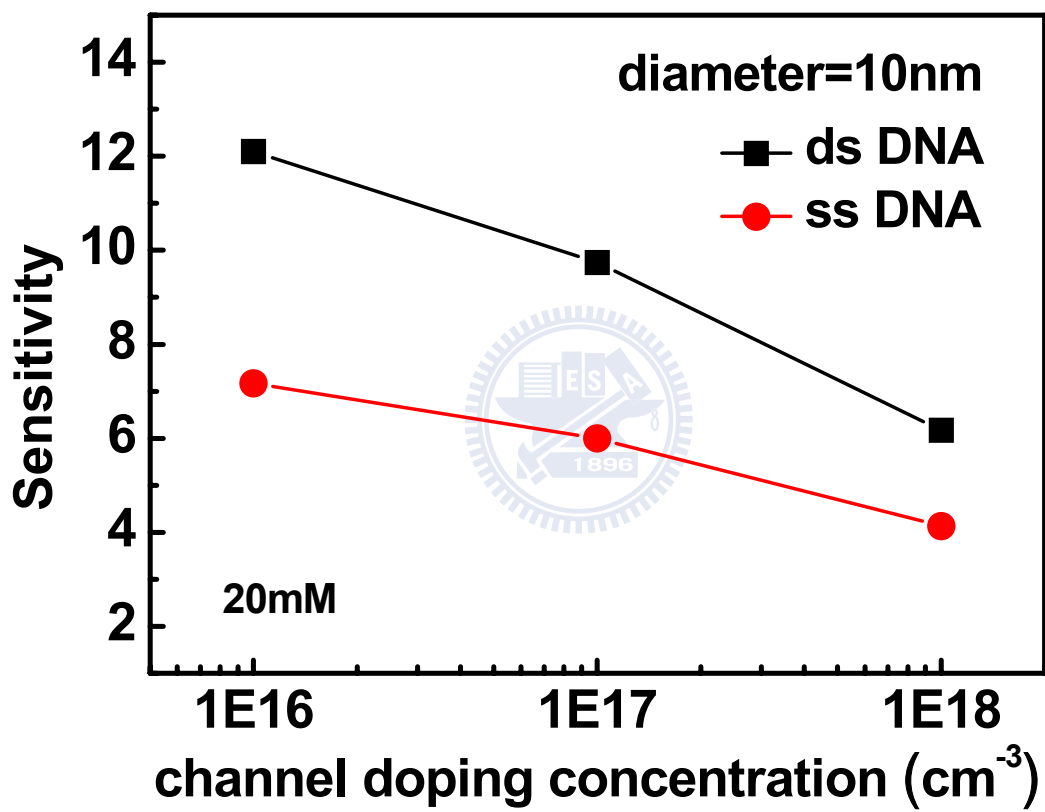


Fig. 3-11. In the accumulation mode, the sensitivity increases with decreasing doping concentration of the nanowire biosensor.

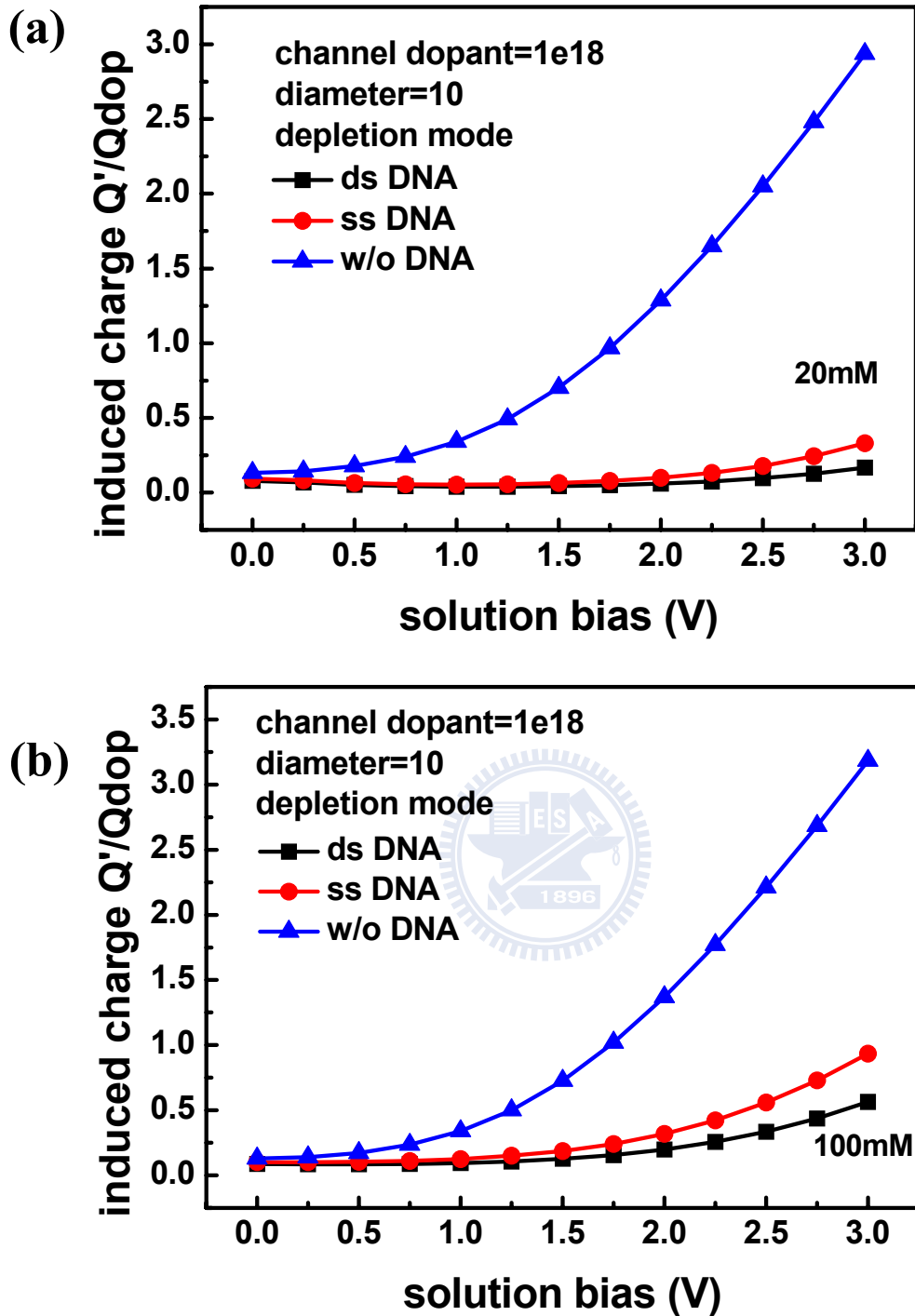


Fig. 3-12. In depletion mode, the induced charge Q' increases rapidly with the solution bias and has an enhancement of $\sim 3.5X/\sim 3X$ compared to the Q_{dop} in 20mM/100mM (at solution bias=3V), respectively. It means the biosensor operating in light ion concentrations has better performance.

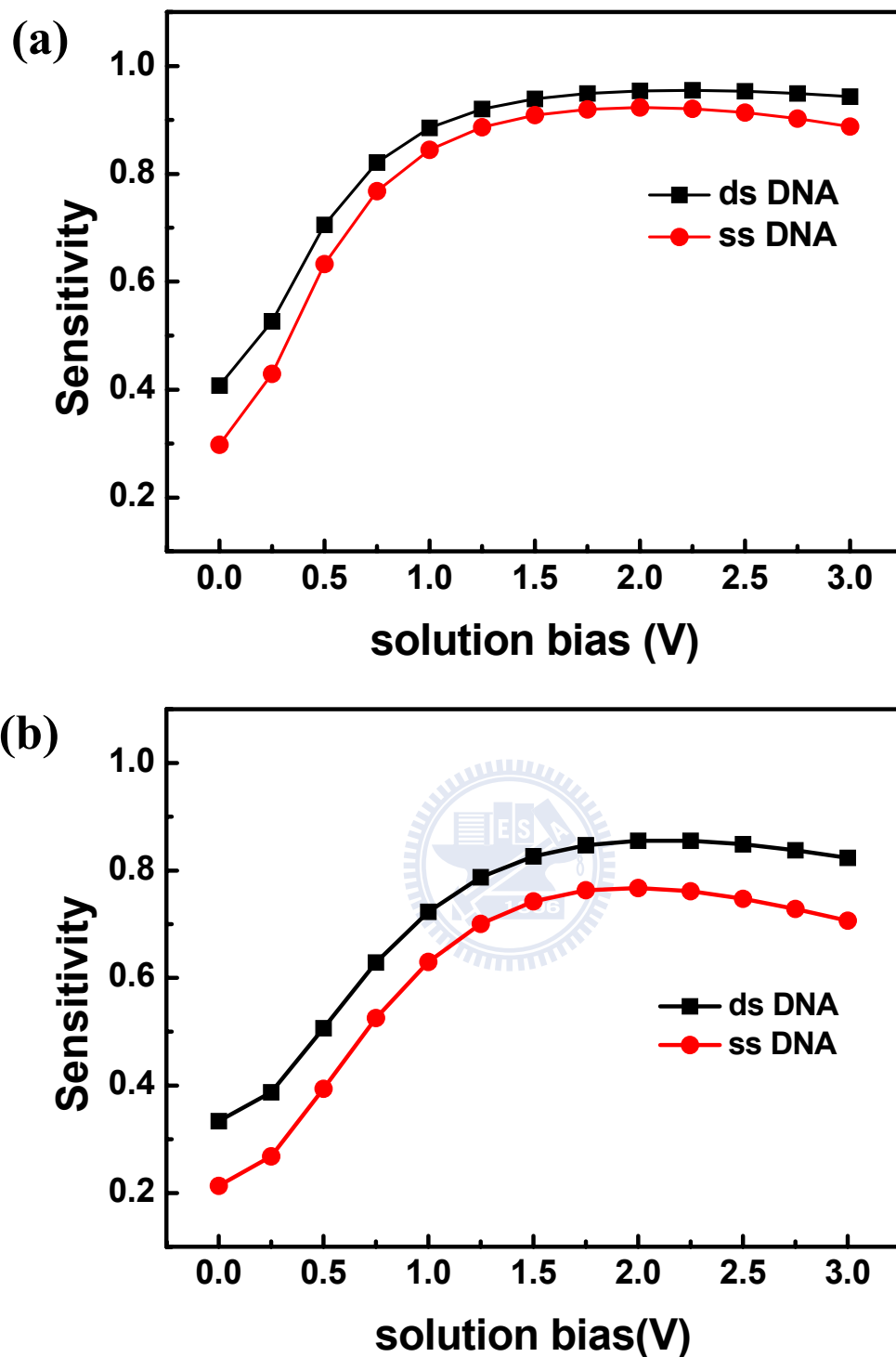


Fig. 3-13. The corresponding largest sensitivity for dsDNA/ssDNA are (a) 0.95/0.92 for the 20mM electrolyte concentration, and (b) 0.86/0.77 for the 100mM electrolyte concentration.

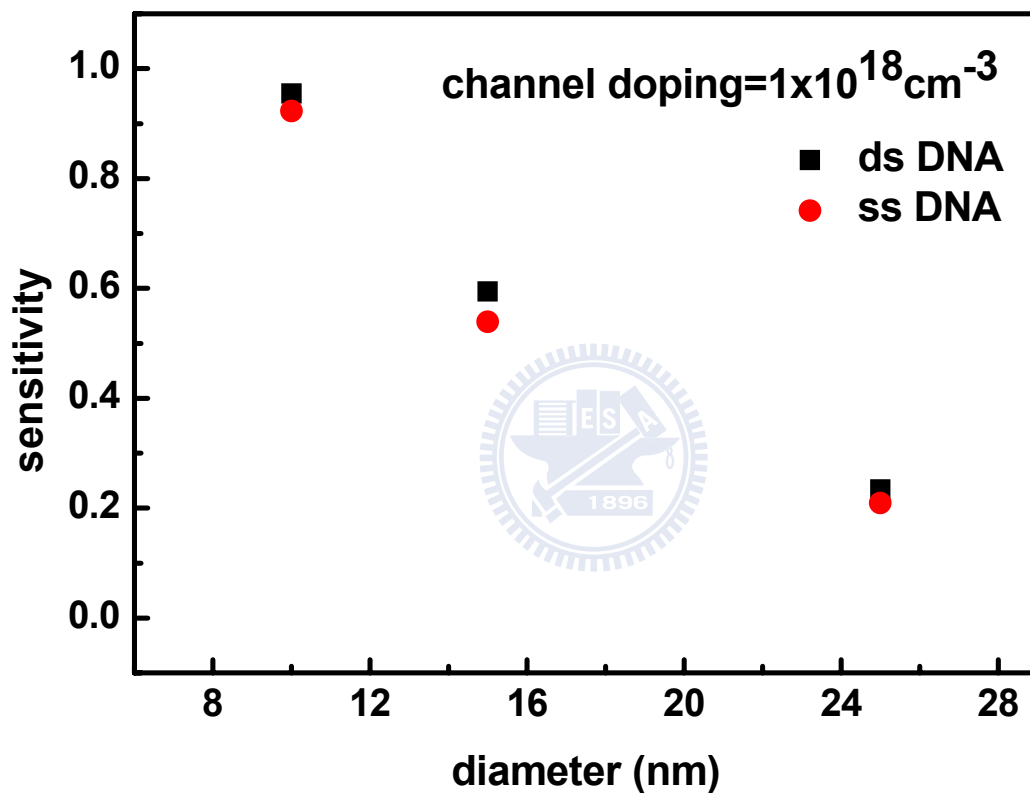


Fig. 3-14. In the depletion mode, the sensitivity of a Si-NW biosensor increases with decreasing diameter because of the increased surface to volume ratio.

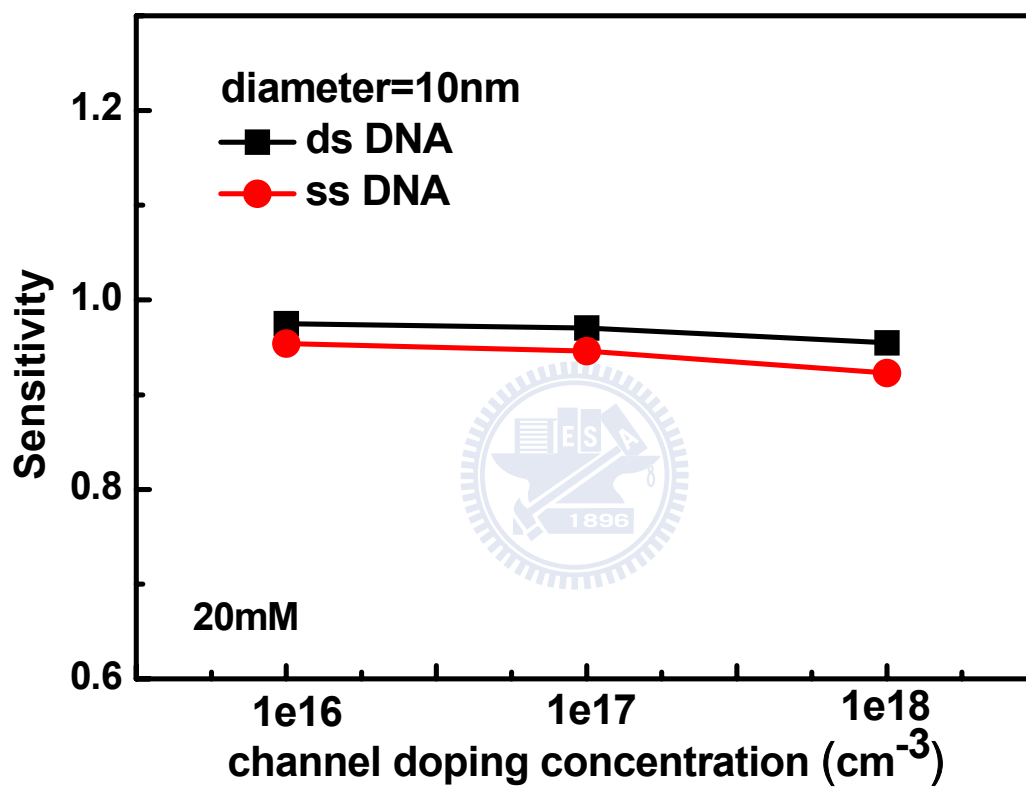


Fig. 3-15. The sensitivity does not increase with decreasing channel doping concentration because the sensitivity is saturated in the depletion mode.

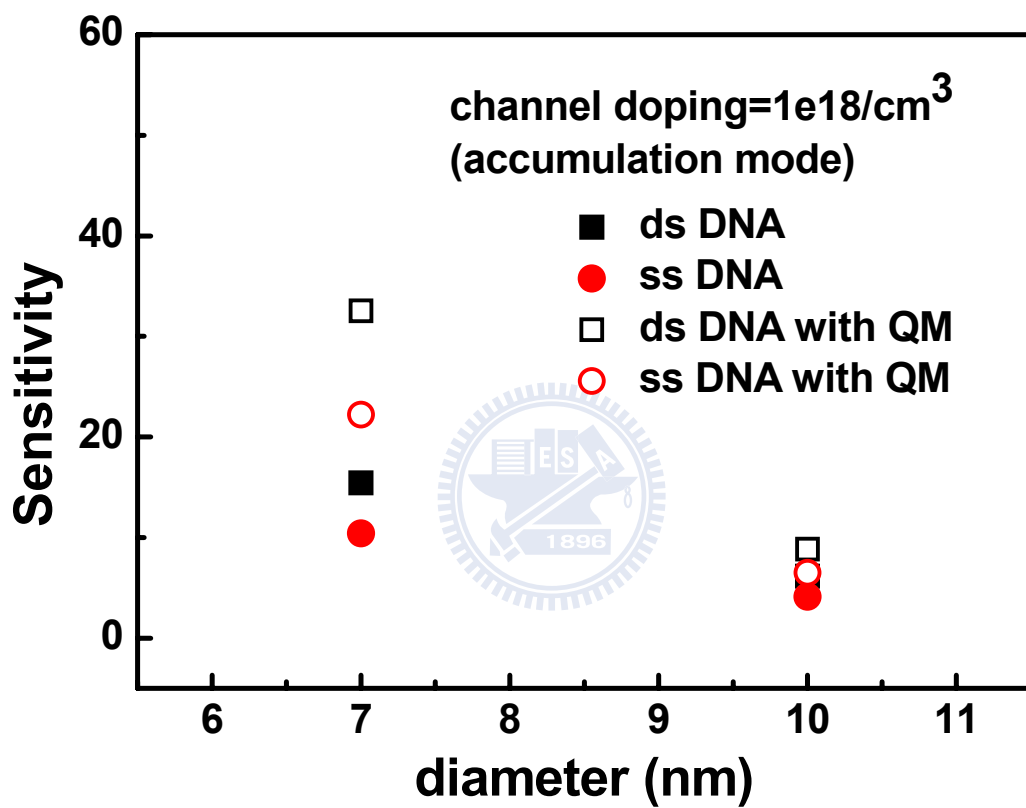


Fig. 3-16. Impact of quantum effects on the sensitivity of small-diameter Si-NW biosensors.

Chapter 4

Simulation and Analysis of Silicon Nanowire

Biosensors with Antenna

4-6 Introduction

The ion-sensitive field effect transistor (ISFET) is one of the most common chemical sensors, and is widely used in many areas. However, many research groups have demonstrated that the ISFETs do not have enough sensitivity [4.1]-[4.2] to detect ultra-low concentration biomolecules. For better performance, scientists and engineers have progressively miniaturized the size of biosensors to raise the surface to volume ratio and thus the sensitivity. In [4.3], the research group in NCTU has proposed a novel structure with antenna for the Si-NW biosensor design. The new structure shows a superior subthreshold swing and higher on/off current ratio than the traditional bulk device [4.3]. Although these advantages can further improve the performance of biosensors, the characteristics of the new structure with antenna have not been well understood.

Therefore, in this chapter, we establish a simulation flow for the proposed biosensor in [4.3]. In addition, we provide an analytical model [4.4] to assess the sensitivity of the Si-NW biosensors operated in subthreshold regime.

4-7 Simulation Approach and Calibration

4-2.1 Simulation Approach

The proposed system of Si-NW biosensors with antenna (Fig. 4-1(a)) can be divided into two sub-regions, as shown in Fig. 4-1(b) and Fig. 4-1(c). The first region, A, is the sensing region which contains a metal antenna with a top layer Al_2O_3 . The surface of the sensing region is immersed in the electrolyte solution. We assume the target biomolecules are uniformly distributed in the electrolyte solution and fully activated within the Debye length. The Debye length depends on the ionic strength concentration [4.5]. The second region, B, is the semiconductor region which contains a Si-NW and oxide. We assume there are no defects and traps in this region. In the following, we discuss the physical models employed and elaborate how to deal with the boundary condition between the region A and region B.

- 1) Region A: According to the Debye-Hückel theory [4.6], the charged biomolecules are attached to the oxide surface which can result in a corresponding change of surface potential. We can use the Graham equation [4.7] to describe it.

$$\sigma = \sqrt{8\varepsilon_e kTn_0} \sinh\left(\frac{zq\Psi}{2kT}\right), \quad (4-1)$$

where σ is the surface charge density, ε_e is the dielectric constant for the electrolyte solution, k is the Boltzmann constant, T is the absolute temperature, z is the valence of ion, n_0 is the ionic strength of electrolyte, q is the fundamental charge, and Ψ is the surface potential on the sensing region. Equation (4-1) is a well-defined function. Therefore, we utilize the inverse function of equation (4-1) to calculate the surface potential change $\Delta\Psi$. The

inverse function can be further simplified [4.8] as below:

$$\Delta\Psi = \frac{2kT}{zq} \left[\sinh^{-1} \left(\frac{\sigma_0 + \sigma_{\text{bio}}}{\sqrt{8\varepsilon_e kT n_0 + \text{bio}}} \right) - \sinh^{-1} \left(\frac{\sigma_0}{\sqrt{8\varepsilon_e kT n_0}} \right) \right], \quad (4-2)$$

where the surface potential change $\Delta\Psi$ is the potential difference between the sensing region with and without detecting the accumulated charge density of biomolecules σ_{bio} within the Debye length. σ_0 is the initial surface charge density which depends on the pH of the electrolyte solution.

- 2) Region B: The carrier transport and the potential distribution in this region can be described by the drift-diffusion equation and Poisson's equation, respectively. The drift-diffusion equation and Poisson's equation are elaborated in the earlier chapter 3-2. The potential change $\Delta\Psi$ derived from the inverse Graham equation is taken as the boundary condition in region B. Then, we can use the semiconductor simulation tool, ISE [4.9], to solve the coupled drift-diffusion equation and Poisson's equation with the boundary condition $\Delta\Psi$.

Equation (4-1)-(4-2) are the physical models used in the estimation of the surface potential change $\Delta\Psi$ on the sensing region. The coupled drift-diffusion equation and Poisson's equation are utilized to describe the carriers transport and the potential distribution in the semiconductor region. We can separate the simulation procedure of Si-NW biosensors with antenna into the following five main steps.

In the first step: Using the numerical solver, MatLab [4.10], the potential change $\Delta\Psi$ on the surface of sensing region can be estimated by solving the inverse Graham equation.

In the second step: In the region B, the coupled drift-diffusion equation and Poisson-Boltzmann equation are solved by the semiconductor simulation tool, ISE. We take the potential change $\Delta\Psi$ as the boundary condition of ISE simulation.

In the third step: With the specified operating bias such as source voltage and drain voltage, we can calculate the sensitivity of Si-NW biosensors by using ISE simulation tool. In this chapter, the sensitivity is defined as the relative conductance change between the sensing region without and with detecting the biomolecules. We assume that the corresponding surface potential of sensing region without/with detecting biomolecules is $0/(0+\Delta\Psi)$ volt.

In the fourth step: Vary the device design parameters in the first, second, and third steps, sequentially. In addition, we collect and categorize the simulation results to build the sensitivity table for various device design parameters.

In the fifth step: We investigate and analyze the sensitivity associated with different device design parameters, and systematically discuss the impact of design parameters on the Si-NW biosensors with antenna.

In summary, the simulation procedure of Si-NW biosensors with antenna is shown in the Fig. 4-2.

4-2.2 Simulation Results

In this section, we calculate the surface potential change $\Delta\Psi$ of DNA molecules in electrolyte solutions with pH 6 and 7 [4.11]. To calculate the surface potential change $\Delta\Psi$, we need to know three parameters: the initial surface charge density σ_0 , the charge density of biomolecules σ_{bio} , and the ionic strength $n_{0+\text{bio}}$. These three parameters can be determined as below:

- 1) The initial surface charge density σ_0 depends on the pH of the solution because the surface potential depends on the pH sensitivity. The dependence of the surface potential and pH is about -50mV/pH . The point of zero charge on the surface is known to be 8 [4.12]. Therefore, in the case of the pH-6 solution [4.11], the initial surface charge σ_0 is approximately 124 nC/cm^2 .
- 2) In order to calculate the charge density of biomolecules σ_{bio} , we assume that the biomolecules are uniformly distributed in the electrolyte solution and fully activated within the Debye length. σ_{bio} can be estimated by integration the valence electrons of charged biomolecules on the surface of sensing region.
- 3) For calculating the ionic strength $n_{0+\text{bio}}$, we assume that the ionic strength of the oligonucleotides solution is 19X higher than that of a 1:1 electrolyte solution because each oligonucleotide has 19-sequential molecules.

Fig. 4-3 shows that our solutions of the inverse Graham equation agree well with the experimental results of Korea Advanced Institute of Science and Technology [4.11].

In the following simulations, the surface potential change is assigned with an appropriate value 50mV and we assume that the channel, source, and drain have the same doping type. Fig. 4-4(a) and Fig. 4-4(b) show that the Si-NW biosensor with

antenna operating in the subthreshold region has better performance than that in the superthreshold region. It can be seen that in the subthreshold region, the sensitivity increases with decreasing diameter, increasing channel length, and decreasing channel doping. This is because the subthreshold swing of Si-NW biosensors with antenna and decreases with decreasing diameter, increasing channel length, and decreasing channel doping as shown in Fig 4-5(a), Fig. 4-5(b), and Fig. 4-5(c), respectively.

4-8 Analytical Sensitivity Model for Long channel Si-NW biosensors with Antenna in Subthreshold Region

In this section, we introduce an analytical sensitivity model for long channel Si-NW biosensors with antenna operated in subthreshold region. Fig. 4-6 shows the Si-NW structure studied in this work [4.4]. In the subthreshold regime, we assume that the Si-channel is fully depleted with negligible mobile carriers, and the nanowire is a device with negligible potential change along the Y-direction. Therefore, the potential distribution $\Phi(r)$ satisfies the following Poisson's equation:

$$\frac{\partial^2 \Phi(r)}{\partial r^2} + \frac{1}{r} \frac{\partial \Phi(r)}{\partial r} = \frac{-qN_a}{\epsilon_{Si}}, \quad (4-3)$$

where N_a is the channel doping concentration, and ϵ_{Si} is the dielectric constant for silicon. The boundary conditions are shown as below:

$$\left. \frac{\partial \Phi(r)}{\partial r} \right|_{r=0} = 0, \quad (4-4a)$$

$$\epsilon_{Si} \left. \frac{\partial \Phi(r)}{\partial r} \right|_{r=\frac{D}{2}} = C_i \cdot [V_{GS} - V_{fb} - \Phi(r = \frac{D}{2})], \quad (4-4b)$$

$$C_i = \frac{2\epsilon_{Si}}{D \cdot \ln(1 + \frac{2t_i}{D})}$$

where D and t_i are the channel diameter and thickness of gate insulator, respectively. V_{GS} is the surface potential on the sensing region, and V_{fb} is the flat-band voltage. C_i is the capacitance per unit length for an infinitely long cylindrical capacitor, which neglects the fringing effect of the field near the edges of the capacitor [4.13]. Solving the boundary value problem in the cylindrical coordinate, the solution can be expressed as [4.4]:

$$\Phi(r) = Ar^2 + B \quad (4-5)$$

$$A = -\frac{qN_a}{4\epsilon_{Si}}$$

$$B = V_{GS} - V_{fb} + \frac{qN_a D}{\epsilon_{Si}} \left(\frac{D}{2} + 2 \frac{\epsilon_{Si}}{C_i} \right)$$

Using the channel potential solution, the subthreshold drain current can be calculated as [4.4]:

$$\begin{aligned} I_{DS} &= q\mu_n \frac{kT}{q} \frac{1}{L_{eff}} \left(\frac{n_i^2}{N_a} \right) \left(1 - e^{-\frac{V_{DS}}{kT}} \right) \left(2\pi \int_0^{\frac{D}{2}} r \cdot e^{\frac{q\Phi(r)}{kT}} dr \right) \\ &= q\mu_n \frac{1}{L_{eff}} \left(\frac{kT}{q} \right)^2 \left(\frac{n_i^2}{N_a} \right) \left(1 - e^{-\frac{V_{DS}}{kT}} \right) e^{\frac{B}{kT}} \left(e^{\frac{A}{q} \frac{D^2}{4}} - 1 \right) \end{aligned} \quad (4-6)$$

where q is the elementary charge, μ_n is the carrier mobility, n_i is the intrinsic carrier density, L_{eff} is the effective channel length, k is the Boltzmann constant, and T is the absolute temperature. The sensitivity model of the Si-NW biosensors can be further derived from the drain current equation as:

$$S = \frac{G - G_0}{G_0} = \frac{\frac{V_{DS}}{I_{DS}} \Big|_{V_{GS}=\Delta\Psi} - \frac{V_{DS}}{I_{DS}} \Big|_{V_{GS}=0}}{\frac{V_{DS}}{I_{DS}} \Big|_{V_{GS}=0}} \quad (4-7)$$

Fig. 4-7(a) and Fig. 4-7(b) show that the subthreshold current model agrees well with the 3-D device simulation. However, it should be noted that the assumption of negligible mobile carriers in the model derivation has set constraints on the channel doping concentration of Si-NW biosensors.

Fig. 4-8 shows that the analytical sensitivity model agrees well with the device simulation results for various doping concentrations. Fig. 4-9 shows that the analytical sensitivity model agrees well with the device simulation results for various channel diameters. It can be seen that the sensitivity of Si-NW biosensors with antenna is insensitive to the channel diameters and doping concentration. This is because the nanowire structure has a superior gate control ability to keep the subthreshold swing near the ideal value, 60mV/dec, at room temperature.

In addition, we can relate the sensitivity of Si-NW biosensors with antenna with the device subthreshold swing as below:

$$\begin{aligned} S_{\text{wing}} &= \ln(10) \frac{dV_{GS}}{d \ln(I_D)} = \ln(10) \frac{\Delta\Psi}{\ln(I_{D,V_{GS}=\Delta\Psi}) - \ln(I_{D,V_{GS}=0})} \\ \Rightarrow \frac{\Delta\Psi}{S_{\text{wing}}} \ln(10) &= \ln(I_{D,V_{GS}=\Delta\Psi}) - \ln(I_{D,V_{GS}=0}) = \ln\left(\frac{I_{D,V_{GS}=\Delta\Psi}}{I_{D,V_{GS}=0}}\right) \\ \Rightarrow \frac{I_{D,V_{GS}=\Delta\Psi}}{I_{D,V_{GS}=0}} &= \exp\left[2.3 \frac{\Delta\Psi}{S_{\text{wing}}}\right] \end{aligned} \quad (4-8)$$

We can rewrite the sensitivity expression in equation (4-8) as below:

$$\text{Sensitivity} = \frac{G-G_0}{G_0} = \frac{\frac{I_{D,V_{GS}=\Delta\Psi}}{V_{DS}} - \frac{I_{D,V_{GS}=0}}{V_{DS}}}{\frac{I_{D,V_{GS}=0}}{V_{DS}}} = \frac{I_{D,V_{GS}=\Delta\Psi}}{I_{D,V_{GS}=0}} - 1$$

$$\Rightarrow \text{Sensitivity} = \exp\left[2.3 \frac{\Delta\Psi}{S_{\text{swing}}}\right] - 1 \quad (4-9)$$

From equation (4-9), we can see that the sensitivity is exponentially dependent on the inverse subthreshold swing. Fig. 4-10 shows the corresponding sensitivity for various subthreshold swings, and it is verified by 3-D device simulation. When the subthreshold swing is ~60mV/dec, the corresponding sensitivity is ~5.9. It is consistent with our previous simulation results in Fig. 4-4. Moreover, equation (4-9) indicates that Si-NW biosensors with antenna has ~3X enhancement in sensitivity compared with the traditional ISFET (bulk) if the subthreshold swing is improved from 100mv/dec (bulk) to 60mv/dec (Si-NW).

4-9 Conclusions

Our conclusions for this chapter are summarized as follows:

- (7) The simulation flow of Si-NW biosensors with antenna has been demonstrated.
- (8) The Si-NW biosensor with antenna operating in the subthreshold region has a better sensitivity than in the superthreshold region.
- (9) The sensitivity is insensitive with diameter and doping concentration. It implies that the proposed structure [4.3] has the potential to suppress the process variations.

- (10) An analytical sensitivity model for Si-NW biosensors with antenna operating in subthreshold regime has been demonstrated.
- (11) We have demonstrated the correlation between the sensitivity and the subthreshold swing. Compared with ISFETs, the Si-NW biosensors with antenna have ~3X sensitivity gain if the subthreshold swing is improved from 100mv/dec (bulk) to 60mv/dec (Si-NW).

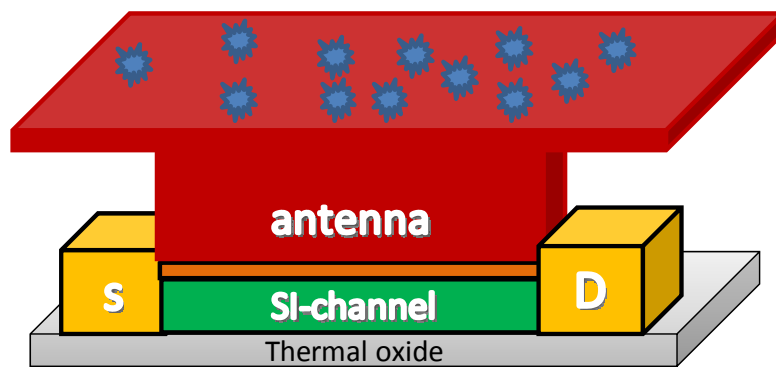
References

- [4.1] P. R. Nair and M. A. Alam, "Performance limits of nanobiosensors," *Applied Physics Letters*, no. 88, 2006.
- [4.2] J. J. Gooding, "Nanoscale biosensors: significant advantages over larger devices?" *Biosensors*, no.3, pp 313-315, 2006.
- [4.3] H. H. Hsu, T. W. Liu, L. Chan, C. D. Lin, T. Y. Huang, and H. C. Lin, "Fabrication and characterization of multiple-gated poly-si nanowire thin-film transistors and impacts of multiple-gate structures on device fluctuations," *IEEE TED*, vol. 55, no. 11, NOV. 2008.
- [4.4] Y. S. Wu, and P. Su, "Sensitivity of gate-all-around nanowire MOSFETs to process variations-a comparison with multigate MOSFETs," *IEEE TED*, vol. 55, no. 11, NOV. 2008.
- [4.5] P. E. Sheehan, and L. J. Whitman, "Detection limits for nanoscale biosensors," *Nano Letters*, vol. 5, no. 4, pp. 803-807, 2005.
- [4.6] M. Holst, "The Poisson-Boltzmann equation: analysis and multilevel numerical solution," in "Applied mathematics and CRPC," California Inst. Technol., Pasadena, CA, 1994. Tech. Rep.
- [4.7] A. J. Bard and L. R. Faulkner, *Electrochemical Method: Fundamentals and Applications*. 2nd ed. (Wiley, New York, 2001), pp. 947-950.
- [4.8] F. Uslu, S. Ingebrände, D. Mayer, S. Böcher-Meffert, M. Odenthal, A. Offenhäusser, "Label-free fully electronic nucleic acid detection system based on a field-effect transistor device," *Biosensors and Bioelectronics*, vol. 19, pp 1723-1731, 2004.
- [4.9] <http://www.synopsys.com/Tools/TCAD/DeviceSimulation/Pages/default.aspx>
- [4.10] <http://www.mathworks.com/>

- [4.11] S. J. Kim, K. Yoo, J. Shim, W. Chung, C. Ko, M. Im, L. S. Kim, and E. Yoon, "Real-time label-free quantitative monitoring of biomolecules without surface binding by floating-gate complementary metal-oxide semiconductor sensor array integrated with readout circuitry," *Applied Physics Letters*, no. 91, 2003.
- [4.12] R. E. G. van Hal, J. C. T. Eijkel, and P. Bergveld, "A general model to describe the electrostatic potential at electrolyte oxide interfaces," *Adv. Colloid Interface Sci.* 69, 31 1996.
- [4.13] D. K. Cheng, *Field and Wave Electromagnetics*. Reading, MA: Addison-Eesley, 1992.



(a) A Si-NW biosensor with antenna



(b) The sensing region

(c) The semiconductor region

Debye length
 $\lambda \sim \frac{0.304}{\sqrt{\text{NaCl}}} [\text{nm}]$

[4.5]

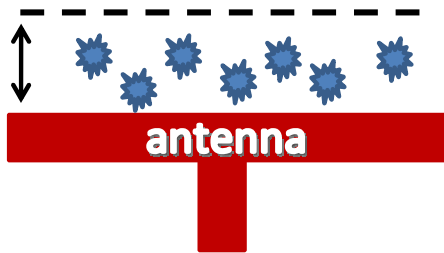


Fig. 4-1. (a) The proposed biomolecules detecting system [4.3] which can be separated to (b) the sensing region, and (c) the semiconductor region.

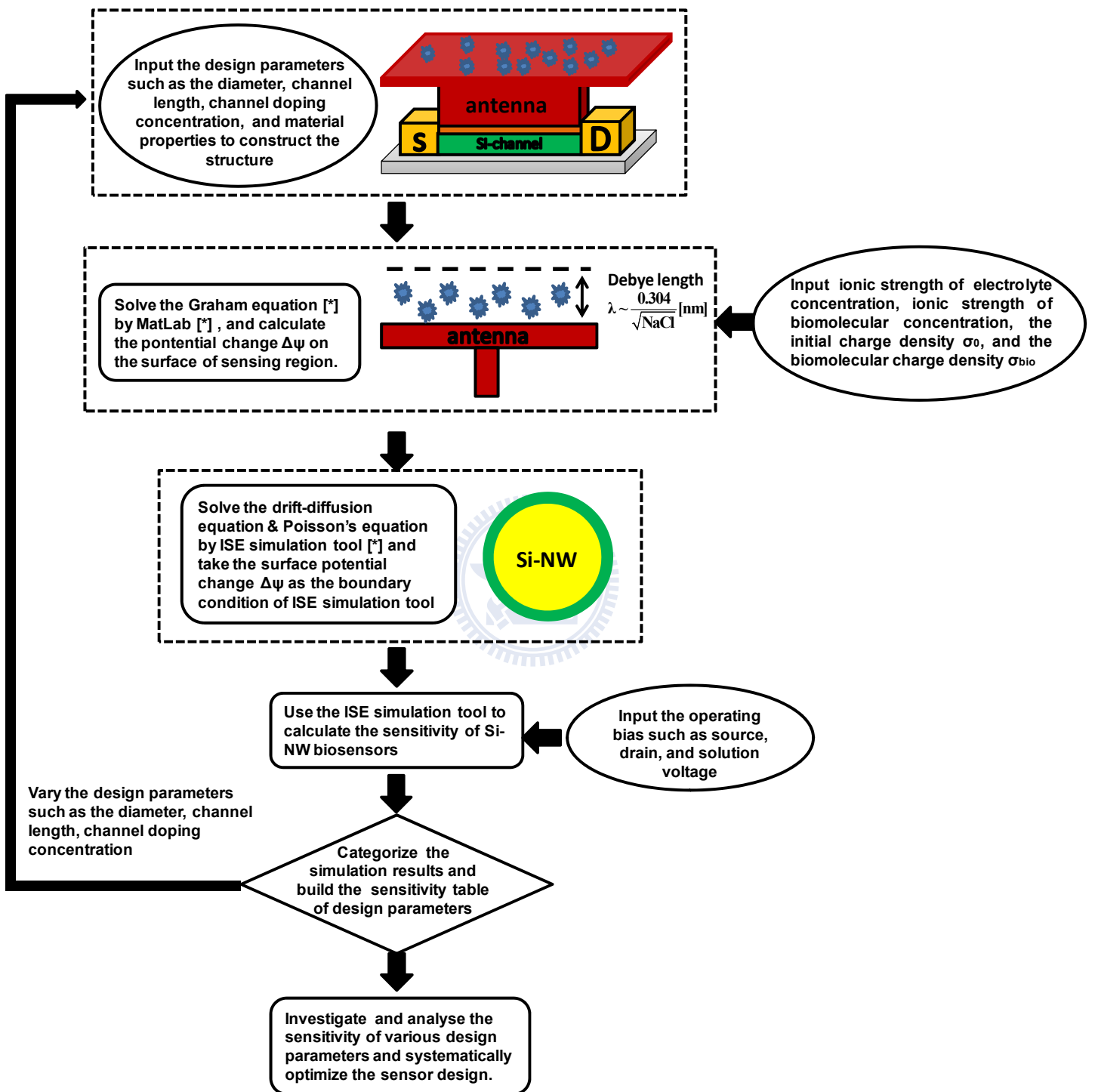


Fig. 4-2. The simulation procedure for a Si-NW biosensor with antenna.

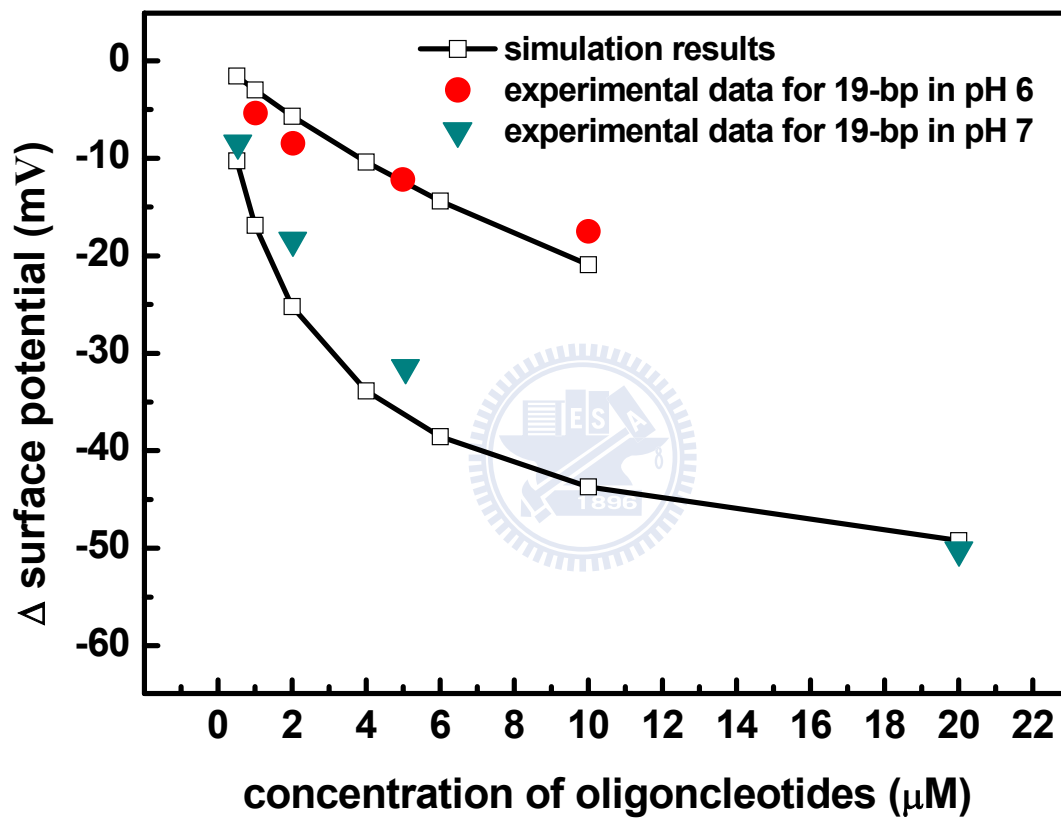


Fig. 4-3. Simulation of the surface potential change in the electrolyte solution with pH 6 and pH 7. Our simulation results agree well with the experimental results [4.11].

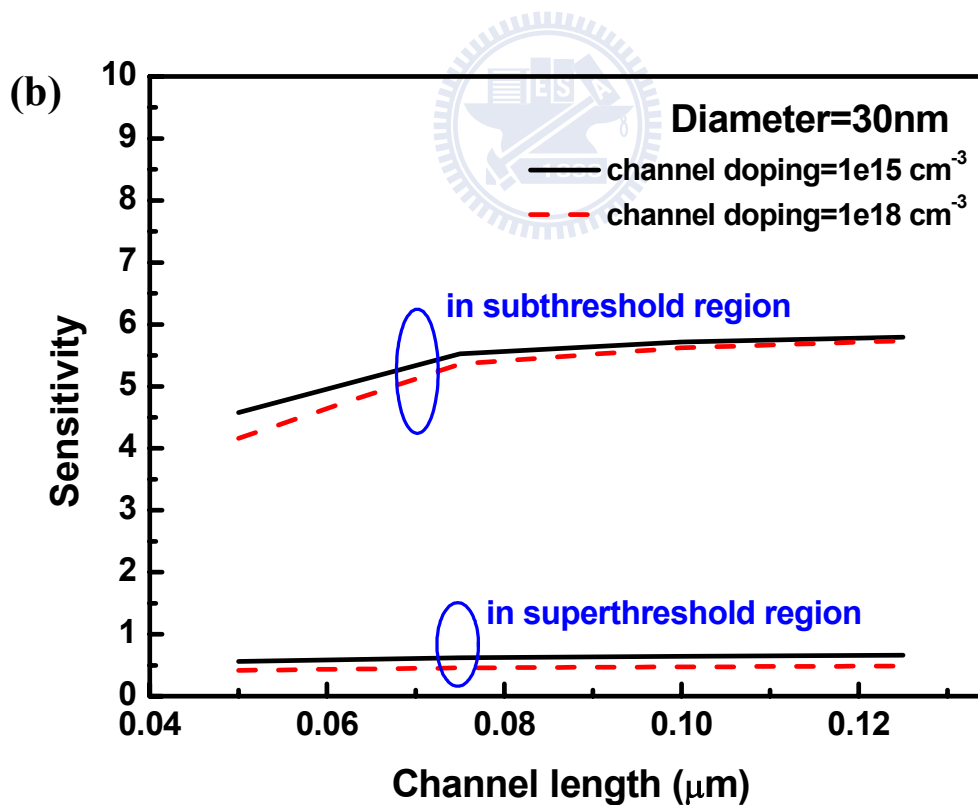
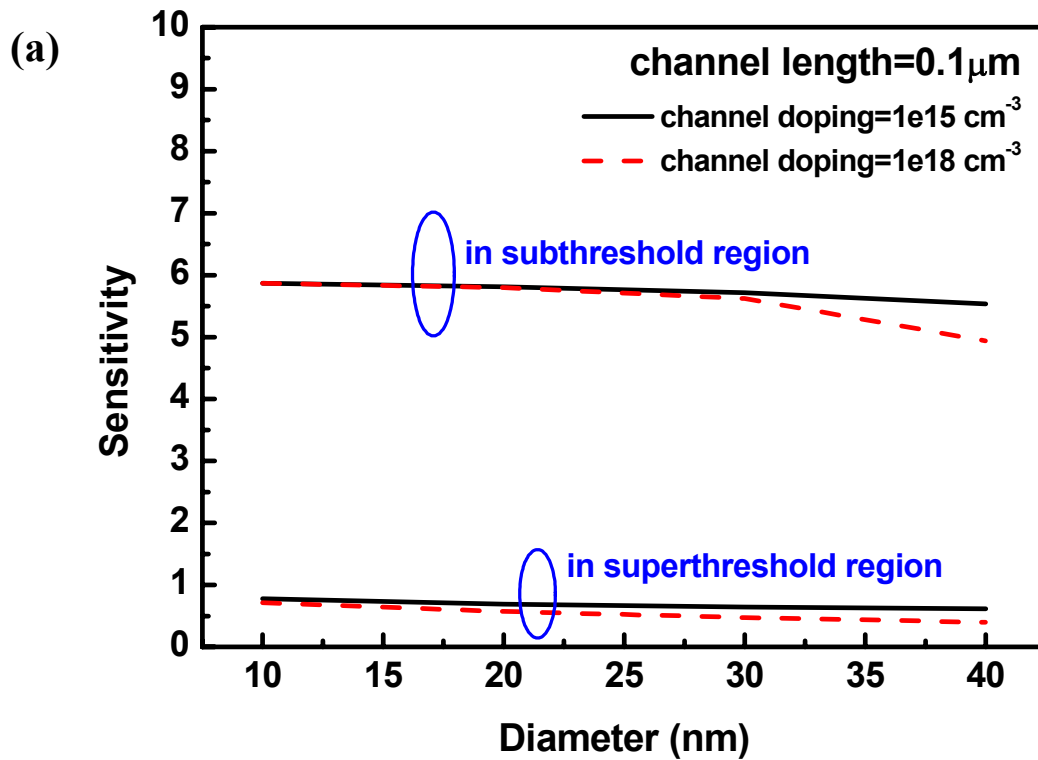


Fig. 4-4. The sensitivity of Si-NW biosensors with antenna operating in the subthreshold and superthreshold region for various (a) channel diameters, and (b) channel lengths.

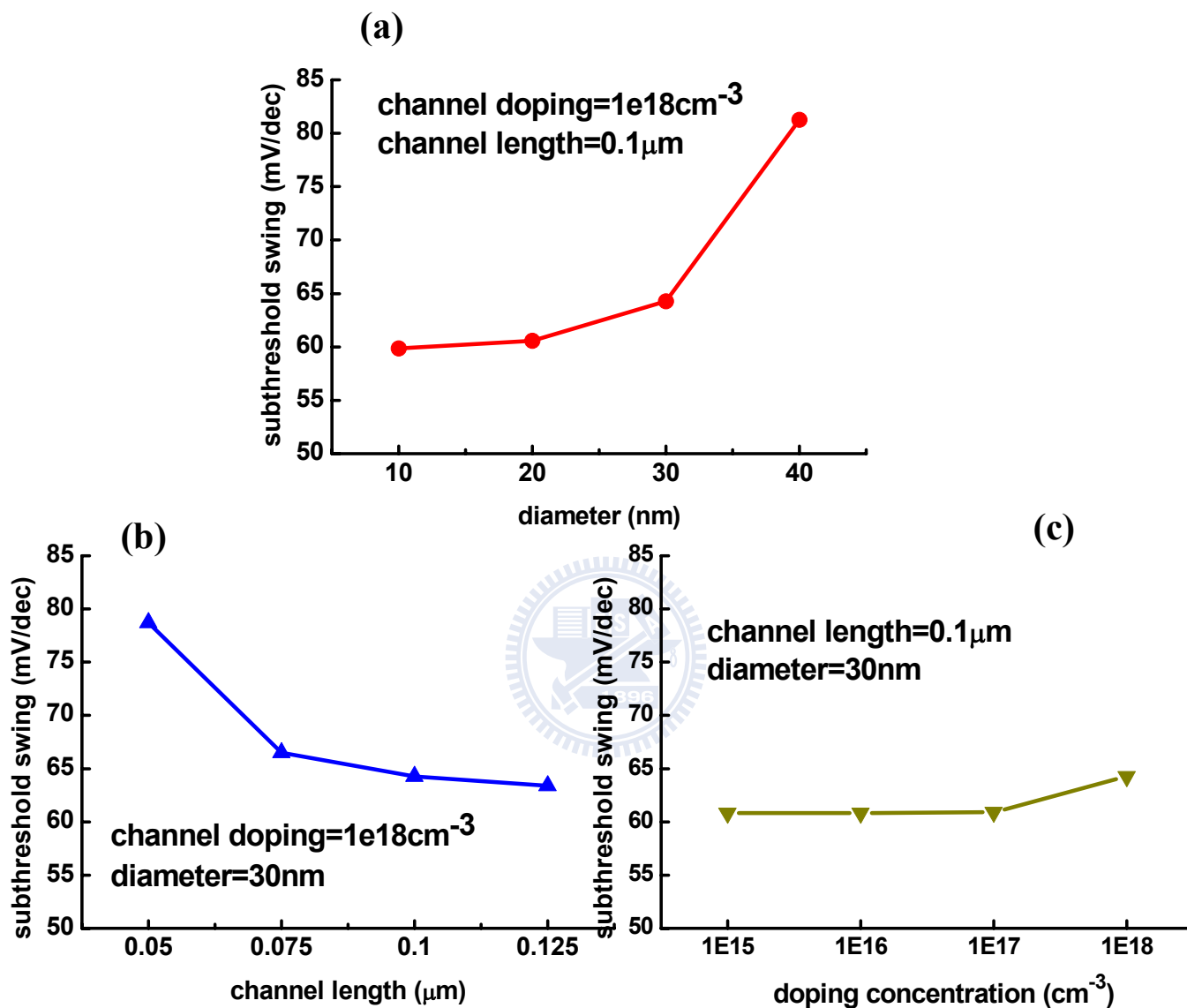


Fig. 4-5. The subthreshold swing of Si-NW biosensors with antenna depends on various device design parameters such as (a) diameter, (b) channel length, and (c) channel doping.

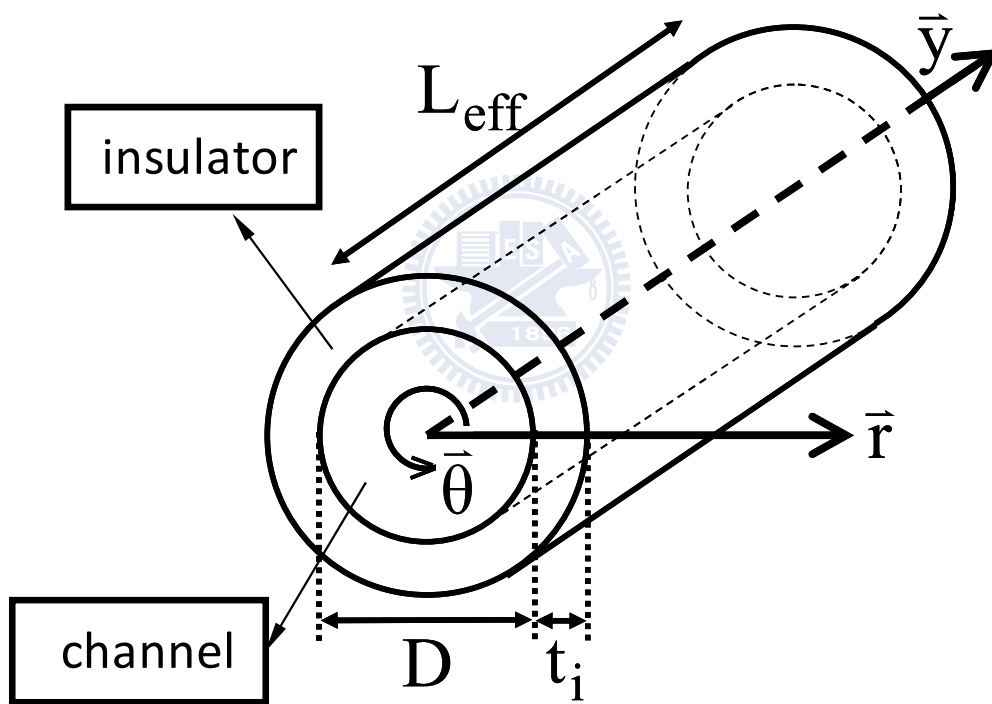


Fig. 4-6. Schematic sketch of a Si-NW structure [4.4]. The origin ($r=0$ and $y=0$) is defined at the center of the channel/source junction.

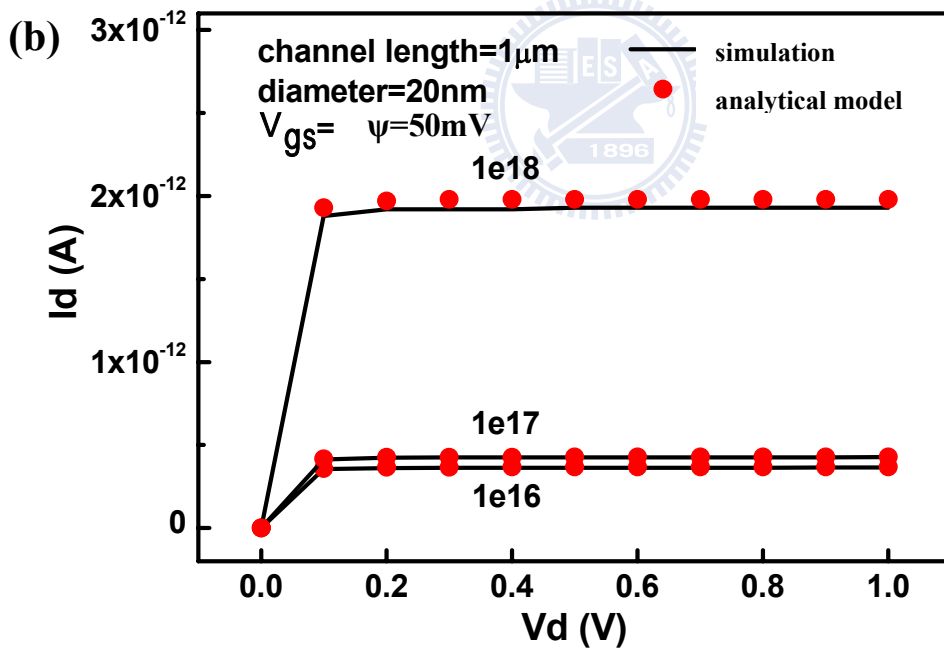
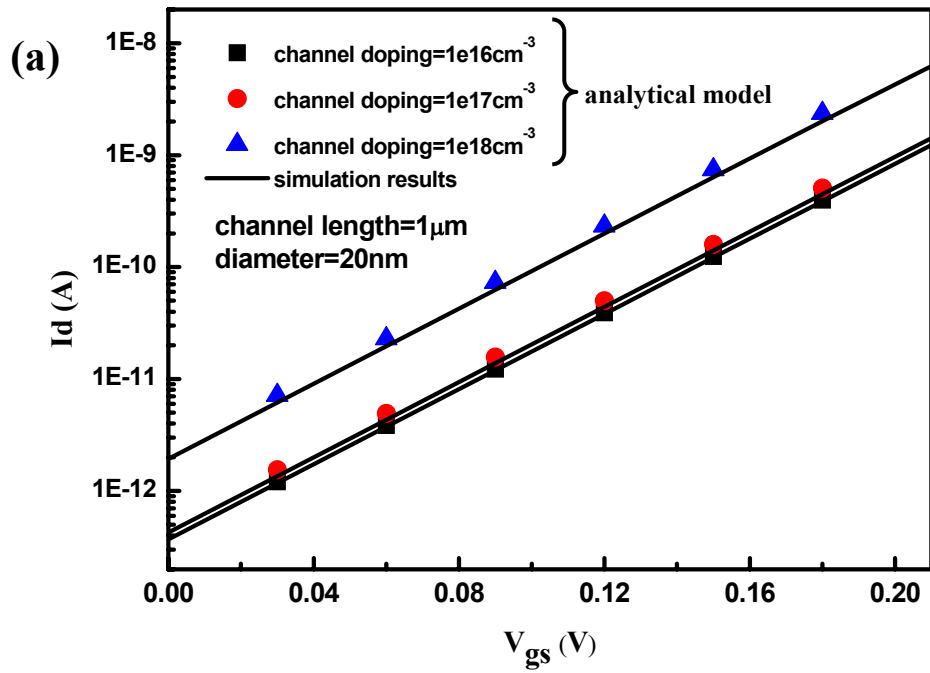


Fig. 4-7. The simulation results are captured well by our analytical model in the (a) I_d versus V_{gs} curves, and (b) I_d versus V_d curves.

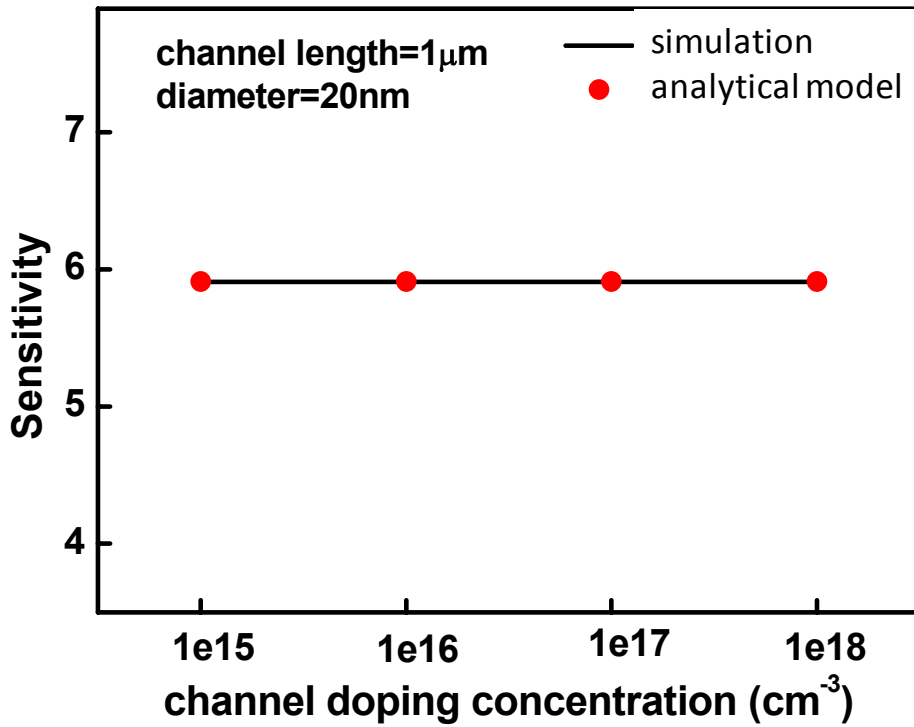


Fig. 4-8. Comparison of the analytical sensitivity model with simulation results for various doping concentrations.

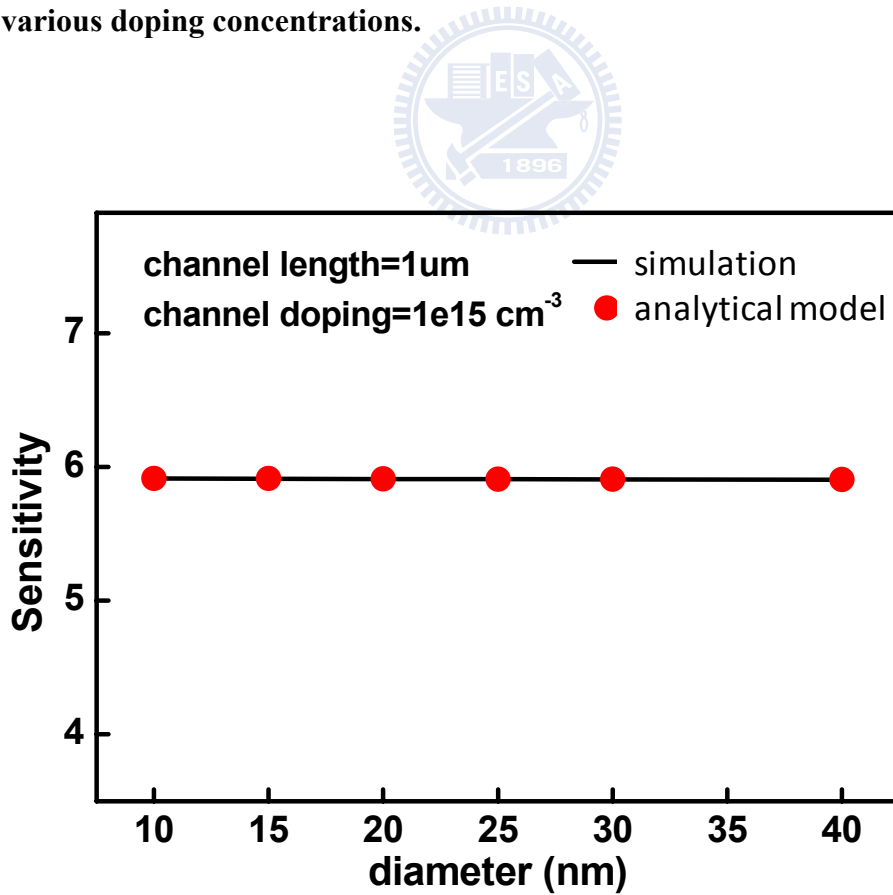


Fig. 4-9. Comparison of the analytical sensitivity model with simulation results for various diameters.

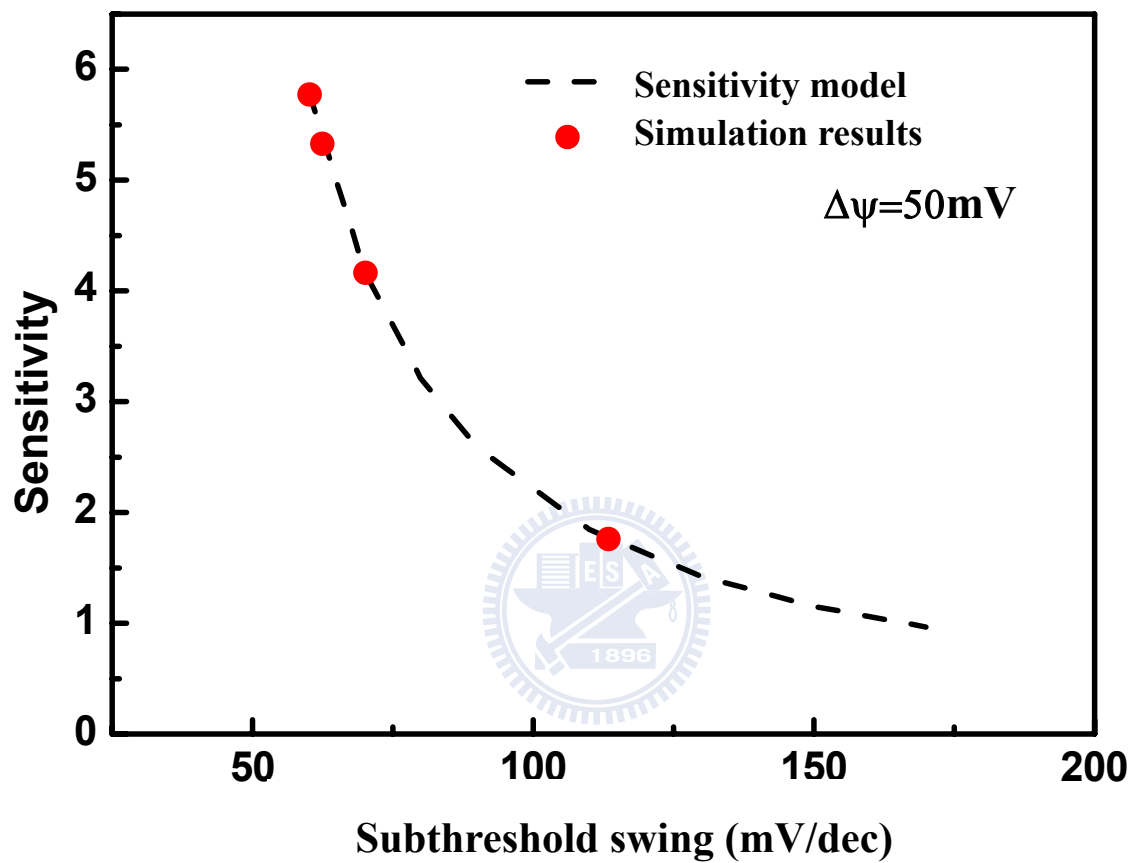


Fig. 4-10. The corresponding sensitivity of Si-NW biosensors for various subthreshold slopes, from 60mV/dec ~180mV/dec.

Chapter 5

Conclusions

In this thesis, we have provided three systematic simulation procedures for Si-NW biosensors considering the intrinsic fluctuations, the screening effect, and the novel structure with antenna.

Our simulation procedure for the direct-detection Si-NW biosensor has been demonstrated and verified with Harvard's experimental results [5.1]. This simulation framework has been employed to systematically investigate the impact of process variations on Si-NW biosensors and the impact of quantum effects on small-diameter Si-NW biosensors. Our results can be summarized as:

- a). We have assessed the impact of diameter variation on the sensitivity of Si-NW biosensors. Our simulation results indicate that Si-NW biosensors should still be designed at lower doping concentrations for the suppression of sensitivity variation.
- b). To assess the impact of channel length variation, we have used the autocorrelation function to generate the pattern of channel length fluctuations. Our simulations indicate that P_{length} is negligible. Hence, lightly-doped channel and short channel length should be employed for higher sensitivity of Si-NW biosensors.
- c). We have performed atomistic simulation to capture the impact of RDF on the sensitivity of SI-NW biosensors. Our simulations indicate that lightly-doped Si-NW biosensors have more advantages in $\langle S_{\text{RDF}} \rangle$ and P_{RDF}

than the heavily-doped case.

- d). The impact of quantum effects on the Si-NW biosensors has been studied for lightly and heavily doped devices. It indicates that the impact of quantum effects for the heavily-doped case is more significant than the lightly-doped case. Even though the sensitivity is enhanced more by the quantum effect in the heavily-doped case, the sensitivity for heavy doping concentration is far less than that for the light doping concentration. Hence, even considering the quantum effect, the lightly-doped channel is still a better choice.

Our simulation procedure for Si-NW biosensors with solution bias has been demonstrated and verified with the Stanford's simulation results [5.2]. We have used a sophisticated method to combine the electrolyte solution region and the semiconductor region. Using our combined simulator is more efficient compared to solving the physical models in the electrolyte solution region and the semiconductor region individually. The screening effect severely limits the performance of Si-NW biosensors. To assess the impact of the electro-diffusion flow in the electrolyte solution, we have utilized our simulation framework to systematically investigate the screening effect for various device design parameters. Our simulation results indicate that the sensitivity of Si-NW biosensors enhances with increasing diameter and decreasing channel doping, no matter in the accumulation or depletion mode. Comparing the two operation modes, we find that Si-NW biosensors operating in the accumulation mode have more benefits in terms of the sensitivity. Moreover, Si-NW biosensors with an optimized solution bias can be employed to obtain the largest sensitivity.

Our simulation flow for Si-NW biosensors with antenna has been demonstrated. We find that Si-NW biosensors with antenna operating in the subthreshold region have a larger sensitivity than that in the superthreshold region. We have provided an analytical sensitivity model to assess the sensitivity of the Si-NW biosensors in the subthreshold regime. Verified with the computer simulation, our analytical sensitivity model is reliable predicting the sensitivity of long channel Si-NW biosensors with antenna. Moreover, we have related the sensitivity model to derive the subthreshold swing. Our study indicates that Si-NW biosensors with antenna has ~3X sensitivity enhancement compared with the traditional ISFET (bulk) as the subthreshold swing improves from 100mV/dec (bulk) to 60mV/dec (Si-NW).



References

- [5.1] G. Zheng, F. Patlowsky, Y. Cui, W. U. Wang, and C. M. Lieber, “Multiplexed electrical detection of cancer markers with nanowire sensor arrays,” *Nat. Biotechnol.*, vol. 23, no. 10, pp. 1294-1301, Oct. 2005.
- [5.2] Y. Liu, K. Lilja, C. Heitzinger, R. W. Dutton, “Overcoming the screening-induced performance limits of nanowire biosensors: a simulation study on the effect of electro-diffusion flow,” *IEDM*, pp. 491-494, 2008.